THE DESIGN OF A TWO-LEVEL SOLID-STATE MASER

Colin Kydd Campbell

A Thesis Submitted for the Degree of PhD
at the
University of St Andrews

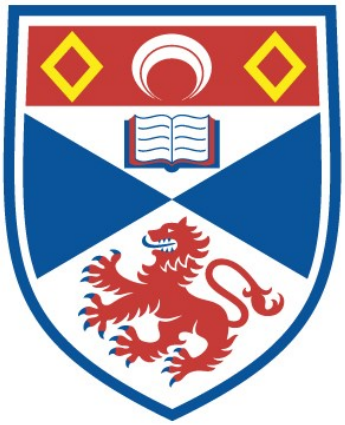

1960

ProQuest LLC.
789 East Eisenhower Parkway
P.O. Box 1346
Ann Arbor, MI 48106 – 1346

THE DESIGN OF A TWO-LEVEL SOLID-STATE MASER

A Thesis

presented by

Colin K. Campbell, B.Sc., S.M., M.I.R.E.

to the

University of St. Andrews

in application for the Degree

of Doctor of Philosophy.

ms 2156

DECLARATION

I hereby declare that this thesis has been composed by me, is a record of work carried out by me and has not previously been presented for a higher degree.

CERTIFICATE

I certify that Colin Kydd Campbell, B.Sc., S.M., M.I.R.E., has spent nine terms as a research student in the Physical Laboratory of the United College of the University of St. Andrews, that he has fulfilled the conditions of Ordinance No. 16 of the University Court of St. Andrews and that he is qualified to submit the accompanying thesis in application for the degree of Doctor of Philosophy.

Research Supervisor

CAREER

I served in the Royal Corps of Signals and the Diplomatic Wireless Service from 1944 - 1948 before matriculation in the University of St. Andrews where I followed a course leading to graduation in 1952 in Electrical Engineering.

I studied at the Massachusetts Institute of Technology in 1951 with the aid of a Caird Travel Grant, and again at that Institute in 1952 and 1953 on the Massachusetts Golf Association Scholarship, and there I was awarded the S.M. Degree in Electrical Engineering in 1953 and elected to Associate Membership of Sigma Xi.

I was an electronics design engineer until October 1957 when I was admitted by the Senatus Academicus as a research student and began the work which is the subject of this thesis. This research was made possible by an award from the Royal Naval Scientific Service.

ACKNOWLEDGMENTS

I should like to express my sincere thanks to

Professor J.F.Allen,F.R.S.	for suggesting the topic and for encouragement throughout
Dr. D.Bijl,F.R.S.E.	for his supervision and for his most helpful advice
Royal Naval Scientific Service	for a research and equipment grant
Dr. D.Osborne	for many stimulating conversations
Mr. J.Gerrard	for help with the photographs
Mr. J.McNab, Mr. M. Bird, Mr. T.Marshall,Mr.G.Dunsire, Mr. F.Akerbaum, Mr. E.Pirie	for their excellent work on the equipment
Mr. R.Mitchell	for the plentiful supply of liquid helium
Mr. H.Cairns	for his generous assistance with components

and to the Research Officers at Harwell, Dounreay, S.R.D.E. Christchurch, and University of Reading for the supply and irradiation of specimens.

TABLE OF CONTENTS

LIST OF ILLUSTRATIONS

CHAPTER 1

INTRODUCTION

1.1 The Maser

Prior to the development of the maser, amplification and oscillation in microwave devices were obtained by the conversion of d-c power to r-f power through the interaction of charged particles with an electromagnetic field. In the maser devices with which we are concerned, energy conversion is achieved through the interaction of an electromagnetic field with a molecular system which may be uncharged.

In the past, prime interest in the field of Microwave Spectroscopy has been confined to the study of the mechanisms governing the absorption of microwave energy by a quantum system. It was realized, nevertheless, that under certain conditions a quantum system could emit microwave energy upon the application of a prescribed stimulant. The name maser is thus derived as an acronym for "Microwave Amplification by Stimulated Emission of Radiation".

Molecular systems which are initially in thermal equilibrium with their surroundings will absorb radiation, for in such equilibrium the energy states of the systems will be populated according to a Boltzmann distribution. If just two energy states of an electron spin-system in a d-c magnetic field are considered, the lower energy state will be more densely populated than the higher energy state. To make the

system emissive, it is necessary to upset this balance and arrange for the higher energy level to contain the larger proportion of the electron population. The ease by which this "inversion" can be obtained will depend upon the mechanisms governing the restoration of thermal equilibrium and upon the sharpness of the energy levels.

Efficient maser operation is highly dependent upon the material which is being excited, and many materials are being investigated for such use. Efficient operation in this context is taken to mean a large gain-bandwidth product if the system acts as an amplifier, and spectral purity if the system acts as an oscillator. In addition, the mechanisms governing the restoration of thermal equilibrium in an activated material are temperature dependent, and thus present day masers operate at temperatures in the liquid nitrogen to liquid helium range.

The principal attraction of a maser system, however, lies in the low noise figure, or noise temperature, that can be attained. Conventional microwave receivers have overall noise temperatures of the order of 1800°K, whereas, one observer[1] has reported a noise temperature of 20°K for a particular maser amplifier. Since the principal noise contribution in a receiver comes from the first stage (if that stage has a reasonably high gain), one can see that a conventional microwave receiver preceeded by a maser operating at the same frequency will constitute a very sensitive receiver indeed. Such a

system would be particularly suitable for radio astronomy and for long range radars, provided that the gain-bandwidth criteria were satisfied in the particular application.

There are in existence two types of maser systems, namely: a) those which utilize emissive material in the gaseous state, and b) those which operate with emissive material in the solid state. It is with a subdivision of the latter type that this thesis will be concerned. For the purpose of completeness, however, a brief review of the evolution of the various maser types follows.

The first literature on stimulated emission was ascribed to Einstein[2] who formulated a treatment relating the probabilities for emission and absorption of radiation in a molecular system when that system was under the influence of an applied radiation field. The first paper exploring the possibilities of maser action was by Weber[3] (Univ. of Maryland, 1953). A gaseous (NH_3) maser was later developed by Gordon, Zeiger and Townes[4] (Columbia University, 1954). This was followed by the experiments of Combrisson and Townes[5] in 1955 on a pulsed two-level solid-state maser. In 1956, Bloembergen[6] (Harvard University) proposed a scheme for a three-level (continuously operating) maser, which was quickly developed by Scovil[7] (Bell Telephone Labs., 1956).

1.2 Scope of Thesis

This thesis is concerned with the development of a two-level, X-band (3 cm.), solid-state maser for operation at liquid helium temperatures. The work was initiated as part of a programme of investigations in the field of electron spin resonance at the University of St. Andrews.

When the thesis programme commenced in 1957, it was planned to develop a two-level, solid-state maser as a microwave amplifier, but it became evident, with the advance of maser technology, that the three-level maser constituted a much more efficient amplifier system. Therefore, the thesis programme was directed toward investigating the possibility of using the two-level, solid-state maser as a pulsed microwave oscillator.

Unlike the three-level maser, the two-level system could theoretically be used to generate pulsed oscillations at a frequency higher than the frequency of inversion, and it was conceivable that useful amounts of power could be generated in the millimetric and sub-millimetric regions of the spectrum by such means. Since any development along this line would be a long term programme, this thesis was restricted to an investigation of the problems associated with inversion and spontaneous (but controlled) oscillation at the same X-band frequency.

The principal materials selected for investigation were crystals of neutron-irradiated diamond and neutron-

irradiated magnesium oxide. To the best of our knowledge, such diamonds had not been previously investigated as potential maser crystals. Neutron-irradiated MgO had been examined by Chester et al.[8,9] who obtained successful maser amplification with this type of material. However, these investigators had not observed spontaneous oscillations with such crystals.

Chapters 2, 3, 4 and 5 of the thesis cover the essentials of electron spin resonance and maser theory as applied to the problems at hand. The theory of two-level, solid-state masers has been covered to a large extent by several authors[10] and will not be fully repeated here. In Chapter 5, details are given of the paramagnetic crystals employed in this thesis. In Chapter 6, the experimental equipment and its design are covered in detail, while the remaining two chapters deal with experimental results, investigations and conclusions.

CHAPTER 2

STIMULATED AND SPONTANEOUS EMISSION OF RADIATION

2.1 Einstein Transition Probabilities

A radiation field can interact with an atomic system to effect transitions between stationary states of the atomic system if the radiation field contains components near a Bohr frequency. Spontaneous transitions can also take place within the system in the absence of an applied radiation field. The probabilities for such transitions were first postulated by Einstein[2] in 1917 in his quantum theory of black-body radiation.

Photons obey Bose-Einstein statistics and can be treated formally as linear oscillators. In this way, Planck obtained an expression for the energy density due to oscillators with frequencies between ν and $\nu + d\nu$, to give his radiation law,

$$\rho(\nu)d\nu = \frac{8\pi h}{c^3} \frac{\nu^3 d\nu}{(e^{h\nu/kT} - 1)} \qquad (2.1)$$

where $\rho(\nu)$ represents the equilibrium energy density in the radiation field.

In the Einstein treatment, if k and l represent states of the atomic system, and N_k and N_l $(N_k < N_l)$ denote the number of atoms in the k^{th} and l^{th} states, respectively (for $E_k > E_l$), the number of atoms, N_{kl}, making a transition

from k to l per second will be

$$N_{kl} = N_k A_{kl} + N_k B_{kl} \rho(\nu_{kl}) \qquad (2.2)$$

in the case of equilibrium between the atoms and a radiation field. The first term on the right hand side of Equation 2.2 represents spontaneous transitions and is proportional to N_k, while the second term represents induced emissions and is proportional to N_k and to the density of the radiation field at the Bohr frequency. The expressions A_{kl} and B_{kl} are time-independent quantities. In the same way, the number of atoms making a transition from l to k per second will be

$$N_{lk} = N_l B_{lk} \rho(\nu_{lk}) \qquad (2.3)$$

corresponding to absorption. The spontaneous transition coefficient in this case is zero. The coefficients, A_{kl}, B_{kl} and B_{lk}, in the above equations are called the Einstein Transition Probabilities. In the state of equilibrium when the number of transitions upwards and downwards must be equal, the above equations will be equal. Then it can be proved that,

$$B_{kl} = B_{lk}$$

$$A_{kl} = \frac{8\pi h(\nu_{kl})^3 B_{kl}}{c^3} \qquad (2.4)$$

and in equilibrium N_k and N_1 are related by the Boltzmann factor

$$\frac{N_k}{N_1} = \exp\left[-(E_K - E_1)/kT\right] \qquad (2.5)$$

From the above relationships we may derive the Planck radiation formula.

The Einstein relationships have been stressed to show that spontaneous (phase incoherent) emission at microwave frequencies is negligible in comparison to the coherent induced emission, for if we substitute values in Equation 2.4 for A_{kl}, at 10 kMc/s, then $A_{kl} \approx B_{kl} \times 6 \times 10^{-28}$ and hence may be neglected in any practical calculations other than on noise.

2.2 The Emissive Condition

It can be seen from Equations 2.2 and 2.3, that if we legitimately neglect the spontaneous transition probability, A_{kl}, the condition for emission of radiation reduces to the simple form $N_k > N_1$. Thus the emissive condition requires that the equilibrium population distribution in the atomic states should be inverted. It is further evident that after inversion, the ratio, N_k/N_1, should be as high as possible for the emitted power will be proportional to the population difference. Now a perfect population inversion in a two-level spin system will correspond mathematically to a spin

temperature change from $+T_{initial}$ to $-T_{initial}$, hence the initial (equilibrium) temperature should be as low as possible. Even at low temperatures population differences at 10 kMc/s are not large. For example, with this two-level system, the population ratios would be

$$\frac{N_k}{N_1} = 99.8\% \qquad \text{for } T = 300^\circ K$$

$$\frac{N_k}{N_1} = 88\% \qquad \text{for } T = 4^\circ K \ .$$

Under "steady-state" conditions with the two-level spin system a negative temperature cannot be realized as the density of the incident radiation field is increased. The best that one can hope to achieve under such conditions is an equality of populations corresponding to a spin temperature of $+\infty$. It is necessary to employ transient techniques to effect a population inversion between two energy levels of a spin system. This will be discussed in Chapter 5.

2.3 Quantum-Mechanical Treatment of Transition Probabilities

The topic of transition probabilities will be discussed briefly from the quantum-mechanical viewpoint, as the results of this treatment are of great importance in our later calculations. The results will be quoted without proof which has been fully derived by various authors[11,12]. For simplicity,

the discussion will be a semi-classical one with the radiation field unquantized, and only coherent radiation will be considered.

In most many-body problems, the exact Hamiltonian-Function cannot be calculated, and consequently the Schrödinger equation can be solved exactly in only a few simple cases. To overcome this drawback, approximation techniques such as the Perturbation Method may be applied. An energy perturbation in an atomic system may be of a time-independent or time-dependent nature. The perturbing influence of an electric field in a paramagnetic salt such as Ti^{3+}, set up by surrounding charges, may be taken as an example of the former perturbation. The influence of electromagnetic radiation on a paramegnetic system (again such as Ti^{3+}) may be regarded as an example of the latter type of perturbation. It is with the time-dependent perturbations that we shall concern ourselves.

The time-dependent Schrödinger equation is of the form

$$H\Psi = i\hbar \frac{d\Psi}{dt} \tag{2.6}$$

where

$H = H_0 + H'$ = Hamiltonian operator for the perturbed system

H_0 = Hamiltonian operator for the unperturbed system

H' = Time dependent energy perturbation operator.

Now since any state function may be expressed in terms of a

linear combination of pure energy state functions (or, using the Dirac terminology, since any ket can be expressed linearly in terms of the basic kets of a representation), the wave function for the perturbed system may be written,

$$\Psi = \sum_n C_n(t)\,\psi_n \tag{2.7}$$

where the ψ_n are independent of time and related to Ψ by,

$$\Psi = \sum_n C_n(t)\,\psi_n \exp(-iE_n \tfrac{t}{\hbar}) \tag{2.8}$$

In Equation 2.8 E_n is the energy of the stationary state ψ_n, $i = \sqrt{-1}$ and $\hbar = h/2\pi$.

Straightforward analysis for the time-dependence of the C_n's then gives

$$\frac{dC_n}{dt} = \frac{1}{i\hbar} \sum_K C_k(t)\ (H'_{nk})\ \exp(2\pi i\, \nu_{nK} t) \tag{2.9}$$

where H'_{nk} is the matrix element forming the representative of the Hamiltonian operator H' for states n and k, such that,

$$(H'_{nk}) = \int_V \psi_n^* H' \psi_K \, dV \tag{2.10}$$

the integration extending over the whole volume, V, of the co-ordinate system. The term ν_{nK} represents the transition frequency between states n and k and is given by $\nu_{nK} = (E_n - E_k)/h$. The term, ψ_n^* is the conjugate complex of ψ_n. If the system is in state k at time $t = 0$, before the perturbation is applied, then $|C_n|^2$ will give the probability

that the system is in state n after time t. In this case, therefore, $C_k = 1$, and all the other C's = 0 at t = 0, so that

$$C_n(t) = \frac{1}{i\hbar}\int_0^t (H'_{nk}) \exp(2\pi i \nu_{nK} t)\,dt \qquad (2.11)$$

$$= \frac{2\pi}{h}(H'_{nk}) \frac{\exp\left\{-2\pi i(E_n - E_k)t/h\right\} - 1}{2\pi(E_n - E_k)/h} \qquad (2.12)$$

In the case of a magnetic dipole transition between states n and k under the influence of a perturbing electromagnetic field ($B\cos 2\pi\nu t$), the nk^{th} element of the perturbation matrix is given by

$$(H'_{nk}) = \int_V \psi_n^* H' \psi_K \, dv$$

$$= B\cos(2\pi\nu t)\int_V \psi_n^* \mu \psi_K \, dv \qquad (2.13)$$

where the integral represents the strength of the magnetic dipole transition coupling the two states; where μ is the magnetic dipole moment.

Thus far, only two exactly defined states have been envisioned. As the energy levels are not entirely sharp, a function, $\rho(\nu)$, must be included to account for the density of the final states. This density function may be expressed in the normalized fashion

$$\int_{-\infty}^{+\infty} \rho(\nu)\,d\nu = 1$$

When this expression is included in the squared probability equation (No. 2.12) for monochromatic states, and the resultant expression integrated over the frequency range $-\infty$ to $+\infty$, the following expression is valid for the overall transition probability P_{nk},

$$P_{nk} = \int_{-\infty}^{+\infty} \left| C_n(t) \right|^2 \rho(\nu)\, d\nu \approx \frac{4\pi^2}{h^2} \left| (H'_{nk}) \right|^2 \rho(\nu)\, t \qquad (2.14)$$

CHAPTER 3

RESONANCE AND RELAXATION PROCESSES IN PARAMAGNETIC SOLIDS

Introduction

This chapter covers briefly those parts of paramagnetic resonance and relaxation phenomena relevant to the problems encountered in this thesis. The transitional probabilities discussed in the previous chapter are applied to the problem of calculating the power flow between a paramagnetic system and an electromagnetic radiation field when relaxation processes are considered. The relationships between power flow and relaxation may also be expressed in macroscopic terms, as in the Bloch equations[13].

3.1 Spin Hamiltonian

As stated in Chapter 2, in order to evaluate the properties of a quantum system, it is necessary to establish a Hamiltonian function, H, representing the total energy (potential and kinetic) of the system before an attempt is made to solve the Schrödinger equation. For the case of a paramagnetic crystal in a d-c magnetic field, B, the Hamiltonian can be expressed (in terms of decreasing energy) by the following:

$$H = W_c + W_V + W_{LS} + W_{ss} + \beta(L + 2S)\cdot B + W_{JI} - \gamma_n\beta_n B\cdot I \qquad (3.1)$$

Here, W_c represents the coulomb interaction of the electrons with the nucleus and with each other. The terms W_{LS} and W_{ss} represent the spin-orbit interactions and the spin-spin interaction, respectively. The W_V term represents the effect of the crystal field where $V(x,y,z)$ is the crystalline potential. In the iron group of hydrated salts, this interaction is large compared with the spin-orbit interactions and small compared with the coulomb interaction. In the rare earth salts, the effect of the crystalline field is smaller than the spin-orbit interactions, but greater than the nuclear interactions. Interaction with an external magnetic field, B, gives rise to the term $\beta(L + 2S).B$ where β is the Bohr magneton, and L and S refer to the orbital and spin momenta of the contributing electrons. Term W_{JI} represents the interaction between the magnetic moment of the nucleus and the magnetic field set up by the orbital and spin moments of the electrons. J refers to the total angular momentum of the electrons and I to the nuclear angular momentum. The final term, $-\gamma_n\beta_n B.I$, refers to the direct interaction between the nuclear moments and the external magnetic field, B, where γ_n = nuclear gyromagnetic ratio, and β_n = nuclear magneton. The magnitude of this latter term is usually negligible. Typical energies involved in such molecular interactions are as follows:

Type of interaction	Magnitude (e-volts)
Optical transition	few e-v
Molecular vibrational transition	10^{-3}
Molecular rotational transition	10^{-4} - 10^{-5}
Orientational energies of paramagnetic ions in usual laboratory fields (3000g)	" " "
Orientation of nuclear moments	10^{-7}

3.2 Paramagnetic Resonance

Paramagnetic resonance occurs when transitions between the Zeeman levels of a spin $\frac{1}{2}$ system are effected under the stimulus of an electromagnetic radiation field. The energy levels are appropriately separated by the application of a d-c magnetic field. Maximum interchange of energy occurs when the magnetic field vectors are orthogonal.

The condition for resonance is,

$$h f = \Delta E = g\beta B \qquad (3.3)$$

where f = transitional frequency; g = spectroscopic splitting factor = 2.0023 for a "free" electron; β = Bohr magneton = $e\hbar/2mc = 0.927 \times 10^{-20}$ erg/gauss; $h = 2\pi\hbar = 6.62 \times 10^{-27}$ erg-sec ; ΔE is the separation of the neighbouring Zeeman levels. One may also relate g in terms of a gyromagnetic ratio γ where $\gamma = g(\beta/\hbar)$.

As will be shown, power absorption is proportional to f^2, and for ultimate sensitivity one should work at as high

a frequency as possible. The upper limit for operation is mainly limited, however, by the availability of components in the high frequency region. Because of such limitations, X-band equipment was selected for this thesis. X-band components were also reasonably plentiful as surplus. At X-band, $f \approx 10$ kMc/s and the d-c magnetic field is required to be in the order of 3500 gauss.

3.3 Spin-Lattice and Spin-Spin Relaxation Processes

If the energy levels of a quantum system were perfectly sharp, as was assumed in the first part of the transition-probability analysis in Chapter 2, energy would only be emitted or absorbed by the system at a monochromatic frequency under the influence of an applied perturbation. In actuality, the width of a spectral line can never be less than that dictated by the Uncertainty Principle,

$$\Delta W \cdot \Delta t \approx h/2\pi \qquad (3.4)$$

where the "width" of a spectral line is defined as that frequency interval in which half of the emitted or absorbed energy is contained. In Equation 3.4, ΔW is the energy spread of an excited state and Δt is the average time spent by the atom or spin in that excited state.

In the absence of an applied perturbation, spontaneous transitions would determine the lifetime of an excited state, and thus the spread in energy of the excited state. This

spread in energy would correspond to a "natural" line width, $(\Delta f)_n$, where

$$(\Delta f)_n \approx \frac{A_{kl}}{2\pi} \tag{3.5}$$

and where A_{kl} is the spontaneous transition probability coefficient given in Equation 2.2. In the microwave region, however, the natural broadening will be negligible in the presence of other broadening processes. As described below, the principal broadening processes encountered in paramagnetic resonance work on solids are due to spin-lattice and spin-spin relaxation effects.

In the presence of a perturbing radiation field, a spin system in a crystal lattice will (in general) absorb energy. Since the spins are coupled to the crystal lattice through spin-orbit and orbit-lattice coupling, the lifetime of an excited state will be shortened by this process. Such a relaxation process is termed a spin-lattice relaxation process. In accordance with the Uncertainty Principle, such a relaxation process would increase the energy spread of an excited state and thus the paramagnetic resonance line would be broadened. For the type of maser considered here, however, an operational requirement is that spin-lattice interactions should be weak. In such instances, therefore, the resonance lines would not be significantly broadened by

this effect. The spin-lattice relaxation processes may be described in terms of a time constant, T_1, and this time constant is defined here as the time taken for the spin system to couple $(1 - 1/e)$ of its excitation energy to the crystal lattice in the absence of an applied perturbation.

The spin-spin interaction arises from the fact that the total d-c magnetic field acting on an electron in a paramagnetic molecule is that of the "external" magnetic field plus a contribution which is due to the magnetic field set up at the electron by the neighbouring electrons. Such a contribution will result in a spread of transition frequencies over the spin system. If the spins are made to precess in phase about the external magnetic field axis, at the instant $t = 0$, a coherent magnetic moment will be set up at that instant in the (x-y) plane orthogonal to that field (z) axis. The spins will subsequently suffer dephasing, and the coherent magnetic moment will decay to zero as the spin system increases to a state of maximum entropy. The time for dephasing may be described as the spin-spin relaxation time. The spin-spin interaction may be reduced by magnetic dilution of the paramagnetic salt, whereas the spin-lattice interaction decreases with decreasing crystal lattice temperature. The two relaxation processes are not, however, mutually exclusive.

3.4 Saturation

Saturation, as will be described here, occurs in the absorption of radiation by a paramagnetic molecule when the absorption is not linearly dependent upon the density of the applied radiation field. In the paramagnetic system, as the density of the applied radiation field is increased (slowly), the number of spin transitions to the excited state will increase. Eventually, as the radiation field density is increased, the relaxation processes are unable to effect a speedy return of the excited spins to the ground state, and the population difference between the spin states will decrease. When this happens, there is no longer a linear dependence between the absorption processes and the applied perturbation, and the spin system is said to approach saturation. Complete saturation occurs when the two population levels of the spin system are equal, and in this case the paramagnetic system may be said to be transparent to the incident radiation.

As has been previously stated, an excess of spins in the excited state cannot be obtained by the application of a "steady state" perturbation. If the state population has been inverted by some means, however, it can be postulated that in the inverted state, a departure from linearity between emitted power and the applied perturbation will occur as the spin system returns through transparency to the ground state.

As shown in Section 4.2, the magnetic properties of a paramagnetic crystal may be described in terms of a complex susceptibility $\chi = \chi' - i\chi''$, where χ'' and χ' relate to the phenomena of absorption and dispersion respectively. The magnitudes of the susceptibility components χ' and χ'' depend upon the degree of saturation of the spin system. Such components will be pzero for the special case of a completely saturated (equal populations) spin $\frac{1}{2}$ system.

3.5 Power Flow between the Paramagnetic Solid and the Radiation Field

The instantaneous rate of energy transfer, $P_{ins.}$, for a spin transition in a paramagnetic molecule is, by the application of probability theory,

$$P_{ins.} = (hf) \times \frac{d}{dt}(\text{spin transition probability}) \qquad (3.6)$$

and the average power flow, $P_{av.}$, between the paramagnetic system and the radiation field (assuming absorption for simplicity) will be found by integrating the above expression over a distribution of times, such that,

$$P_{av.} = \int_o^t P_{ins.} \cdot Pr(t)dt \qquad (3.7)$$

where Pr(t) represents the probability for transitions as a function of t. Wittke[14] has derived an expression for the average power flow due to a single electron undergoing

transitions as the result of a perturbation by a microwave electric field. The expression is derived by the method indicated in Equation 3.7, but includes the result of a more specific probability treatment than that given in Equation 2.12. When the effect of spin-lattice and spin-spin interactions is considered, we have:

$$(P_{av.})_{E.Field} = \frac{f\,p^2E^2}{2T_2h} \cdot \frac{1}{(f-f_o)^2 + (\frac{1}{2\pi T_2})^2 + \frac{T_1(pE)^2}{T_2\,h^2}} \qquad (3.8)$$

where

p = electric dipole moment

E = amplitude of microwave electric field

f_o = resonant frequency for transitions

T_1 = spin-lattice relaxation time

T_2 = spin-spin relaxation time

For a single electron in a microwave magnetic field, Equation 3.8 would hold if p were replaced by the magnetic dipole moment, μ, and E were replaced by the amplitude of the microwave magnetic field, B_1,

$$(P_{av.})_{B.Field} = \frac{f\mu^2B_1^2}{2T_2h} \cdot \frac{1}{(f-f_o)^2 + (\frac{1}{2\pi T_2})^2} \qquad (3.9)$$

neglecting the last term in the denominator of Equation 3.8 if linear operation is assumed. Examination of the denominator in Equation 3.9 will show that it is possible to ascribe

a "molecular" bandwidth, (Δf), to the system, namely,

$$(\Delta f) \approx \frac{1}{\pi T_2} \tag{3.10}$$

Now the power absorbed by the spin system at resonance will be **twice** that observed at the frequency half power points. If therefore, in Equation 3.9, we select the $(f - f_0)$ term to equal $(\Delta f)/2$, the power interchange will be

$$P_{av.} = 2 \cdot \frac{f \mu^2 B_1^2}{2 T_2 h} \cdot \frac{1}{\frac{(\Delta f)^2}{2}}$$

$$= \frac{2 f \mu^2 B_1^2}{h} \cdot \frac{\pi}{(\Delta f)} \tag{3.11}$$

The above is the result derived from consideration of the transitions of a single electron. For a spin $\frac{1}{2}$ system containing N spins, Equation 3.11 would be multiplied by the population difference, dN, between neighbouring Zeeman levels. Since to a good approximation,

$$dN = \frac{h f}{2k T} \cdot N \tag{3.12}$$

the expression for the power absorption in a spin $\frac{1}{2}$ paramagnetic crystal containing N spins becomes

$$(P_{av.})_{p.Crystal} = \frac{\pi f^2 \mu^2 B_1^2 N}{k T (\Delta f)} \tag{3.13}$$

which is in agreement with the expression quoted by Combrisson and Townes[5]. Note that this equation has been derived in the Gaussian system of units.

In all the above expressions, B_1 has been taken to represent the amplitude of a pulsating microwave magnetic field. Circularly polarized microwave magnetic fields are required for transitions, however, but any pulsating field may be expressed in terms of two half-amplitude circularly polarized components rotating in opposite directions.

3.6 The Bloch Formulation

The Bloch equations[13], originally applied to the nuclear magnetic resonance phenomena[15], may be applied to electron spin resonance phenomena, if one is interested in a classical understanding of the transient and steady state response of an electron spin system under the stimulus of an applied radiation field. These equations, now written to relate relaxation processes and magnetization changes in an electron spin system are

$$\frac{dM_x}{dt} = \gamma(M_y B_o + M_z B_1 \sin\omega t) - \frac{M_x}{T_2}$$

$$\frac{dM_y}{dt} = \gamma(M_z B_1 \cos\omega t - M_x B_o) - \frac{M_y}{T_2}$$

$$\frac{dM_z}{dt} = \gamma(- M_x B_1 \sin\omega t - M_y B_1 \cos\omega t) + \frac{M_o - M_z}{T_1} \qquad (3.14)$$

where B_0 is the density of the d-c magnetic field which is applied along an arbitrary Z-axis; M_0 is the steady state magnetization along the Z-axis in the absence of a perturbing radiation field; M_z represents the time dependent component of the magnetization along the Z-axis as the result of such a perturbation ($B = 2B_1 \sin \omega t$); M_x and M_y are the projections in the x-y plane of the precessing magnetization vector M;; γ is the gyromagnetic ratio for electron spins and T_1 and T_2 are the relaxation terms previously described.

The real and imaginary component of the magnetic susceptibility of a paramagnetic solid may be derived from the solutions to the above equations[15], namely

$$\chi' = \tfrac{1}{2}\chi_0\omega_0 T_2 \left(\frac{(\omega_0 - \omega)T_2}{1 + (\omega_0-\omega)^2T_2^2 + \gamma^2B_1^2T_1T_2}\right)$$

$$\chi'' = \tfrac{1}{2}\chi_0\omega_0 T_2 \left(\frac{1}{1 + (\omega_0-\omega)^2T_2^2 + \gamma^2B_1^2T_1T_2}\right) \qquad (3.-5)$$

where the expressions are in Gaussian units. The $\gamma^2B_1^2T_1T_2$ term in the denominators may be called the saturation term. The effect of this term on the susceptibility components is illustrated in Fig. 1, where the normalized susceptibilities are plotted against the dimensionless product $(\omega_0 - \omega)T_2$ for conditions of negligible and non-negligible saturation.

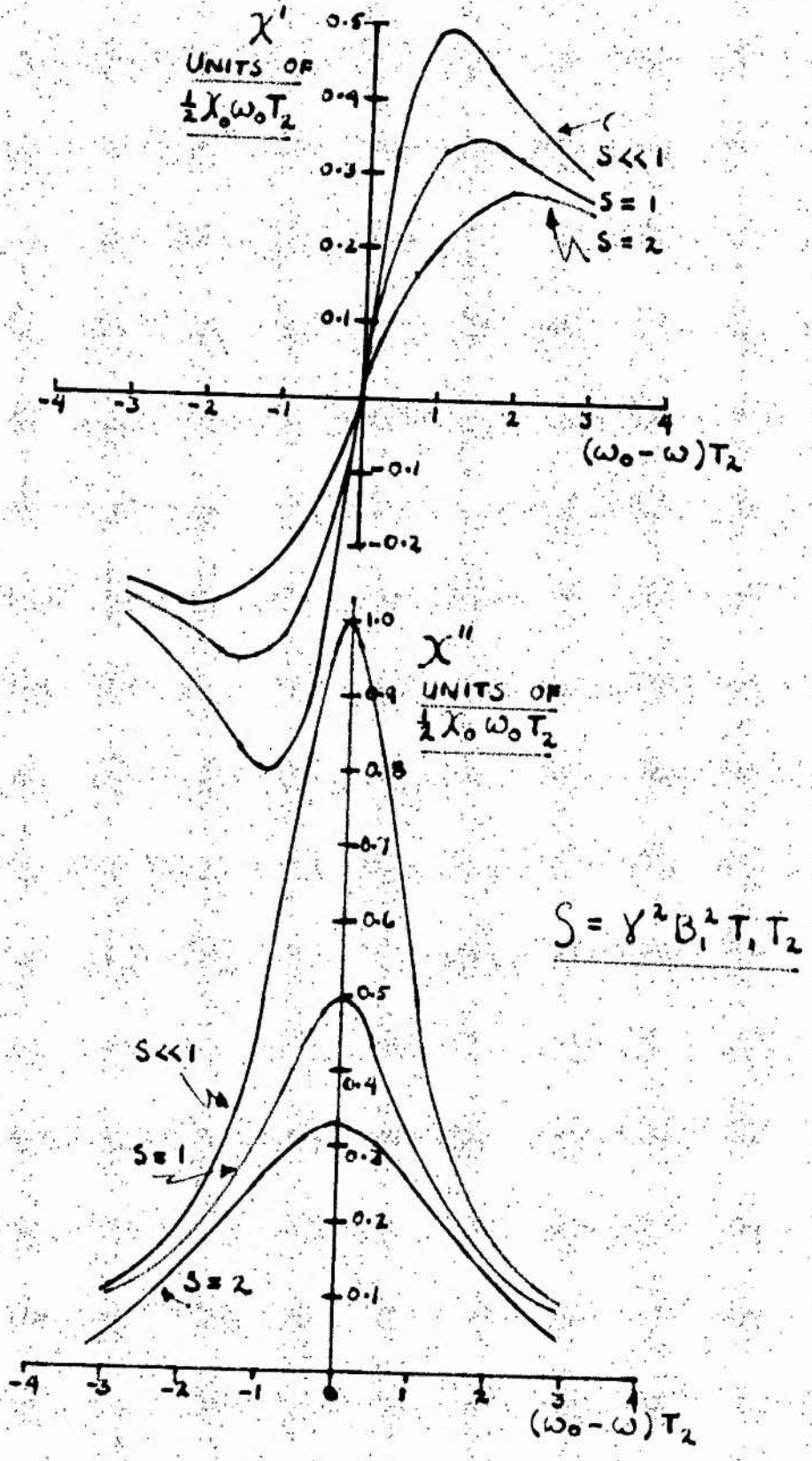

FIGURE 1

SUSCEPTIBILITY COMPONENTS AS FUNCTION OF SATURATION

An examination of the characteristics of a reflection-cavity paramagnetic resonance spectrometer, operating under steady state conditions will show that the signal reflected from the cavity will, in general, be a function of χ' and χ''. In practice with ordinary diode detectors there will be no response to phase modulation, and the detector output will be proportional only to $\chi'' B_1^2$. If phase sensitive elements are included in the cavity arm of such a circuit (e.g., for coupling adjustments), distortion might occur in the wings of the absorption characteristic if the dispersive effects are large enough to affect the coupling of the cavity.

It will be seen that if the saturation term is included in the power expression (Equation 4.11, or in Equation 3.9 when applied to the case of a spin density of N spins/c.c), and if the density of the perturbing microwave field approaches ∞, the power absorbed by the spin system will, in this limit, approach the maximum value,

$$P(\infty) = \frac{M_o B_o}{T_1}$$

$$= \frac{\chi_o B_o^2}{T_1} \text{ / unit vol.} \qquad (3.16)$$

where χ_o is the static magnetic susceptibility per unit volume, and B_o is the density of the level-splitting field.

From Equation 3.16 it will be seen that the temperature of the spin system will approach ∞ as the spin lattice relaxation time (T_1) approaches infinity.

Experimentally, the magnitude of the saturation term may be calculated by noting the deviation of the absorption characteristic from linearity as a function of the incident microwave power. The ratio of the anticipated to the experimentally observed absorptions will give the saturation term directly. These observations will hold for the case of homogeneously broadened lines. The molecular response, however, will be a more complicated function of frequency for inhomogeneously broadened lines. As indicated by Ingram[16], the change in power absorption, together with the change in line width on saturation, allows the broadening mechanism to be determined.

CHAPTER 4

CIRCUIT RELATIONSHIPS FOR A PARAMAGNETIC SOLID IN A MICROWAVE REFLECTION CAVITY RESONATOR

Introduction

As shown in the previous chapter, the absorption of energy by a paramagnetic solid is proportional to the power density of the perturbing microwave magnetic field. This radiation density may be conveniently increased if the paramagnetic specimen is located in a resonant cavity. Reflection-type cavity resonators were employed in this thesis in preference to transmission-type resonators, to simplify the problems associated with cavity coupling, and with heat conduction into the cryostat.

The circuit properties of reflection-type cavity resonators are briefly discussed in this chapter, as they relate to the absorption (or emission) of energy by a paramagnetic solid. Conditions for amplification and oscillation are derived, and illustrative examples given, and a figure of merit for the system is derived, in terms of a gain-bandwidth product.

4.1 Resonant Cavity Q Factor

The efficiency of an unloaded cavity resonator may be expressed in terms of a "Q" factor, Q_o, such that

$$Q_o = \omega_o \frac{W}{P} \qquad (4.1)$$

where

W = energy contained by the microwave fields in the cavity

P = power loss to the cavity walls

$\omega_o = 2\pi f_o$, where f_o is the resonant frequency

Furthermore we may express the energy storage in terms of the oscillating magnetic (or electric) field intensity. For a TE 101 or a TE 102 resonator, this expression reduces to

$$W = \frac{(2B_1)^2}{8\,u_o} \cdot (\text{volume of resonator}) \qquad (4.2)$$

where

$(2B_1)$ = peak amplitude of the microwave magnetic field density (webers/p.s.m.) over the cavity

u_o = magnetic permeability of free space = 10^{-7}

and where the relation is expressed in unrationalized m.k.s. units.

In practice the cavity must be coupled to a signal source. As a result it is necessary to define an overall Q for the system, (Q_T), in terms of the Q's associated with the cavity and the coupling losses, as follows,

$$\frac{1}{Q_T} = \frac{1}{Q_o} + \frac{1}{Q_c} \qquad (4.3)$$

where Q_c is the Q associated with the coupling.

4.2 Effect of a Paramagnetic Solid in the Cavity

As shown in Equation 3.13, the power absorbed by a spin $\frac{1}{2}$ paramagnetic crystal in a radiation field will be

$$P_{av.} \approx \frac{\pi f^2 \mu^2 B_1^2 N}{kT(\Delta f)}$$

when the spin system is unsaturated. This equation may be applied to the case of a paramagnetic solid filling a resonant cavity, if the density of the magnetic field, B_1, is redefined as in Equation 4.2. The effect of this solid on the power losses within the cavity system may be expressed in terms of a magnetic Q factor, Q_m. In this event, the overall Q may be written in the form,

$$\frac{1}{Q_T} = \frac{1}{Q_o} + \frac{1}{Q_c} + \frac{1}{Q_m} \qquad (4.4)$$

where the magnetic Q factor, Q_m, is positive in the case of an absorption, and negative in the case of an emission of power by the paramagnetic solid.

The magnetic Q factor may also be expressed in terms of the imaginary part of a complex magnetic susceptibility χ, where

$$\chi = \chi' - i\chi'' \qquad (4.5)$$

and where χ' and χ'' relate to the dispersion and absorption of radiation, respectively. The power absorbed from an

electromagnetic radiation field of amplitude B_1 by an unit volume of the magnetic specimen per cycle will be

$$P_{cyc} = \oint B \, dM \qquad (4.6)$$

where M = magnetization per unit volume = $\chi B/u_o$

$B = B_1 \sin\omega t$

$u_o = 10^{-7}$

Thus

$$dB = B_1 \cos\omega t \cdot d(\omega t)$$

and

$$P_{cyc} = \oint \frac{(\chi' - i\chi'')B_1^2 \sin\omega t \cos\omega t \, d(\omega t)}{u_o} \qquad (4.7)$$

On integration the term in χ' drops out and the expression for P_{cyc} reduces to

$$P_{cyc} = \frac{\pi \chi'' B_1^2}{u_o} \text{ / unit vol.} \qquad (4.8)$$

For the general case of a paramagnetic solid in an uniform electromagnetic field, the energy storage in the field per unit volume will be[17]

$$W = \frac{B_1^2}{8\pi u_o} \qquad (4.9)$$

so that

$$P_{cyc} = 8\pi^2 \chi'' W/\text{cycle/unit vol.} \qquad (4.10)$$

or

$$P = \frac{\pi f \chi'' B_1^2}{u_o} \text{/unit volume} \qquad (4.11)$$

which agrees with the expression derived by Gordon, Zeiger, and Townes[4].

An expression for the magnetic Q factor of the paramagnetic solid may be derived from Equations 4.4 and 4.11, namely,

$$Q_m = \frac{1}{4\pi\chi''} \qquad (4.12)$$

where the complex susceptibility component χ'' becomes negative when the paramagnetic solid is emissive*.

4.3 Conditions for Regenerative and Super-regenerative Maser Action

A necessary condition for regenerative amplification in the maser system is that the power supplied by the paramagnetic specimen in the resonant cavity shall exceed the wall losses in the resonant cavity; that is,

$$\left| -\frac{1}{Q_m} \right| > \frac{1}{Q_o} \qquad (4.13)$$

---

* In the general case, the coupling of the electromagnetic energy to the spin system should be taken into consideration, in which case, the expression Q_m in Equation 4.12 would be multiplied by a "filling factor", η, and η may be defined as: $\eta\chi'' = (\int_V B_1^2 \chi'' \cdot dV_s)/(\int_V B_1^2 \cdot dV_c)$ where the upper integration extends over the volume of the specimen, and the lower integration extends over the volume of the cavity. For the case of maximum coupling $\eta = 1$.

It can be postulated that Equations 3.13 and 4.11 will hold for emission as well as for absorption if the spin temperatures (negative or positive) are low in both instances. If this is accepted, Equations 3.13 and 4.11 may be equated for emissive behaviour. If the relationship is expressed in Gaussian units on a per unit volume basis, we have,

$$\frac{\pi f^2 \mu^2 B_1^2 (N' V_s)}{kT\ (\Delta f)} = \pi f \chi''(B_1^2) V_s \qquad (4.14)$$

where N' is now the number of participating spins per c.c., and where V_s is the volume of the paramagnetic solid. Whence

$$4\pi\chi''\eta = \frac{4\pi^2 \eta \mu^2 f(NT_2)}{kTV_s} \qquad (4.15)$$

where N is the total number of participating spins.

As an illustration, let $Q_o = 2 \times 10^4$; $f = 9.1 \times 10^9$ cps $V_s = 5$ cc; $T = 4^oK$; $\eta = \frac{1}{2}$. Then (since $\mu = 0.92 \times 10^{-20}$ erg/gauss; $k = 1.37 \times 10^{-16}$ erg/degree) the condition for amplification expressed in Equation 4.13 reduces to the condition that $(NT_2) > \sim 4.5 \times 10^9$. For a line width of 1 gauss*, T_2 in this illustration is approximately $\frac{1}{\pi(\Delta f)} = 3.6 \times 10^{-7}$ sec. (since $df = 2.8dB \times 10^6$ cps.), and the condition for

* For simplicity, we assume that the broadening is entirely due to spin-spin interaction, and not to any broadening that might arise from inhomogeneities in the d-c magnetic field.

amplification in the illustration reduces to

$$N > \sim 1.2 \times 10^{16} \text{ spins}$$

The condition for oscillation, on the other hand, is that the total Q of the system should be negative. This necessitates that

$$\left| -\frac{1}{Q_m} \right| > \frac{1}{Q_o} + \frac{1}{Q_c} \qquad (4.16)$$

If the resonant cavity is nearly matched to the source waveguide, we have

$$\frac{1}{Q_o} + \frac{1}{Q_c} \approx \frac{2}{Q_o}$$

If this approximation is assumed to be valid for the above illustration, the condition for oscillation becomes,

$$N > \sim 2.4 \times 10^{16} \text{ spins}$$

4.4 Gain-Bandwidth Product

The gain-bandwidth expression for a reflection cavity, regenerative maser with circulator, has been derived by Burkhardt et al.[10] The power gain, G, of the system with a circulator in the reflection arm is $\Gamma\Gamma^*$ where Γ^* is the cavity reflection coefficient. It can be shown that,

$$G = \Gamma\Gamma^* = \frac{\frac{4}{Q_c}\left(\frac{1}{Q_T} - \frac{1}{Q_c}\right)}{\left(\frac{1}{Q_T}\right)^2 + \left(\frac{\omega}{\omega_o} - \frac{\omega_o}{\omega}\right)^2} \qquad (4.17)$$

where G is the mid-band power gain; $1/Q_T = 1/Q_o + 1/Q_c + 1/Q_m$. Equation 4.17 may be reduced to,

$$(G^{\frac{1}{2}} - 1)\frac{B}{\omega_o} \approx -\frac{2}{Q_T} \qquad (4.18)$$

where B is the bandwidth between half-amplitude points on the response curve.

As shown in Fig. 3, page 51, a 10 db directional coupler was employed in the reflection path of the maser in this investigation (for reasons of economy) and in this case, the system gain to this point would be,

$$(G^{\frac{1}{2}} - 1)\frac{B}{\omega_o} \approx \frac{-2}{\sqrt{10}} \cdot \frac{1}{Q_T}$$

CHAPTER 5

INVERSION CRITERIA AND CHOICE OF PARAMAGNETIC CRYSTALS

Introduction

The discussion has so far been limited to the behaviour of the spin system following inversion. In this chapter, inversion techniques will be discussed as they apply to the problems of this investigation. The rest of the chapter will be devoted to a detailed statement on the paramagnetic media employed.

5.1 Inversion Techniques

At this time there are three methods for exciting a paramagnetic crystal in a two-level spin system. These are:

1) Pulse inversion

2) Adiabatic fast passage -- frequency sweep method

3) Adiabatic fast passage -- field sweep method.

1) In pulse inversion, a short, intense pulse of microwave radiation is applied to the spin system at the resonance frequency while the d-c magnetic field is held constant at the resonance value. With this method, since the rates of frequency sweep are large, it is necessary to evaluate the quantum mechanical transitional probabilities before the height and duration of the inverting pulse can be determined. Torrey[31] has shown that, if a two-state system is exposed to

a pulse of microwave power at the resonance frequency for a time, t, such that

$$\frac{\mu B_1 t}{h} = \frac{1}{2} \qquad (5.1)$$

(where μ is the magnetic dipole moment and B_1 the amplitude of the microwave field), then the state populations will be inverted. It can be seen, however, that both the magnetic field and the perturbing frequency have to be held at the resonance value, whilst in addition, the pulse time has to be critically set. Thus, this method would not be too easy to apply in practice.

2) In the frequency sweep method, the d-c magnetic field is held at the resonance value and the power klystron frequency swept through cavity resonance under the following conditions:

a) The passage must be adiabatic -- that is, the magnetization, M, must follow the changes in the effective magnetic field. For convenience, the motion of M can be referred to a co-ordinate frame rotating at angular frequency ω, about the d-c magnetic field vector, $\vec{B_o}$, when the paramagnetic sample is subject to a microwave field, B_1, circularly polarized about the d-c field vector. The co-ordinate system rotates with the same frequency

as the microwave field. The effective magnetic field will be

$$\vec{B}_{eff} = \vec{B}_1 + (\vec{B}_o - 2\pi\vec{f}/\gamma) \qquad (5.2)$$

where γ is the electron gyromagnetic ratio. At resonance, the expression reduces to $B_{eff} = B_1$. The magnetization, M, will precess about B_{eff} with angular frequency Ω where

$$\Omega = \gamma B_{eff} \qquad (5.3)$$

When viewed in the stationary system, M will nutate about the Z-axis at the same frequency Ω. The effective magnetic field reverses as the perturbing radiation passes through resonance, and the orientation of M with respect to B_o will be reversed.

The adiabatic condition is thus[18],

$$(\gamma B_1)^{-1} \ll t \qquad (5.4)$$

where t is the time taken to pass through the resonance half width of the spin system (assuming that this resonance is much sharper than the cavity resonance) and where $(2B_1)$ is the amplitude of the pulsating microwave field at the specimen in the resonant cavity. As will be shown in Section 7.4, a typical value for $(2B_1)$, with the resonant cavity system employed in this investigation, would be 2.5 gauss. Thus, since the gyromagnetic ratio, γ =

2γ x 2.8 Mc/gauss, the adiabatic condition would reduce to

$$t \gg 4.5 \times 10^{-8} \text{ secs.}$$

b) The "fast" condition means that the resonance passage in time, t, should be very much less than the spin-lattice relaxation time, T_1. Thus, if $t = 100(4.5 \times 10^{-8})$ sec = 4.5 microsec, and T_1 is in the same ratio, it can be seen that in this particular instance, T_1 would have to be greater than about 450 microsecs for efficient inversion.

c) A third condition is that the inverting power level should be sufficient to produce an appreciable saturation of the spin system under steady state conditions.

Note that with this technique, the molecular resonance should be much sharper than the cavity resonance. If this is not so, then only a portion of the spins in the paramagnetic sample will be inverted. Furthermore, after inversion, unless special precautions[19] are taken, there will be a high probability that the stored spin energy will be re-radiated spontaneously immediately after inversion. Both drawbacks can be avoided by the use of method 3.

3) In the field sweep method, the frequency is held constant at the cavity resonance value while the magnetic field is swept through the resonance condition. To an observer moving with the rotating system of co-ordinates, the effect will be the same as described in paragraph a) above.

With the field sweep method, however, the tendency for spontaneous re-radiation is avoided as the magnetic field is taken off the resonance value immediately after inversion is effected. Furthermore, all the spins in the resonance distribution will be affected provided that the field sweep amplitude is greater than the "full" width of the spectral line concerned. Note that with methods 2) and 3), the passage through resonance can be in either direction.

5.2 Paramagnetic Crystals Investigated

In the previous section the restrictions on spin-lattice relaxation time have been discussed with respect to the requirements for this investigation. In addition it can be deduced that if the system is to act as a narrow-band amplifier or oscillator, the width of the resonance line associated with the paramagnetic crystal should be as narrow as possible. Also, the paramagnetic resonance line width should be less than the field sweep magnitude if this adiabatic fast passage method is used. Thus paramagnetic crystals with spectral line widths in the order of 1 gauss or less would be likely to fit the field and other requirements. With the frequency sweep method, however, the spectral line width would have to be much smaller than the resonant cavity bandwidth. A typical operational bandwidth for such a resonant cavity is approximately 1.5 Mc/s -- thus the spectral line width in this case would have to be much less than 0.5 gauss for efficient

inversion. With these points in mind, a statement will now be given on the paramagnetic crystals employed in this investigation.

5.2 (a) Neutron Irradiated Magnesium Oxide

It has been found that defects (F centres) may be introduced into certain crystals as a result of neutron irradiation[20]. In particular, Weeks[21] has studied the electron spin resonance spectrum of such induced F centres in irradiated MgO. He postulates that after an oxide atom is displaced from its normal position by neutrons, an electron, donated by divalent impurities present, may become trapped at the vacancy. Such F centres which have only Mg^{24} and Mg^{26} neighbours give a single resonance line with $g = 2.0023$, while those with one or more Mg^{25} neighbours give hyperfine patterns corresponding to the nuclear spin value of 5/2 (six spectral lines).

Furthermore, Chester[8,9] examined crystals of neutron irradiated quartz and neutron irradiated MgO in a two-level maser system. He observed maser amplification and oscillation with the quartz specimens at $4.2^{o}K$, and maser amplification (but not oscillation) with the MgO specimens at the same temperature.

In part of this programme of investigations, neutron-irradiated MgO was employed as the maser medium for such crystals seemed to fit the initial requirements. Furthermore the crystals could be obtained and irradiated fairly readily.

Three MgO crystal specimens were irradiated as follows.

1) Dounreay MgO Specimen

By the courtesy of the Industrial Group at the Dounreay Works of the United Kingdom Atomic Energy Authority, Thurso, Scotland, an MgO crystal was irradiated at that Establishment, in a reactor commissioned to run at a full flux of 10^{14} n/cm^2/sec. From irradiation details quoted by Weeks[22], the following irradiation specifications were drawn up:

1) Material -- MgO single crystal (slice)
2) Weight, 1.78 gms; diam., 1 cm; thickness, 2mm.
3) Type of irradiation -- fast neutrons (~1 Mev)
4) Dosage -- 5 x 10^{19} neutrons/cm^2
5) Temp. during irradiation -- preferably below 100°C
6) Radioactivity of specimen -- within safe handling range (0.3 milliroentgen/week)

At Dounreay the specimen was irradiated with an estimated dose of 10^{18} - 10^{19} neutrons of energy greater than 1.5 Mev (date, August 1959). On receipt of this specimen (which had a count rate for γ radiations of ~ 0.2 milliroentgen per week), it was observed to be almost black in colour. After a month, however, it had changed to a (permanent ?) royal blue colour. From Weeks' estimate[21] of 5.7 neutrons per F centre created, the number of spins in this crystal was adjudged to be between 2 x 10^{17} and 2 x 10^{18}.

2) Harwell MgO Specimens

By courtesy of the Atomic Energy Research Establishment, two MgO crystals were irradiated at Harwell. In this case the specimens weighed 0.88 gms and 0.91 gms, respectively. Each specimen was a slice of a single crystal and was of diameter 1.3 cms and thickness 2 mm. The same irradiation specifications were submitted as for the Dounreay specimen.

At Harwell each crystal received approximately 2.4 x 10^{18} fast neutrons at a temperature of 45°C (date: August 1959) The radiation count was negligible. Each of the crystals (originally opaque) returned with a royal blue (permanent) colouration. From Weeks' irradiation estimate of 5.7 fast neutrons per F centre, the number of centres was adjudged to be 4 x 10^{17} per crystal.

The crystals were later truncated to fit the smaller dimension of the TE 102 resonator described in Chapter 6 -- the truncated dimensions were 0.9 mm, and the weight of each crystal was now 0.72 gms. Thus, by Weeks' criteria the number of spins in the reduced specimens would be 3.3 x 10^{17} spins per crystal.

5.2 (b) Neutron Irradiated Diamond Specimens

It was postulated that neutron-irradiated diamond might satisfy the inversion criteria, and several such specimens were obtained for investigation. As far as was known, irradiated diamonds had not been investigated as maser crystals.

The microwave spectrum of neutron-irradiated diamonds has been studied by Griffiths et al.[23], who show that there are two main types of absorption lines: a) a single isotropic line with a g value of 2.0028 (for a free electron spin, g = 2.0023) the intensity of which can be greatly reduced by heating the diamond to about 1000°C, and b) many less intense anisotropic lines whose intensity is not much affected by heat treatment, and which appear to arise from centres with electronic spin S = 1.

These investigators have observed the diamond colouration and line width (ΔB) as a function of irradiation, as follows:

Irradiation time:	10 hours	120 hours	1850 hours
Colour:	pale green	dark green	black
ΔB at 290°K:	20 gauss	47 gauss	70 gauss
ΔB at 90°K:	15 gauss	21 gauss	26 gauss

(where the integrated neutron flux for an 1800 hour exposure was 9×10^{18} n/cm^2.)

The diamonds employed in our investigations were kindly supplied by the Physics Research Laboratory, University of Reading. Six specimens were obtained with the specifications as shown in the table on the following page. The crystals were irregular slices approximately 0.5 mm thick and 4 mm in diameter.

Specimen	Colour	n_o dose at pile factor 6 (hours)	Weight (cts)
D23	clear	1	0.52
D24	clear	3	0.41
D25	pale green	10	0.17
D26	pale green	30	0.27
D27	dark green	120	0.33
D29	black	1000	0.35

The diamonds were irradiated in the B.E.P.O. reactor and the exact details of the dosage were unknown. The doses listed above were based on a comparison of the absorption spectra of the specimens with other neutron irradiated diamonds (at the University of Reading). From Griffiths' data one would estimate that specimens D27 and D29 were exposed to a dosage of $\sim 6 \times 10^{17}$ n/cm^2 and $\sim 8.5 \times 10^{18}$ n/cm^2, respectively.

5.2 (c) Phosphorous Doped Silicon Crystals

Two crystals (slices) of phosphorous doped silicon were kindly supplied by the Services Research and Development Establishment (Admiralty), Christchurch, Hants., for experimentation Such material had been employed successfully in a two-level maser system at that Establishment. In each case the doping concentration was $2\text{-}5 \times 10^{16}$ P atoms/cc and the crystal

specifications were:

Specimen A	Weight	1.55 grms
	Shape	Half moon
	Thickness	3 mm
	Volume	0.65 cc
	Total Spins	$1.4 - 3.4 \times 10^{16}$
Specimen B	Weight	0.82 grms
	Shape	circular
	Thickness	3 mm
	Volume	0.36 cc
	Total Spins	$0.7 - 1.8 \times 10^{16}$

Bagguley and Owen[20] give the following data for phosphorous-doped silicon:

Donor nucleus	^{31}P
Nuclear spin	1/2
Magnetic moment (nm)	1.13
Hyperfine structure constant $A/g\beta$ (gauss)	42
g-value	2.000

Feher[30] has observed in the temperature range 1.2 - 4°K. that for 10^{16} P atoms/cc in Si the relaxation time T_1 = 1 min.; for 5×10^{17} P atoms/cc, $T_1 = 10^{-5}$ secs. Furthermore, if there are more than 10^{18} donors/cc the hyperfine structure is narrowed out by exchange and there is only one absorption line (instead of two equal lines as with a lower impurity concentration).

CHAPTER 6

DESCRIPTION OF THE APPARATUS

Introduction

This chapter is devoted to a design discussion of the two level, X-band maser, designed for operation at liquid helium temperatures. The design aim was for rapid passage inversion and subsequent monitoring of the resonance signal by either the field sweep or the frequency sweep method. Operation was envisioned with paramagnetic crystals having spin-lattice relaxation times of the order of milliseconds, or larger.

The system could also be employed as an electron spin resonance superheterodyne spectrometer to aid the study of the paramagnetic behaviour and saturation characteristics of potential maser crystals. Since only short term stability was required of the system, electronic klystron stabilization was not employed.

6.1 Microwave Circuitry

The microwave system design was as shown in Figure 2 and Figure 3. As shown, the maser was of the reflection-cavity type. Briefly, its operation was as follows: the paramagnetic crystal was contained in the cavity and subjected to a pulse of "inverting" power from a medium-power klystron. The power reflected from the cavity was fed by a directional coupler to a crystal detector circuit, for oscilloscope presentation. Straight or superheterodyne detection could be employed prior

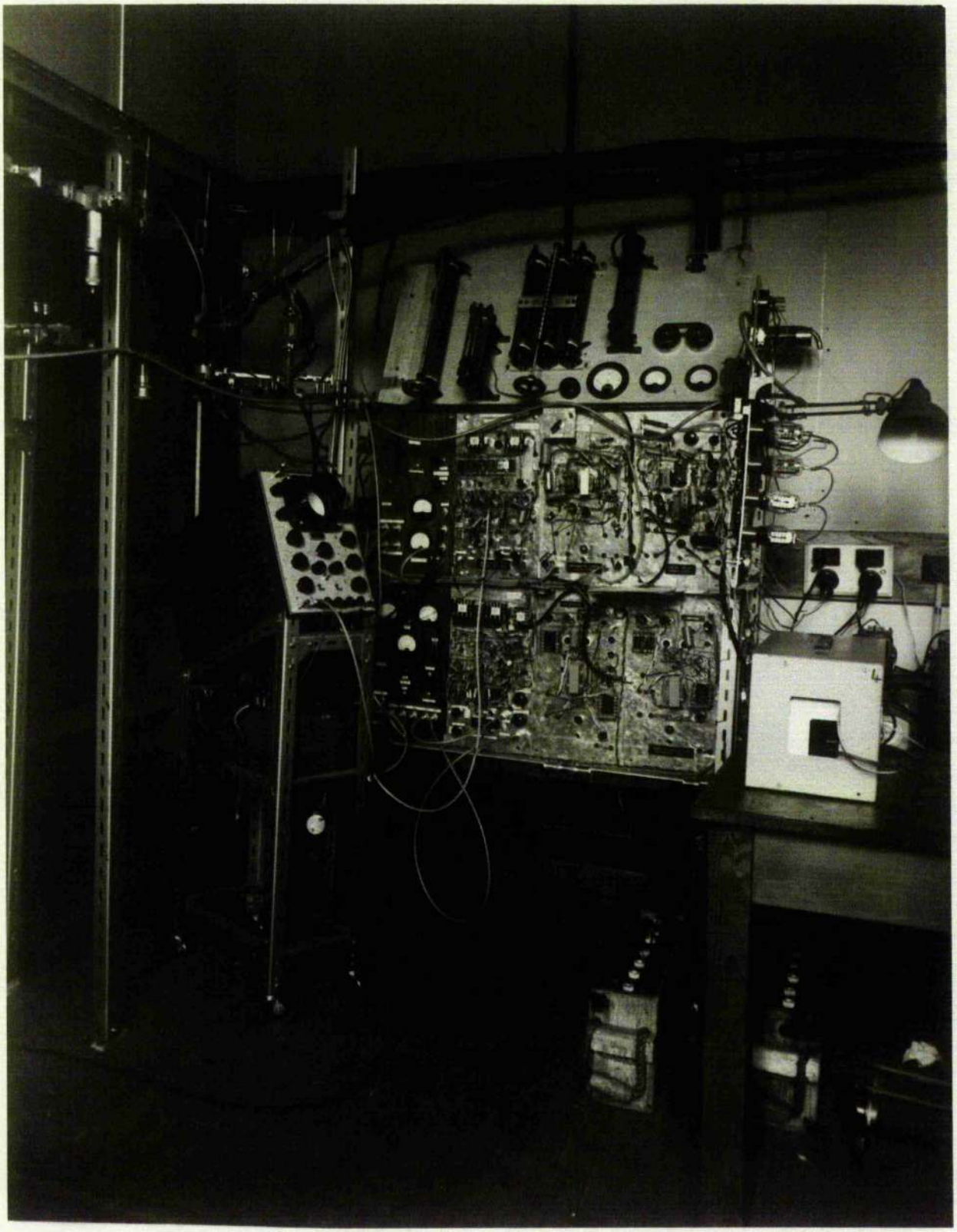

FIGURE 2 MASER ELECTRONICS LAYOUT

to presentation. Observations on the results of such power pulse applications were made possible by the use of a monitor klystron weakly coupled to the reflection-cavity arm.

The system employed X-band (3 cm) equipment throughout, for reasons of economy in the purchase of waveguide components and in the selection of a d-c electromagnet. Type numbers for commercial components are given in Appendix A.

A design description of the circuit now follows.

6.1 (a) Input Circuit

A one-port cavity resonator circuit was built to minimize the design problems associated with the cavity itself and the cross sectional area of waveguide wall entering into the liquid helium dewar. The next step was to supply the power necessary for inversion. The inversion circuit was designed around a Varian X-13 medium power klystron ($\frac{1}{2}$ watt max.) and all of the power from this klystron was made available to the resonant cavity.

In the inversion circuit, the sliding-stub tuner adjacent to the X-13 klystron was used for adjustment of the matching of this klystron. As stated in the specifications, 250 m.watts power output was obtained when the klystron operated into a matched load, and approximately $\frac{1}{2}$ watt output was obtained when the klystron operated into an optimum load as set by the sliding-stub tuner. The 20 db ferrite isolator included in the circuit at this point minimized frequency

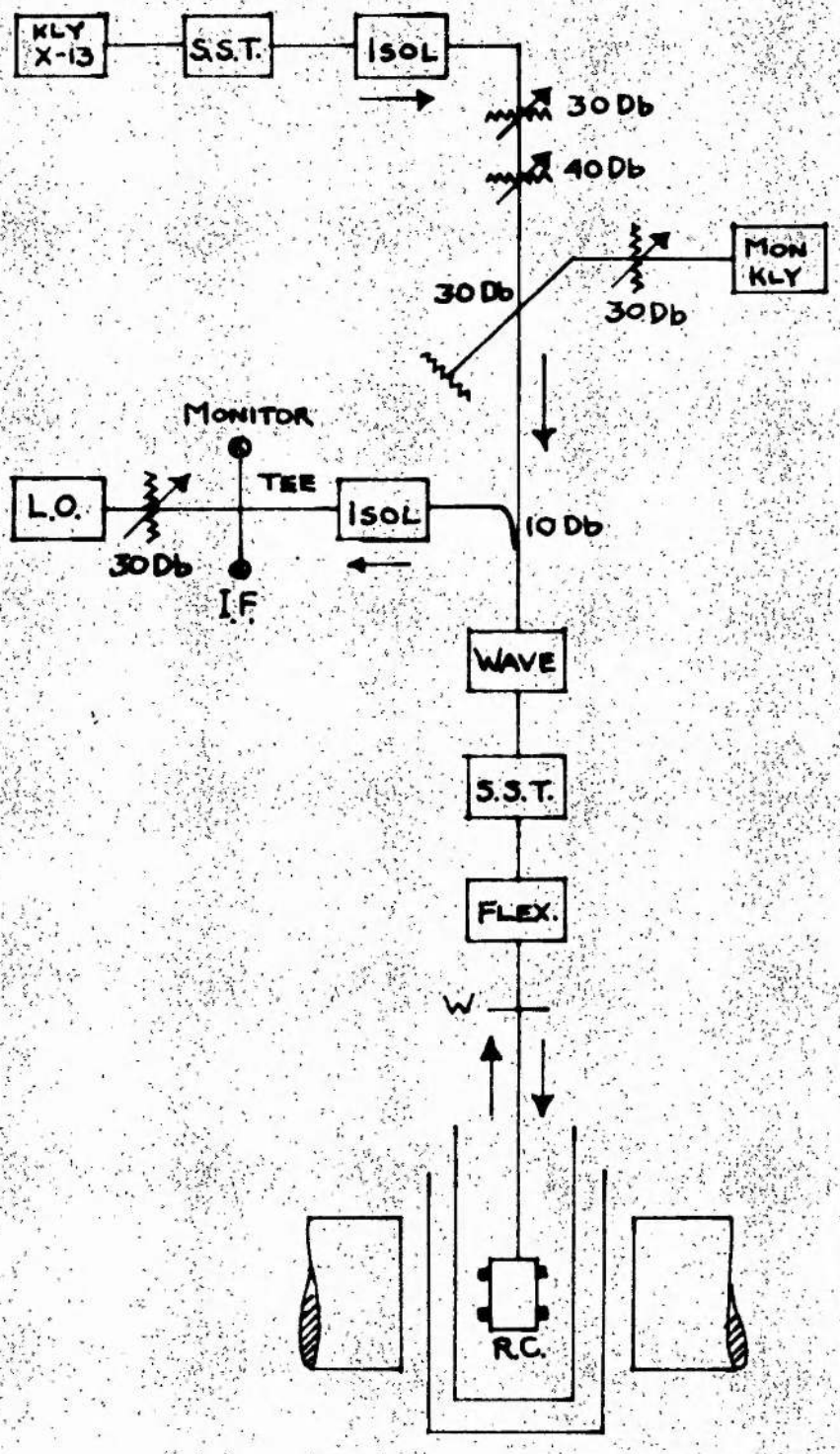

FIGURE 3 MICROWAVE CIRCUIT (SCHEMATIC)

pulling of the klystron by the other circuit elements. A second sliding-stub tuner in the resonant cavity arm was used for coupling adjustments to the resonant cavity.

An uncalibrated 30 db variable attenuator and a calibrated 40 db attenuator provided the variable attenuation required for spectrometer operation. The attenuators could be calibrated against each other, however, when it was necessary to know the total attenuation at any setting.

At the cryostat end of the waveguide, a flexible waveguide and snap coupler enabled the cryostat to be disconnected easily from the rest of the system, for removal to the helium liquefier. The flexible waveguide also served to reduce microphonic vibrations at the cryostat. A 5/1000 in. mica sheet window was located between the coupler and the cryostat proper so that the cryostat could be evacuated or pumped. The window was fitted between a plain and a choke waveguide flange, and was made vacuum tight by inserting a thick rimmed "Gaco" rubber ring in each of the flanges.

The incident wave was coupled into the cryostat through a custom built 2½ in. radius, E-plane bend, with 3 in. straight arms. A quartz-rod, tuning system was mounted on this bend for external adjustment of the resonant cavity frequency. The waveguide in the cryostat itself was of 11/1000 in. copper-nickel with a resonant cavity termination. Design details of the resonant cavities used are described in Section 6.2(d).

6.1 (b) Reflection Circuit

As a ferrite circulator was not available, the reflected signal was coupled out to the main amplifier by means of a 10 db directional coupler. Straight detection and superheterodyne detection could be applied simultaneously to the reflected wave with the Magic T-crystal detector system shown.

A 723/AB klystron ($\sim$ 25 m.watt) provided the local oscillator power, and a 30 db variable attenuator provided the degree of attenuation required. Isolation between the local oscillator and the resonant cavity was effected by the Magic T, in conjunction with a 20 db ferrite isolator.

The Magic T was made in the workshop for economy, and was of the post and bar type, with double matching stubs in the E-plane and H-plane arms. Minimum standing wave ratios of 1.04 and 1.06 were realized for the E and the H arms, respectively, when the T was initially adjusted on a microwave test bench. The crystal detector mounts were also made in the workshop, and were provided with double matching stubs and an adjustable shorted end. Standing wave ratios in the order of 1.06 were realized when the crystals operated into a matched cable.

6.1(c) Monitor Circuit

Provision was made, as shown in Fig. 3, for monitoring the spin resonance signal after inversion or deviation from equilibrium. A 723/AB monitor klystron was originally

incorporated in this circuit, but the stability of this type was found to be unsatisfactory for this function, and an English Electric klystron K311 (approx. 28 m.watt) was later used successfully.

Coupling of the monitor signal into the main waveguide was effected with a 30 db Bethe coupler made in the workshop. A ¼ in. coupling hole was employed here, in conjunction with a coupling angle between waveguides of about 45°. A 30 db variable attenuator was included in the monitor circuit to provide additional reduction of the monitor amplitude. Finally, a wooden fishtail load was made for the monitor klystron, and this type of termination proved to be highly satisfactory.

6.2 The Cryostat

Photographs of the cryostat are reproduced in Figs. 4 and 5, while a schematic drawing (not to scale) is shown in Fig. 6. Constructional details follow.

6.2 (a) Glass Dewars

The liquid air and liquid helium dewars were made of Monax glass and tailed to fit inside the 2 in. magnet gap. The liquid air dewar was pumped to a hard vacuum, but the helium dewar was left slightly soft (5 mm air). In this way, pre-cooling of the inner dewar could be speeded up at no expense to operational efficiency, for the air between the walls of the inner dewar would solidify when in thermal contact with the liquid helium and thereby minimize the heat exchange across this dewar during operation.

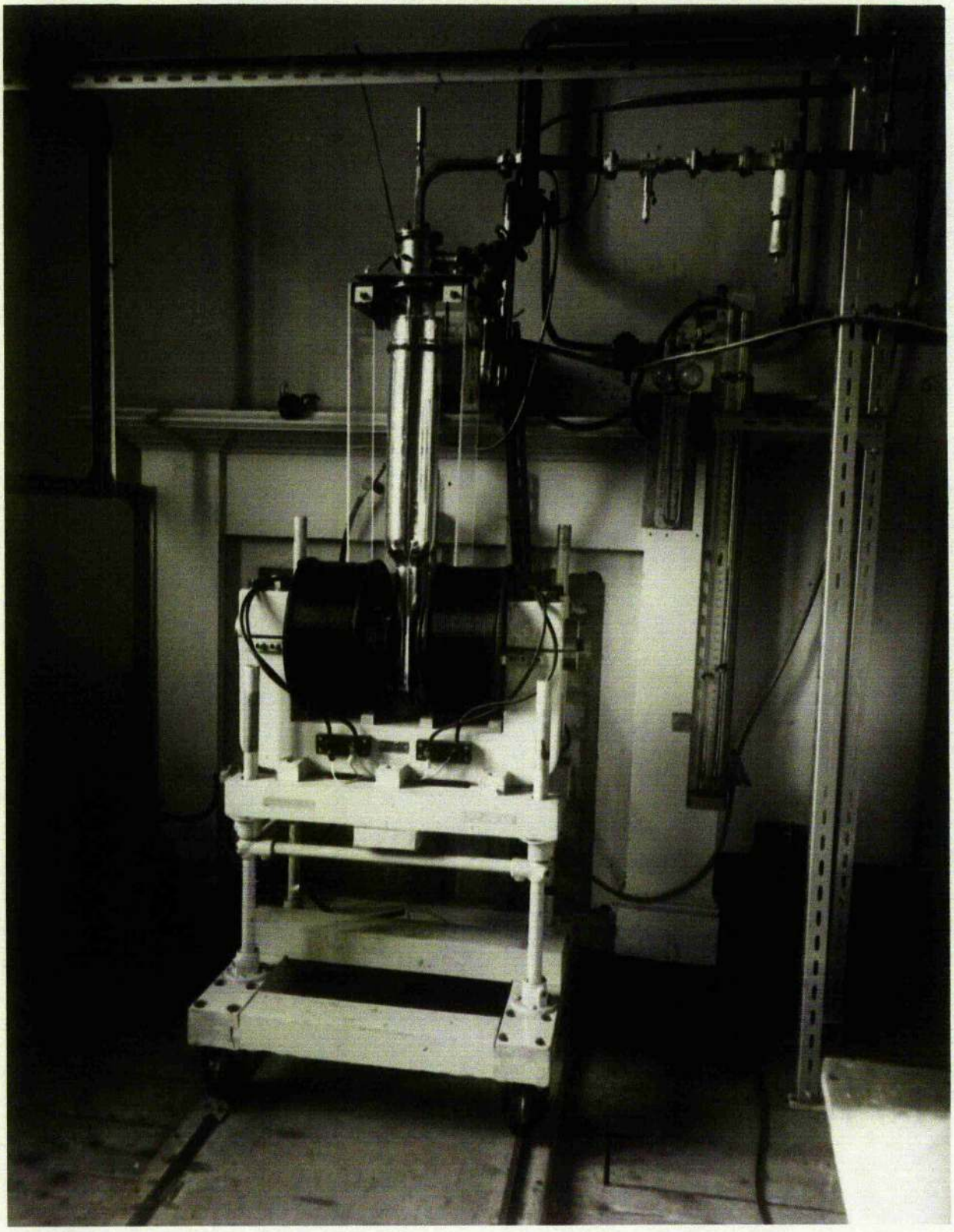

FIGURE 4 MAGNET AND CRYOSTAT

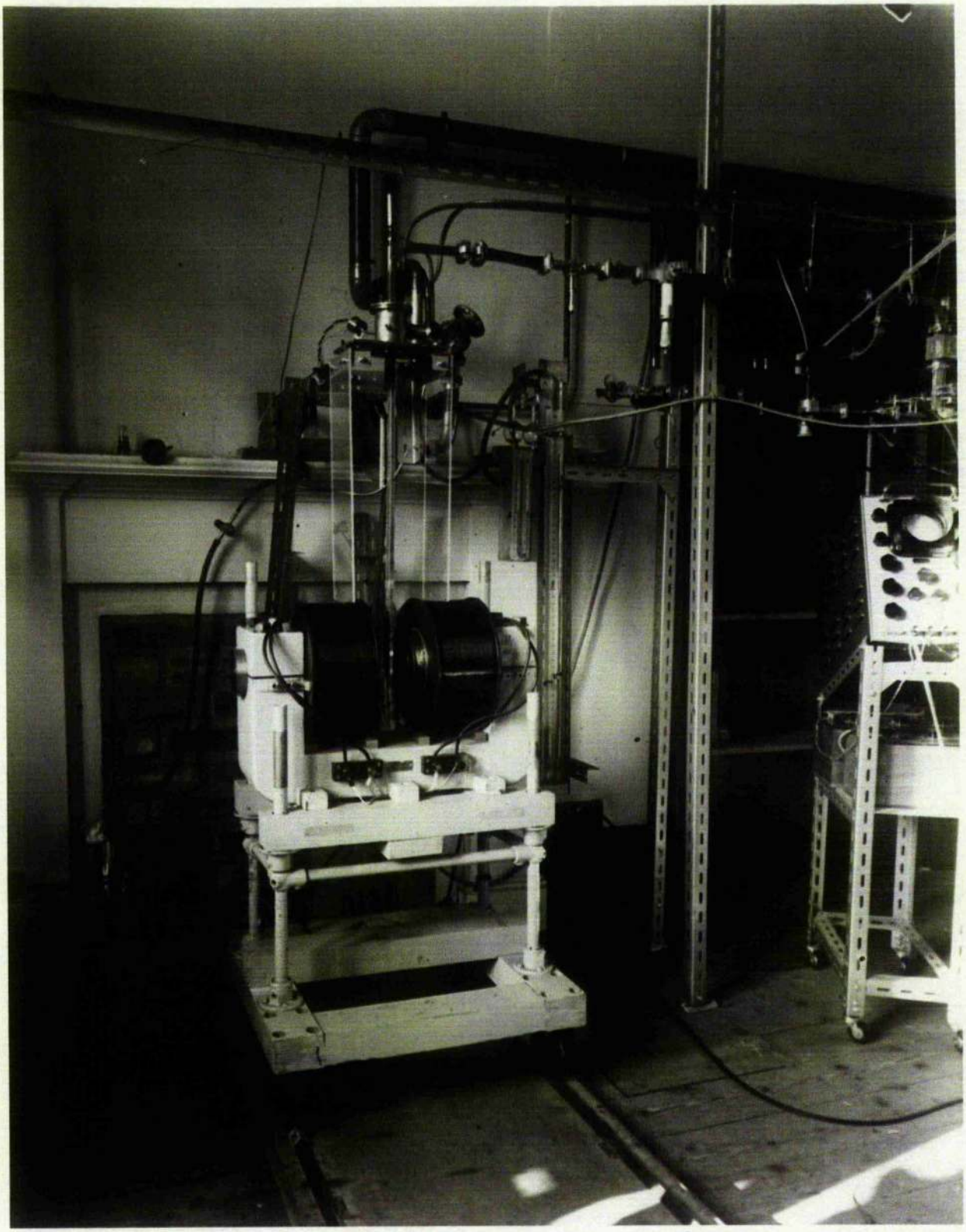

FIGURE 5 MAGNET AND MICROWAVE SYSTEM

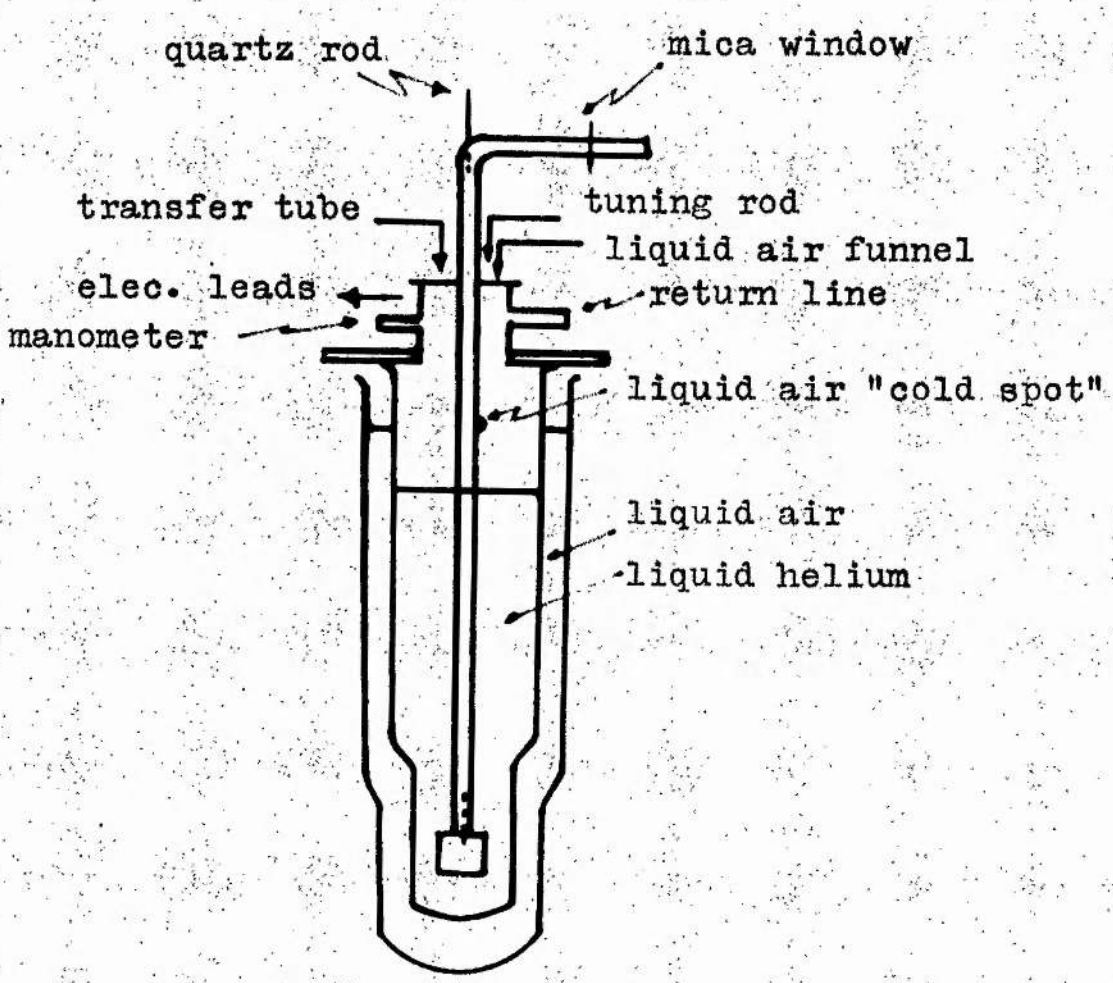

FIGURE 6

CRYOSTAT (SCHEMATIC)

As the overall cross section of the resonant cavity was about 32 mm, it was necessary to make both dewar vessel tails from ½ mm selected material. The upper dewar sections were not restricted in thickness, however, so were made from 1 - 2 mm stock. The dewar dimensions were as follows:

1. Liquid helium dewar

Length of tail	20 cm
Inner wall	34.5 mm O.D.
Outer wall	37.5 mm O.D.
Overall length	72 cm
Main body - inner wall	55.5 mm O.D.
Main body - outer wall	69 mm O.D.
Capacity	~ 1 litre

The upper 12 cm of this dewar was single walled, with a 10 mm terminating rim. A brass collar with a Gaco ring insert fitted around this termination, and the assembly butted against a similar Gaco ring on the main support plate, to which it was clamped by three O BA screws. The upper section (12 cm) of the dewar was left unsilvered. The lower section was silvered except for a vertical strip (½ in. wide) on either side for observation purposes.

2. Liquid air dewar

Length of tail	25 cm
Inner wall	43.5 mm O.D.
Outer wall	47.5 mm O.D.
Overall length	77 cm
Main body - inner wall	90.5 mm O.D.
Main body - outer wall	101 mm O.D.

This liquid air dewar was supported by a brass ring which fitted around a 5 mm swelling at the top of the dewar. Three $\frac{1}{8}$ in. screwed brass rods extended from this ring to the support plate and were fastened there with knurled nuts. By this means, a fine adjustment of the dewar clearance at the pole-pieces could be effected. The dewar was also silvered in the manner described above.

6.2 (b) Cryostat Construction

The main cryostat support section consisted of an 8 x 6 x $\frac{1}{4}$ in. brass plate, which clamped with four wing-nuts to a Handy Angle frame. This point was 5 feet from floor level, so that the glass dewars could be fitted, or removed, in situ. Into the brass plate and along its central axis, a 3 in. section of $2\frac{5}{8}$ in.O.D. x $\frac{1}{8}$ in. brass piping was fitted. A $3\frac{1}{2}$ in. O.D. x 3/16 in. flange, tapped for six 2-BA screws, and stepped to accept a $2\frac{1}{2}$ in. Gaco rubber ring, butted against this pipe section and provided the support for the detachable wave guide assembly. All joints were soft-soldered, vacuum tight joints.

The top plate was cut to accept the E-plane wave guide bend, and the remaining top plate space was allocated to,

a) The helium transfer tube support
b) A 1/16 in. stainless steel tuning rod assembly for external control of the resonant cavity frequency
c) A liquid air reservoir funnel.

The helium transfer tube support (a $\frac{1}{2}$ in. threaded CuNi tube)

and the tuning rod fitted against each broad face of the wave guide (with the tuning rod under the bend). The tuning rod passed through a rubber hat-gland assembly on the top plate which provided a vacuum-tight joint while it allowed the tuning rod to be turned under operational conditions.

The liquid air funnel (6 mm CuNi tubing) terminated inside the helium dewar in a 10 cc reservoir of 10 mm CuNi tubing This reservoir provided a "cold spot" on the entrant wave guide at a point 10 cm from the top plate. Its function was to decrease the thermal gradient along the wave guide in this dewar during operation, and thereby reduce the liquid helium losses due to heat flow along the guide. In operation, however, this attachment made no appreciable difference to the running time.

The helium circuit was a closed circuit, and the return path from the cryostat top section to the main gas bags proceeded via a 1 in. Saunders valve, a threaded coupler, and a U-shaped 1 in. double bellows system in that order. By means of the Saunders valve and threaded coupler the cryostat could be disconnected from the helium return line for the transfer operation. The double bellows system minimized the mechanical twisting at the cryostat whilst the system was being pumped for operation below the λ point -- this was essential in view of the limited clearances between the cryostat and electromagnet.

The helium pressure was monitored with a mercury gauge and a differential oil gauge (butyl pthalate, density 1.046)

connected by a rubber tube to a 10 mm exit tube at the cryostat top plate. This exit tube also served as a return path for cold helium gas during the transfer period, and was double walled for this reason.

Two electrical circuits were brought into the cryostat through a coupler (with glass-metal seal feed-through lugs) at the top plate. One circuit was a 2 watt (6.3 volt a-c) resistance-wire heater wound around the wave guide at its lowest point. The other was the drive for the field sweep coil that was used with the TE 102 resonator.

6.2 (c) Thin-Wall Wave Guide

To keep the heat influx into the helium dewar to a minimum, it was necessary to use other than the standard wave guide. The Royal Radar Establishment kindly supplied some lengths of 11/1000-in. CuNi guide that had been drawn to X-band internal dimensions (0.9 x 0.4 in.) from cylindrical tubing. A 69 cm length was required for the cryostat, but the longest single piece of unkinked guide was about 63 cm. In the first resonant cavity system (TE 111 resonator), the 6 cm lower length of guide in the cryostat was No. 16 standard brass guide. As the weight of wave guide in the dewar was thus about 150 gms., a 2 hour pre-cooling period was required to reduce the wave guide temperature to that of liquid air. In addition more helium was used in the transfer process. Once the helium transfer had been completed, however, operation was satisfactory as far as the helium loss rate was concerned.

The method adopted for joining the thin-wall to the standard wave guide was to file a short section of No. 16 guide until it slipped over the thin-wall guide. The soldered combination was then butted against the main guide, and soldered to the latter with the aid of a collar of No. 15 guide. Later, when the TE 102 resonator was used, the section of brass was replaced by another section of CuNi guide, and the two lengths of CuNi in the cryostat were soldered together with a collar of filed No. 16 guide.

For constructional simplicity, the wave guide in the cryostat was left open to the liquid helium, as was the cavity resonator. An $\frac{1}{8}$-in. hole, drilled in the broad face of the wave guide at the top and bottom of the cryostat, provided an entrance and exit path for the helium, and additionally, served to reduce the possibility of a thermal oscillation in the wave guide during transfer.

6.2 (d) Resonant Cavity Design

Two resonant cavities were designed for thie thesis investigation as shown in Figure 7. The first was a TE 111 cylindrical cavity that could be externally tuned by two methods, while the second was a TE 102 thin-wall rectangular resonator that could be externally tuned over a smaller range with a single mechanism. The resonators will now be discussed in detail.

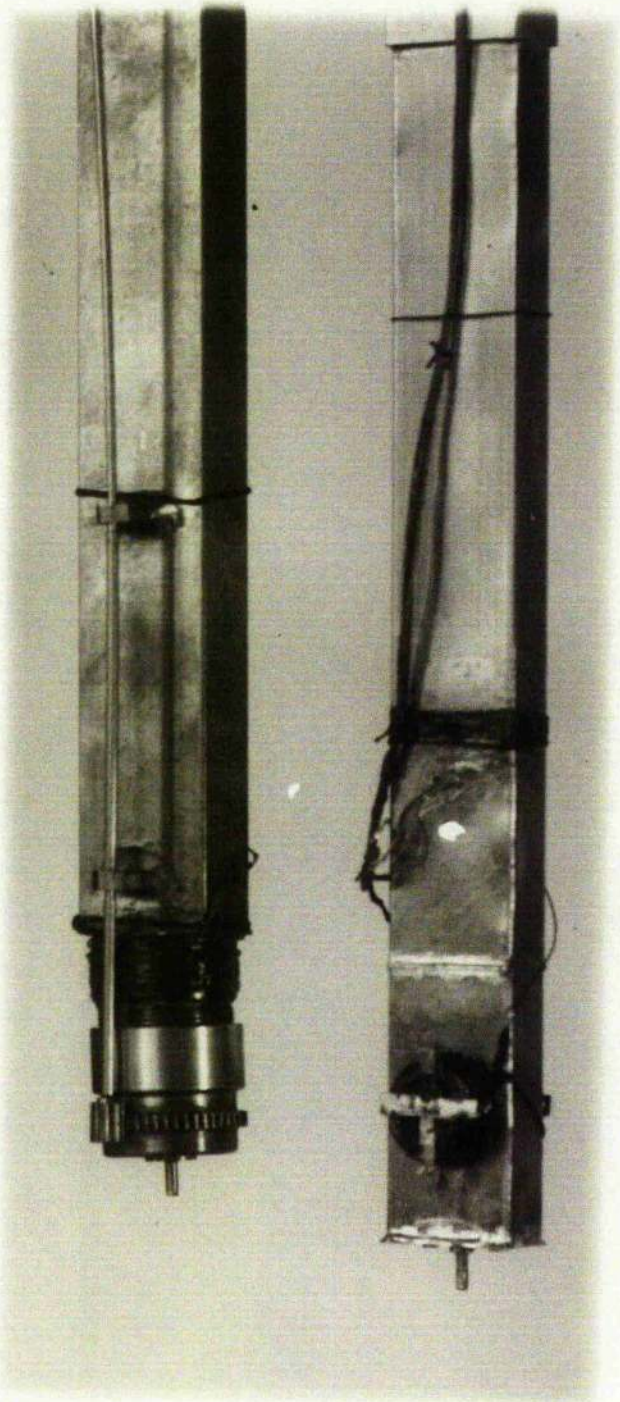

FIGURE 7

TE111 AND TE102 CAVITY RESONATORS

TE 111 Cylindrical resonant cavity

A cylindrical brass resonator was designed first of all, as it was felt that this type would be the easiest to fabricate, in the range of high Q resonators. The resonator was designed from the formula[24],

$$(fD)^2 = A + Bn^2(D/L)^2 \qquad (6.1)$$

where
- f = Frequency in Mc/s
- D = Diameter of the cavity in inches
- L = Length of the cavity in inches
- n = Number of half-wavelengths
- A = A constant
- B = Another constant

and where (D/L) is the primarily selected ratio. It was apparent that the TE 011 cylindrical cavity (highest Q) would be too large, and the TE 111 mode was taken as the one least likely to give trouble from degeneracies.

For preliminary work, it was planned that the resonator should be mechanically tunable over a range of about 300 Mc/s. As a consequence, the resonator was made from brass stock in the shape of two pillboxes threaded together (to minimize wall losses). Design dimensions and operational characteristics for the TE 111 resonator were:

Medium	= silver-plated brass
Internal diameter	= 2.12 cm
Maximum length	= 3.65 cm
Minimum length	= 3.15 cm
Wall thickness	= 1 mm

Coupling thread	= 32 TPI
Coupling hole	= 5/16 in.
Tuning range:	
air at 300°K	= ~9.28 - 9.58 kMc/s
helium at 4.2°K	= ~9.1 - 9.4 kMc/s

The coupling to the resonator was effected by a single coupling hole in the centre of the end wall, and the size of the coupling hole was chosen by experimentation. The selected value of 5/16 in. left the cavity in a slightly overcoupled state.

The resonator itself was soft soldered to the cryostat wave guide through an intermediate 10/1000 in. end plate. With this arrangement, a loaded Q of ~2000 at 300°K and ~7000 at 4.2°K was observed. The Q was calculated by noting the half-power points in the reflected signal when sweeping the driving klystron through the cavity resonance. Note that this method only gives an approximate result since the reflected power is a function of the loaded and unloaded Q's.

The cavity could be tuned mechanically with a 4.5:1 reduction drive made from brass clockwork gears. The drive gear fitted to a 1/16 in. stainless steel rod which extended from the cryostat top plate, via some small bushings soldered along the entrant wave guide. No stops were provided on the tuning mechanisms.

For fine tuning, and additional purposes, an $\frac{1}{8}$ in. quartz rod was fitted on and through the E-plane bend and thence through the cavity coupling hole (1.5 cm maximum penetration).

To prevent excessive side play of the quartz rod in the cavity coupling hole, it was centred with the aid of a mica sheet. The mica sheet was stuck with nail varnish inside the cavity, and against the upper wall, and the clearance hole in the mica (3/16 in.) was made sufficiently large for helium entry. With this quartz rod, tuning could be adjusted smoothly over a range of about 50 Mc/s, which was the electrical tuning range of the klystrons employed. This quartz rod system had no evident detrimental effect on the Q of the resonant cavity, unless the penetration was excessive.

Paramagnetic specimens were mounted on the bottom (centre) of the cavity for with the TE 111 mode, maximum B fields are encountered at such positions on the end plates. Specimens were usually mounted with nail varnish or with vaseline.

Care had to be taken in the pre-cooling stages of operation to ensure that the cavity threads were sufficiently exhausted of air. This was illustrated in one experiment at $4.2^{o}K$ in which the cavity was completely jammed because of an accumulation of solid air between the threads.

TE 102 Rectangular resonant cavity

As will be indicated in the next chapter, the TE 102 rectangular thin-wall resonator was designed to minimize the eddy-current effect experienced with the TE 111 resonator in an alternating magnetic field. The resonator was designed from the equation,

$$(K/\lambda_o)^2 = (1/\lambda_g)^2 + (1/\lambda_{co})^2 \qquad (6.2)$$

where λ_g = guide wavelength; λ_{co} = cut-off wavelength; λ_o = free-space wavelength; K = dielectric constant of the media filling the cavity.

The resonant cavity was made from a section and pieces of the thin-walled CuNi wave guide previously described. A "fixed" frequency cavity with a quartz-rod fine tuning was contemplated. Furthermore, the resonator was to incorporate field modulation coils (Helmholtz pair) on each of its broad faces to effect a variation in magnetic field strength at the paramagnetic crystal. A TE 101 cavity was first considered for simplicity. In this mode, the B field maxima are at the end plates and thus the modulation coil axis would, of necessity, be level with the bottom of the cavity. This was considered undesirable from a mechanical point of view, and also from space considerations. The TE 102 resonator design was then considered and adopted. This mode exhibits B field maxima at the centre and end plates of the cavity.

The length of the cavity was calculated with consideration given to the dielectric constant of the paramagnetic media that would partially fill the cavity (principally irradiated MgO). The cavity was then completed by the addition of CuNi end plates. The upper end plate was soft soldered to the main section, while the lower end plate was soldered with Wood's metal. Coupling and quartz rod tuning were effected

in the manner described for the TE 111 resonator.

Resonant cavity frequency changes could be made prior to low temperature experimentation by building up the lower end plate internally with rectangular plugs of German Silver (1 mm thick) and soldering the combination to the resonator with Wood's metal. A single 1 mm plug would increase the resonant frequency by about 100 Mc/s. (Large plugs would, however, destroy the symmetry of the modulation coils about the resonator central plane.)

The modulation coils were wound on 12 mm CuNi tubing formers, soldered to the broad faces of the cavity at the symmetry plane. Each coil was wound with 100 turns of No. 30 SWG enamelled copper wire, and the coils were connected in series. These coils were designed to execute a magnetic field sweep of 10 gauss, with a current sweep of 1 amp, at the centrally located paramagnetic specimen.

Location of the paramagnetic specimens at the centre of the cavity was quite a problem. After many trials with different supporting media (which gave an excessive resonance shift), the foam cellular material "Jabolite" was employed as a supporting cushion, and the paramagnetic crystals were embedded in this material which completely filled the bottom half of the cavity. While the "Jabolite" had negligible effect on the resonant frequency of the cavity, it did suffer the drawback that it would shrink under normal solder heat -- hence the use of the Wood's metal in this application.

The TE 102 cavity, again slightly overcoupled, exhibited a loaded Q of ~ 2000 at 300°K and ~ 7000 at 4.2°K. Other pertinent design figures were:

Material	= CuNi (silvered)
Length	= 43 mm
Internal dimensions	= 0.4 x 0.9 in.
Thickness	= 11/1000 in.
Coupling hole	= 5/16 in.
Frequency in air at 300°K	= ~ 9.3 kMc/s
Frequency in helium at 4.2°K with Jabolite, plus MgO crystal	= ~ 9.1 kMc/s

6.3 The Magnet System

The Zeeman level-splitting electromagnet was a Newport Instrument Type A, air-cooled magnet, mounted on a rail carriage for easy access to the cryostat. The magnet was supplied with standard (flat) pole pieces of mild steel, 100 mm in diameter. Each coil was wound with 2000 turns of rectangular copper wire (0.05 x 0.15 in.). The magnetic field was approximately 800 gauss/amp for a pole-piece spacing of 50 mm.

The field inhomogeneity was estimated by comparing the observed line width of a speck of DPPH with the observed line width of a large sample of known paramagnetic material -- in this case, irradiated MgO at 4.2°K with a measured line width of ~ 4 gauss. By this method, the field inhomogeneity at the centre of the magnetic field was estimated to be ~ 3 gauss/cm. As a consequence, the pole pieces were machined to display Rose "shims" around their perimeters. The "shim" dimensions

selected from Rose's criteria[25] were:

shim width = 3.85 ± 0.01 mm

shim thickness = 3.75 ± 0.01 mm

With this modification completed, the field inhomogeneity reduction could be calculated by comparing the line widths of the MgO specimen for the shimmed and unshimmed conditions. In this manner, the field inhomogeneity at the centre of the magnetic field was estimated to be less than 1 gauss/cm after shimming. Figures 8 and 9 illustrate the line shape for the MgO specimen, before and after shimming.

For smoothness, the power supply for the magnet was a bank of six 12 volt Admiralty surplus batteries, each with a 40 AH rating. With this battery bank, a field current of over 4 amps could be maintained over the operational period which varied from 4 to 8 hours. A mercury vapour rectifier d-c power unit was adapted to serve as a battery charger, and the system operated in trouble-free fashion over a period of two years.

Current flow to the magnet was regulated by a combination of power rheostats. Great accuracy in the measurement of field currents was not a major requirement in this investigation, and a high quality ammeter was thus sufficient for this purpose. The ammeter could be read to ± 0.01 amps which corresponded to ± 8 gauss.

For 50 cps modulation of the magnetic field, a modulation coil of 225 turns was wound on brass formers on each of

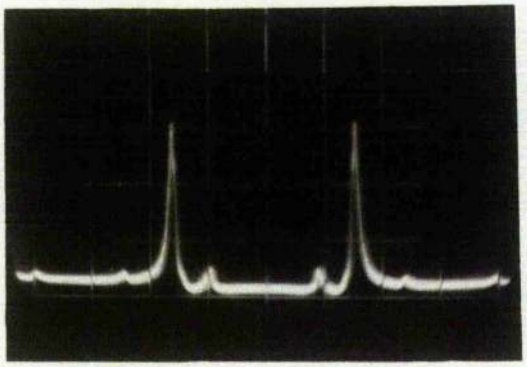

FIGURE 8

MgO RESONANCE LINE WITH TWO SATELLITES

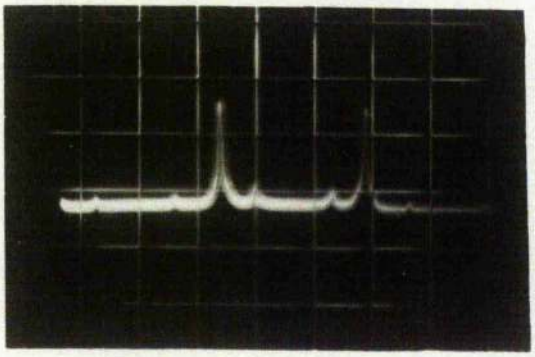

FIGURE 9

MgO RESONANCE LINE WITH TWO SATELLITES
(shimmed pole pieces)

the pole pieces. The normal sweep current applied to the coils (connected in series) for spectroscopic observation was 3 amp. rms. This effected a field sweep of about 60 gauss.

6.4 Electronics

Details of the electronic control systems are now given. For constructional and maintainance ease, each electronic block unit (except the IF amplifier) was constructed in computer fashion on vertically mounted panels of aluminium; the valve-base side of the equipment was left open and facing toward the observer. Standard valves were used in these block units wherever possible.

6.4.(a) Klystron Power Supplies

The common power supply for the resonators of the monitor and local oscillator klystrons was a -300 volt, 75 mA supply, as shown in Figure 10a. The supply was connected to the klystrons as indicated in Figure 11. The power supply was designed to regulate the output noise voltage to within 3 mV rms.

The power supply for the resonator of the X-13 (medium) power klystron was a -500 volt 100 mA supply designed for the same noise voltage regulation. This supply was more troublesome to develop because of the higher voltage ratings demanded by the components. The diagram for this power supply is given in Figure 12. As shown, a facility was included for fine tuning of the output voltage about the 500 volt level.

FIGURE 10 POWER SUPPLIES

a) Klystron supply = -300 v
b) I.F. supply = + 200 v

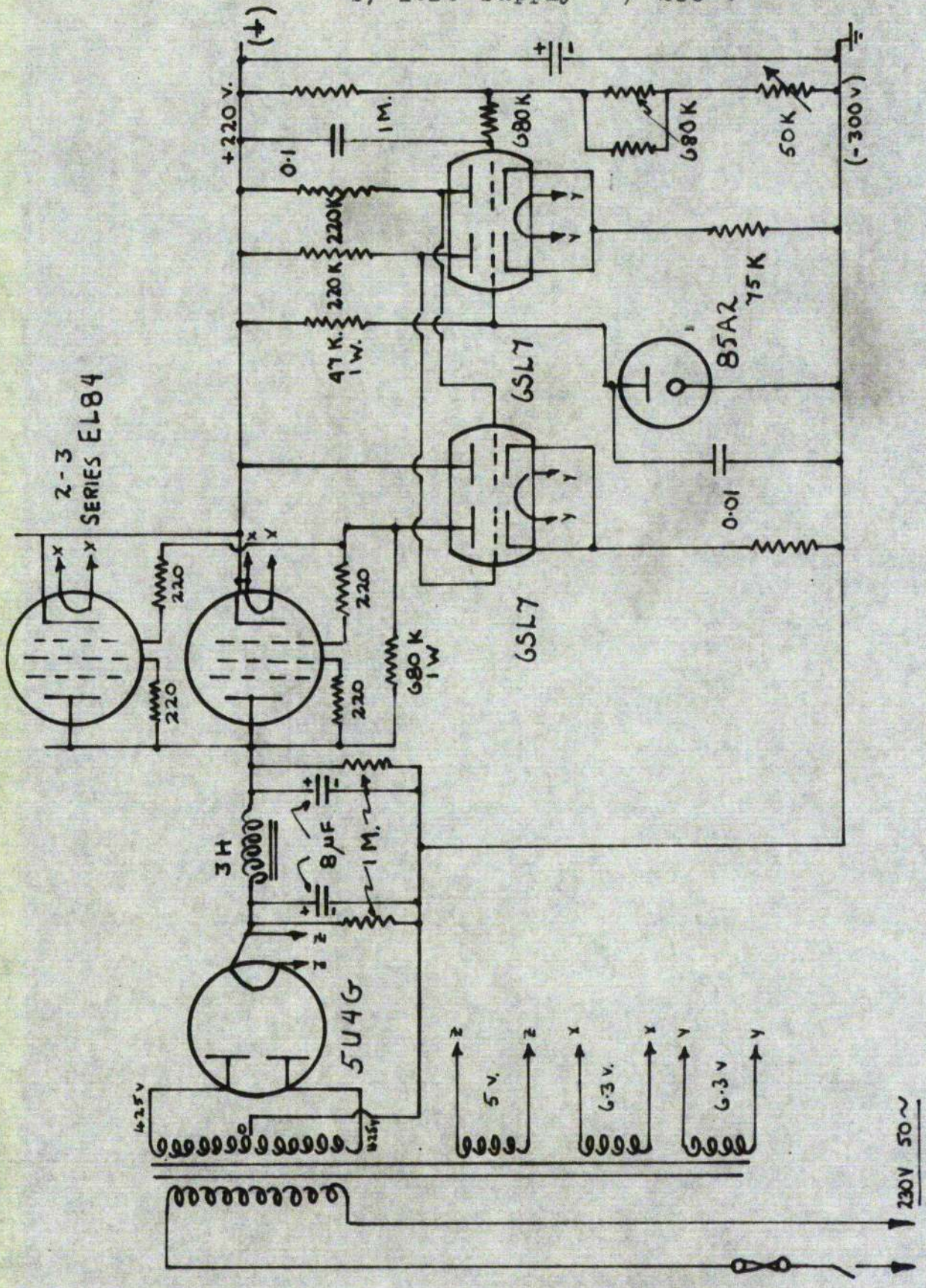

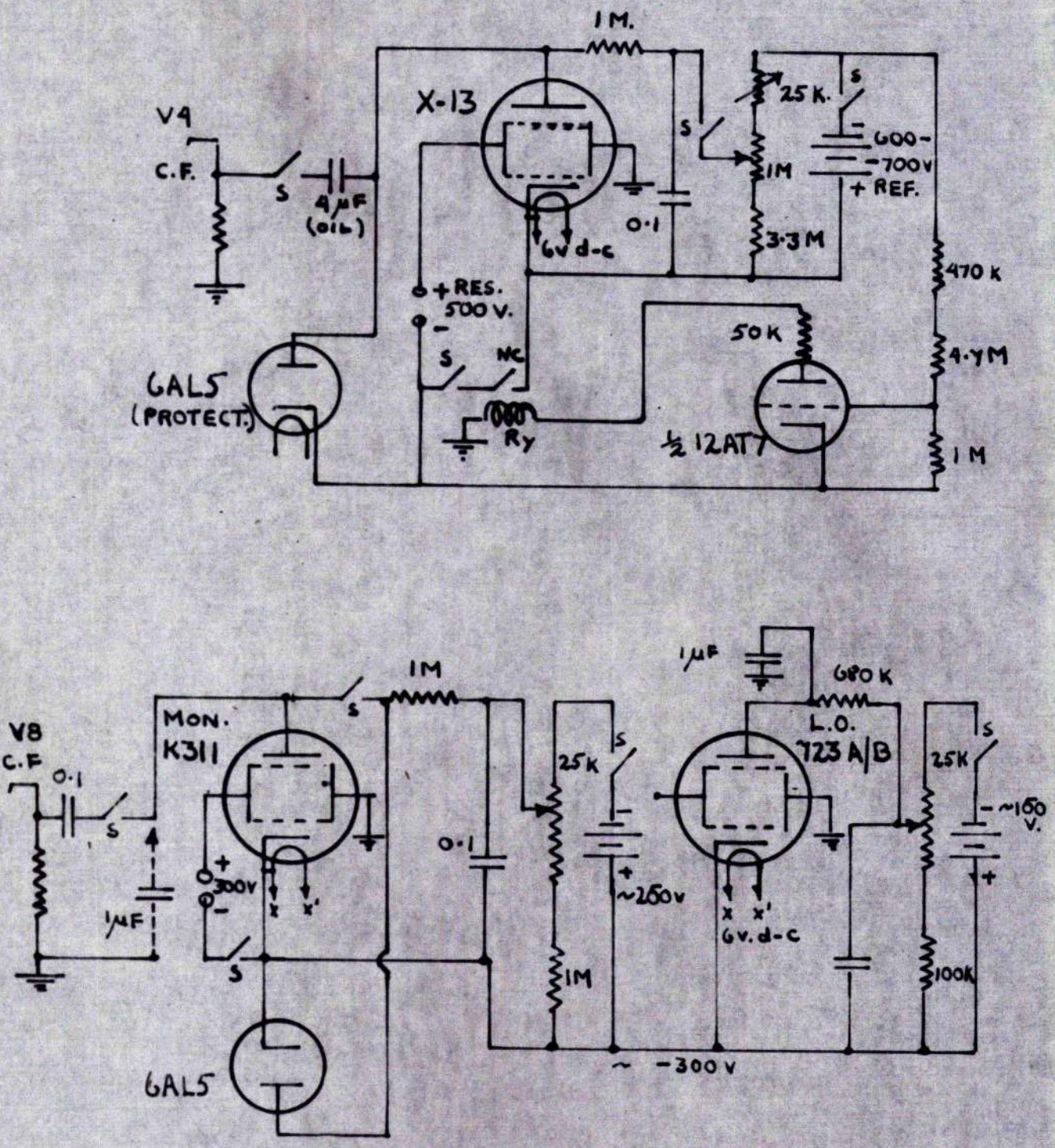

FIGURE 11

CIRCUIT CONNECTIONS FOR KLYSTRONS

FIGURE 12 X-13 KLYSTRON POWER SUPPLY

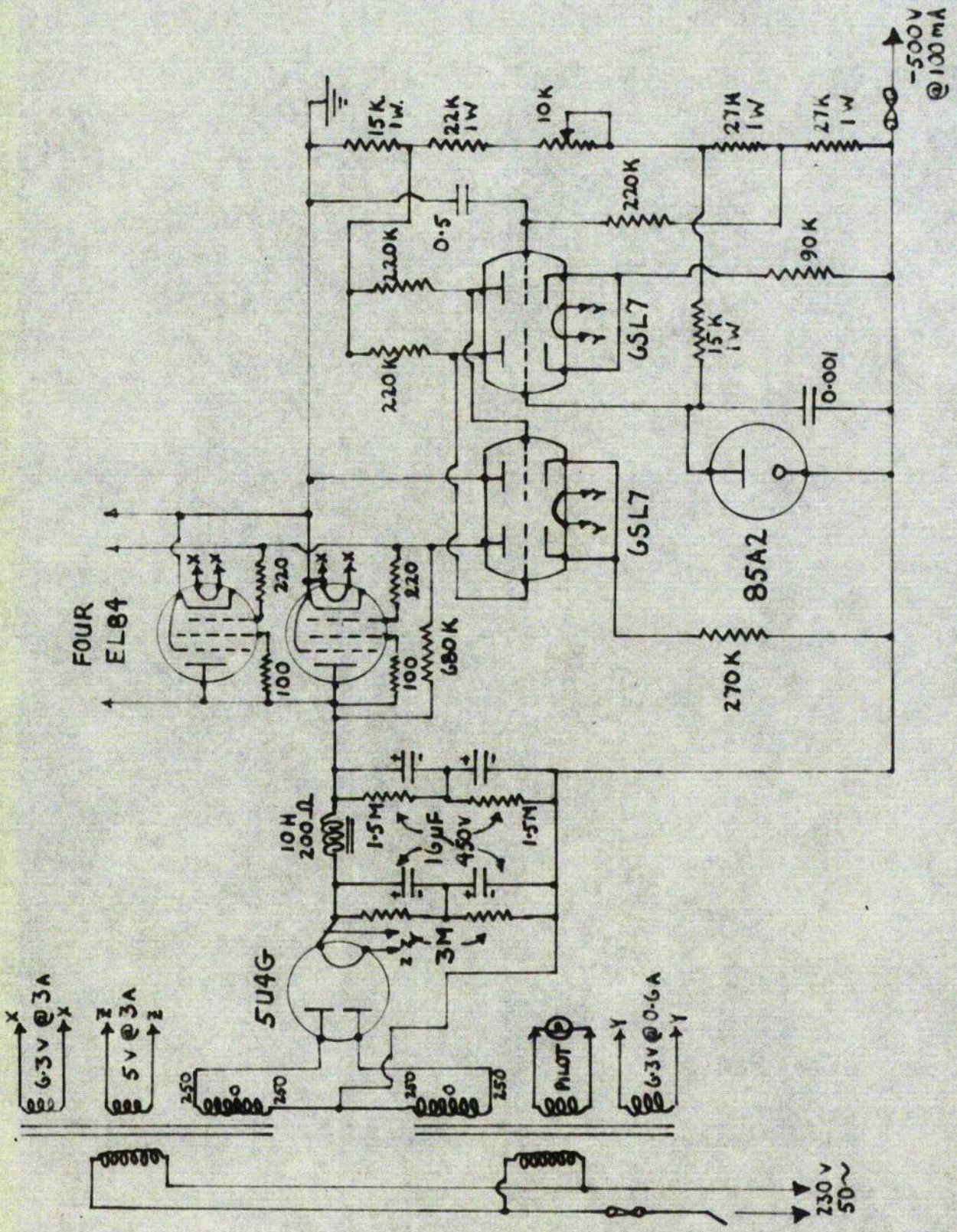

The group of EL84 series regulator valves could possibly be replaced by a single 12E1 power pentode for more efficient construction -- the circuit was otherwise satisfactory.

The reflector potentials of all the klystrons were obtained from standard 120 volt radio batteries. By this means, undesirable frequency modulation of the klystrons was minimized. The drain on the batteries was negligible; indeed the set of batteries lasted for about a year before becoming weak. The klystron reflector potentials were:

Klystron	Reflector voltage
K311	250
723A/B	150
X-13 (3/4 mode)	400

Frequency modulation of the monitor and of the power klystron could be achieved through the application of a sweep voltage, R-C coupled to the reflectors. When a constant klystron frequency was required, the coupling condenser was connected to ground directly, to provide R-C integration at the reflector electrode, and consequent frequency stabilization (as in the local oscillator klystron).

As an added restraint against undesirable frequency modulation, all the klystron heaters were driven from 6-volt wet batteries. A battery charger was built into the apparatus to maintain this facility.

No protective devices were required in the 723A/B klystron circuits. (The main safeguard of longevity, however,

is to ensure that the reflector voltage is applied to the klystron after the heater voltage application and before the resonator voltage application.) In the K311 circuit, a 6AL5 protective diode was connected between reflector and cathode to ensure that the reflector would not become positive with respect to the cathode at any instant. A similar 6AL5 protective diode circuit was associated with the X-13 klystron. In addition, however, a relay fail-safe circuit was connected in series with the output from the -500 volt resonator power supply to ensure that this voltage would be removed if the reflector voltage failed.

The monitor and reflector klystrons, when frequency modulated, were swept with positive pulses or waveforms at the reflector electrodes. As a consequence, for such operation the quiescent reflector voltage was required to be at the most negative voltage experienced over the operating mode.

6.4 (b) I.F. Amplifier

The I.F. amplifier was a war-surplus, single-ended, "Pye strip" with a centre frequency of 45Mc/s and 10% bandwidth. The original circuit incorporated five VR91 pentodes in the pre-detector stage, followed by a detector and VR91 cathode follower operating into a 100 ohm cable. The power consumed was approximately 100 mA at 250 volts, with a 6 volt heater drain of 1.8 amp.

As it stood, the amplifier generated too much high frequency and 50 cycle noise. The 50 cycle noise was virtually eliminated by running the heaters from a six-volt battery, and the high frequency noise was reduced by by-passing the first I.F., wide-band stage. With this done, the maximum gain of the strip was about 1800, and the high frequency noise output was reduced to 20 mV rms. The gain could be controlled by grid bias adjustment, but as the valves had a sharp cut-off, it was usually undesirable, from a stability point of view, to work too close to this point.

Provision was made for connecting a variable condenser bank (1 μF max) across the output, to reduce the background noise still further. The amount of integration that could be applied was, of course, dependent on the shape of the waveform under investigation. The output signal was displayed on a Solartron oscilloscope Type 513-2, with a maximum sensitivity of 1 mV/cm. Furthermore a milliammeter was connected into the second detector circuit as a signal level monitor.

The power supply for the I.F. amplifier "Pye strip" was as shown in Figure 10b. The supply was designed to furnish 100mA at 200-220 volts, with a noise level of less than 3 mV rms. The heater current for this amplifier was supplied by a 6-volt battery.

6.4 (c) Pulse Circuit Power

The power supply for the pulse circuits was as shown in Figure 13. The design rating of this supply was 65 mA at +300 volts and 5 mA at -150 volts. The noise ripple on the 300 volt output line was less than 3 mV rms on no load; ½ volt spikes were obtained, however, when the supply was loaded to the limit. Stabilization of the -150 volt output was less critical, and restricted to voltage reference tube (VR150) stabilization. The ripple level at this output was approximately 1 volt.

6.4 (d) Pulse Circuit Design

The sweep and pulse circuit design is shown in Figures 14 15. The system block diagram and timing sequence are shown in Figures 16 and 17, respectively.

The pulse system was originally designed to effect adiabatic fast passage transitions by the frequency sweep method. Inversions were not obtained with this method, however, and the circuit was modified to effect inversions by adiabatic fast passage of the magnetic field. The frequency sweep method was used effectively to measure the spin lattice relaxation time, T_1.

To achieve field-sweep inversion, it was necessary to pulse the X-13 klystron to the resonant cavity frequency, while sweeping the magnetic field through the resonance condition. In addition, while setting up the system for operation, it was convenient to sweep the reflector of this

FIGURE 13 PULSE CIRCUIT POWER SUPPLY

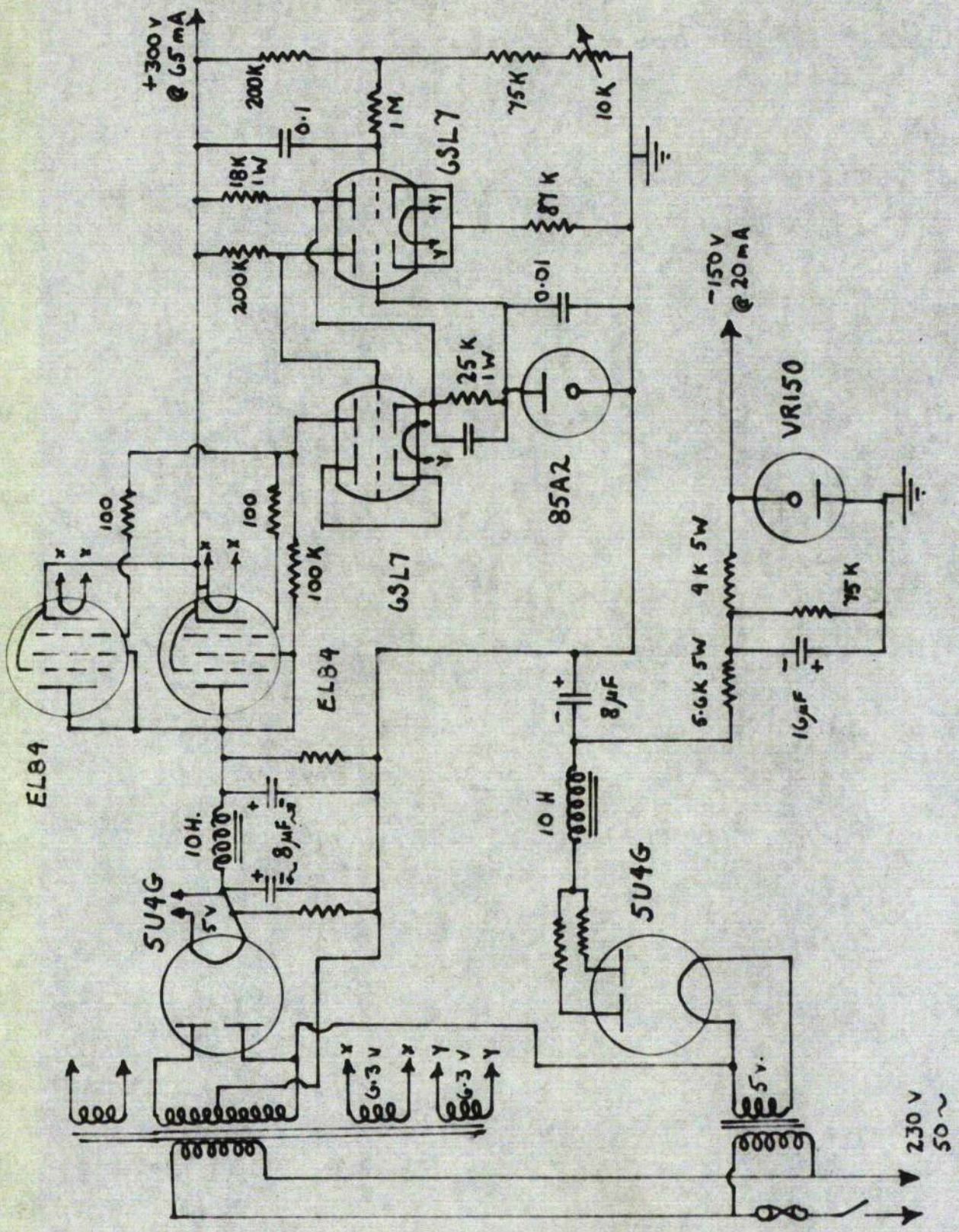

FIGURE 14 MASER PULSE CIRCUITRY -- PART 1

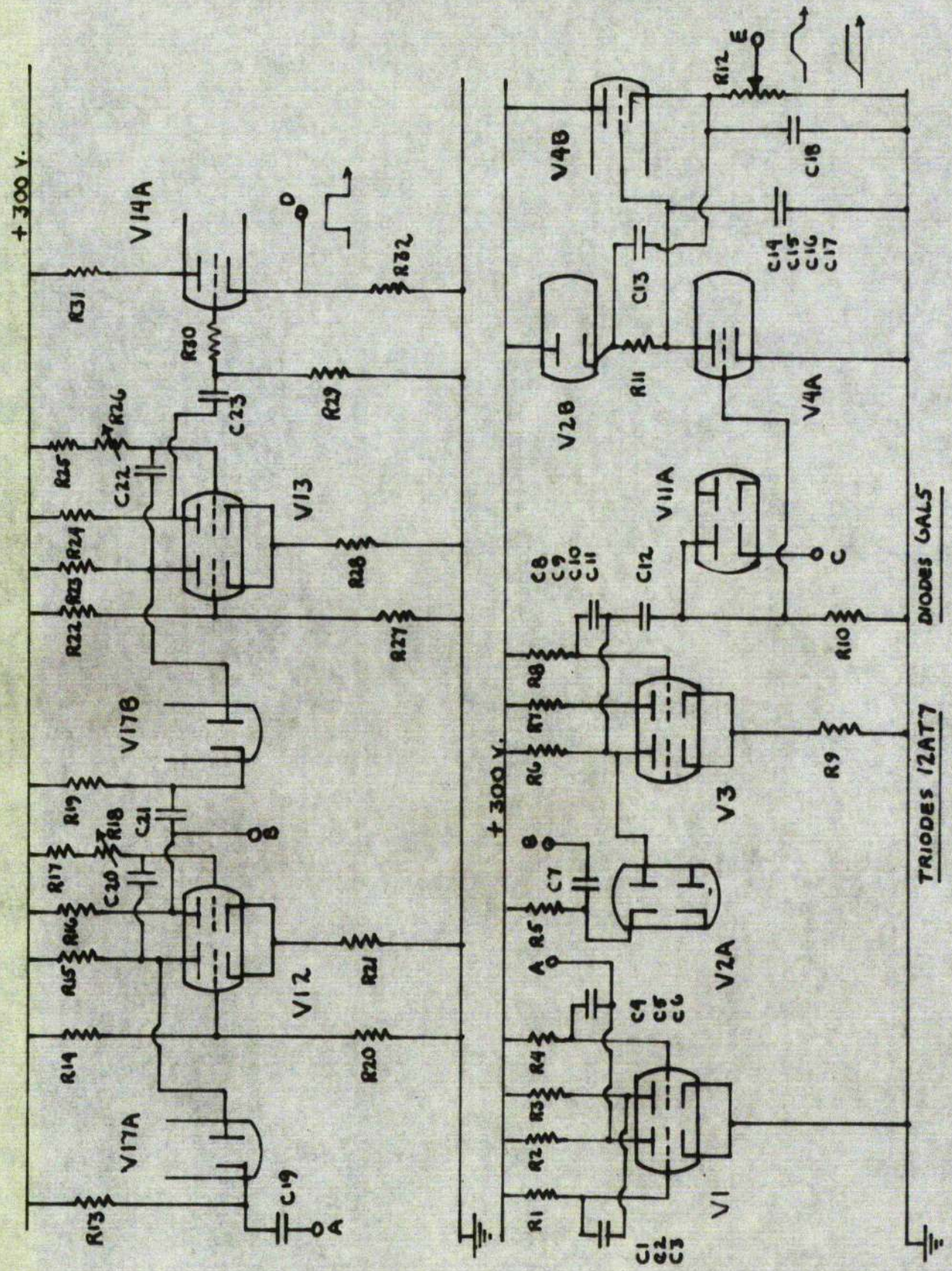

FIGURE 15 MASER PULSE CIRCUITRY -- PART 2

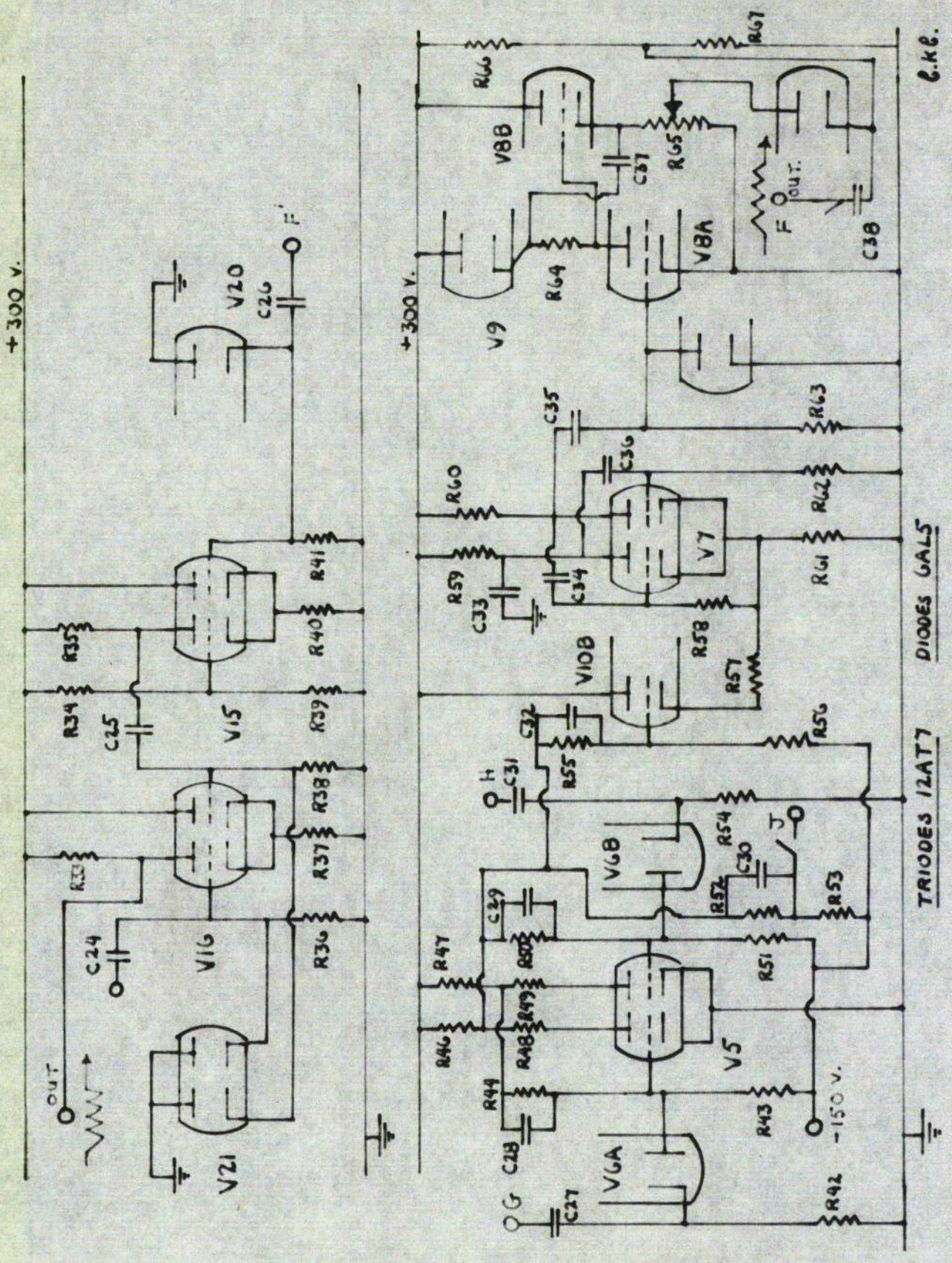

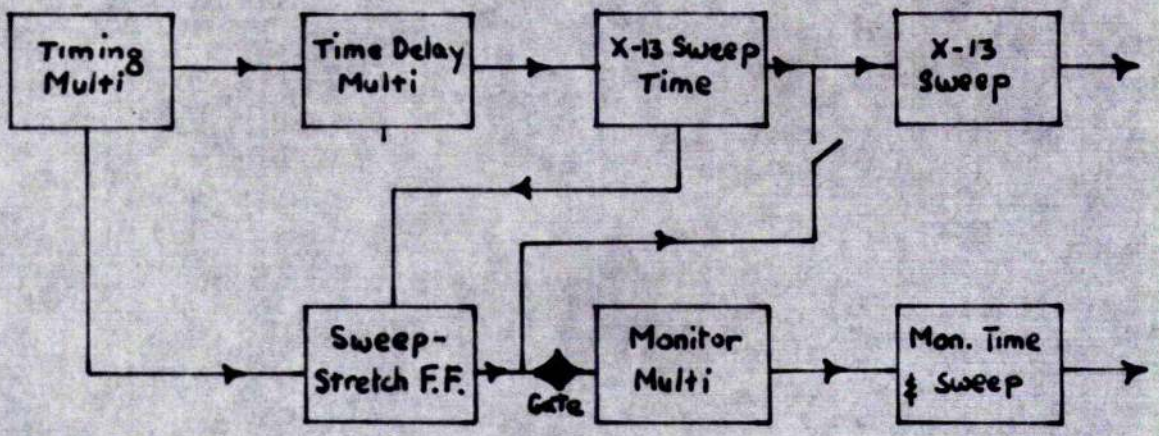

FREQUENCY SWEEP METHOD

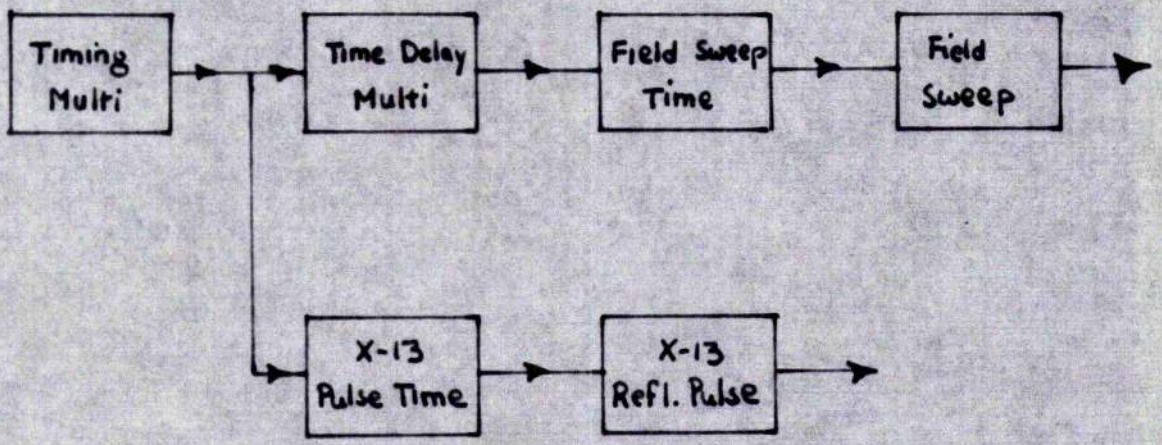

FIELD SWEEP METHOD

FIGURE 16

PULSE CIRCUITRY FOR ADIABATIC FAST PASSAGE INVERSION

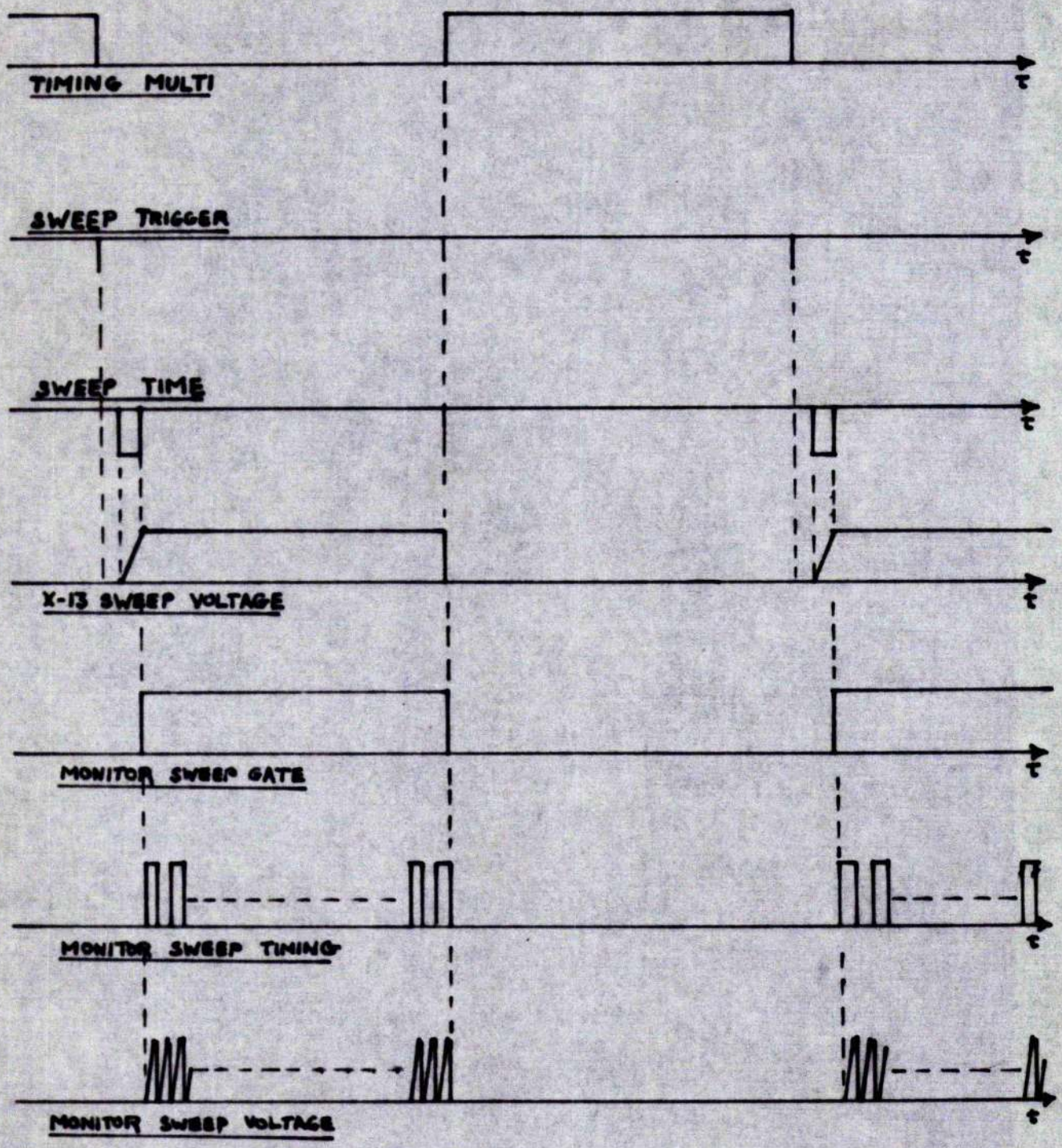

NOT TO SCALE

DCR

FIGURE 17a TIMING SEQUENCE -- FREQUENCY SWEEP METHOD

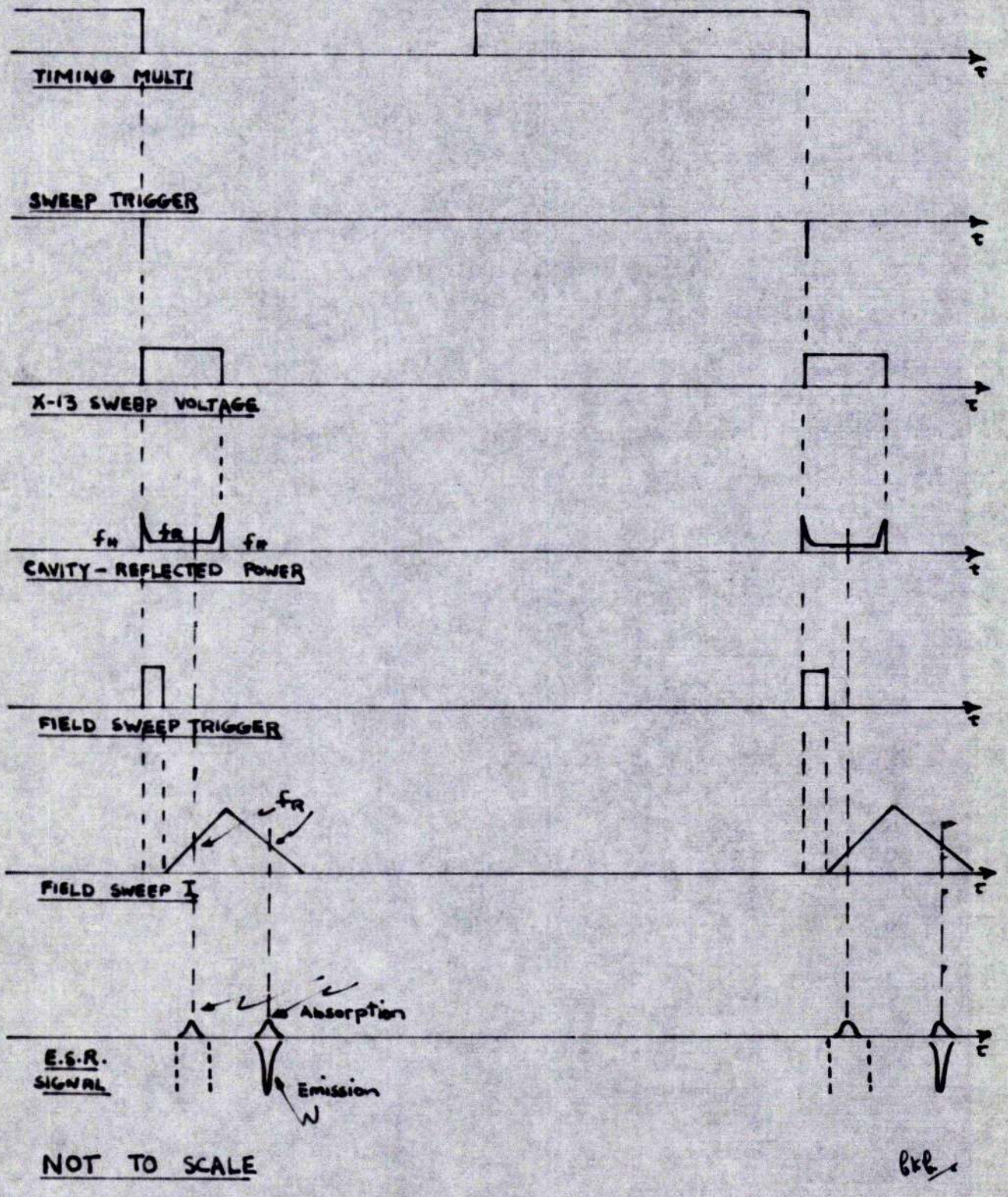

FIGURE 17b TIMING SEQUENCE -- FIELD SWEEP METHOD

klystron with a trapezoidal voltage waveform. The circuit based on valves V1, V2, V3, and V4 constituted the X-13 klystron reflector sweep circuit, and alternatively provided the driving waveform for the field sweep circuit. The circuit based on valves V12, V13, V14-A, and V17, provided the waveforms and timing sequences necessary for pulsing this klystron during the adiabatic fast passage period.

The V1 circuit was a free-running multivibrator circuit, with the grids returned to the supply voltage for efficient triggering action. A switched condenser bank provided repetition rates of 1.5 cps, 12 cps, and 25 cps, and a visual indication of the repetition rate was provided by a 65 volt neon bulb connected across one of the anode loads. The output from point A was connected to the input B of a one-shot multivibrator time delay circuit (50 - 700 μsec) based on V12 and V17-A. The waveform at B was also applied simultaneously to another multivibrator time delay circuit, based on valves V13 and V17-B. The positive-going output signal from V13 was fed to a cathode follower clipper circuit V14-A from which was obtained an essentially rectangular 100 volt pulse of variable duration (40 μsec - 1.5 msec) achieved by variation of the time constants in the V13 circuit. This 100 volt positive pulse was applied when necessary to the reflector of the X-13 klystron, which was normally biased to the high frequency end of the operating mode ($3\frac{3}{4}$ mode width $\approx$ 150 volt). Thus

this klystron could be pulsed to the resonant cavity or other frequency for controllable periods. R-C coupling to the klystron reflector would, of course, produce some "sag" in the waveform at the reflector, and thus the coupling condenser was made as large as possible (2 μF) to minimize this effect.

It was also necessary to produce a magnetic field sweep through the cavity resonance frequency, while the power klystron was pulsed to the resonance frequency. This sweep was initiated by the triggered V12 time delay circuit, which delayed the sequence until the pulsed power klystron reached the resonant cavity frequency. The output from V12 was applied to the sweep-generating and shaping circuit based on valves V2, V3, V4, and V11-A. This was essentially a pulse-timing circuit followed by a bootstrap, trapezoidal, voltage-sweep circuit. Trapezoidal sweep parameters were:

Amplitude (volts)	Leading edge (μsec)	Flat top (μsec)	Trailing edge (μsec)
180	30	100	250
180	75	100	250
170	100	0	200
150	200	0	200

A facility was also included for frequency sweeping the monitor klystron with a fast repetitive triangular voltage sweep (amplitude, $\pm$ 90 volts; sweep time, 100 - 400 μsec; sweep interval, 400 - 600 μsec). This sweep circuit was gated on at the end of the power klystron sweep interval, and gated off after half an operating period by the main control

multivibrator (V1). The gate circuit was a bi-stable flip-flop circuit (V5, V10-B, V16). Sweep timing was derived from a gated free-running multivibrator circuit (V7, V10-B), and the bootstrap voltage sweep output was obtained from V8 and V9.

Under certain conditions, it was desirable that the inverting klystron sweep voltage should not return through the resonance condition while the spin resonance relaxation processes were being monitored. To effect this delay, it was necessary to introduce the clamping diode, V11-A. With this diode switched into the circuit, the grid of V4-A would be pulled down to below cut-off whenever the monitor klystron sweep gate was opened. In this way, the output voltage from V4-B would be clamped at ~ 180 volts during the monitoring period.

The power amplifier circuit, designed for magnetic field modulation, was as shown in Figure 18. This amplifier was powered by a 150 volt battery combination (75 volts of which acted as the magnet supply) as the maximum total current in the anode circuit of this amplifier was 1200 mA. The internal modulation coils (previously described) were coupled to the amplifier through a 3:1 step-down transformer. As the d-c currents involved were fairly large by radio component standards, it was postulated that the transformer would operate more efficiently if choke coupled to the driver valves, as shown. The amplifier, normally biased near cut-

FIGURE 18 FIELD SWEEP POWER AMPLIFIER

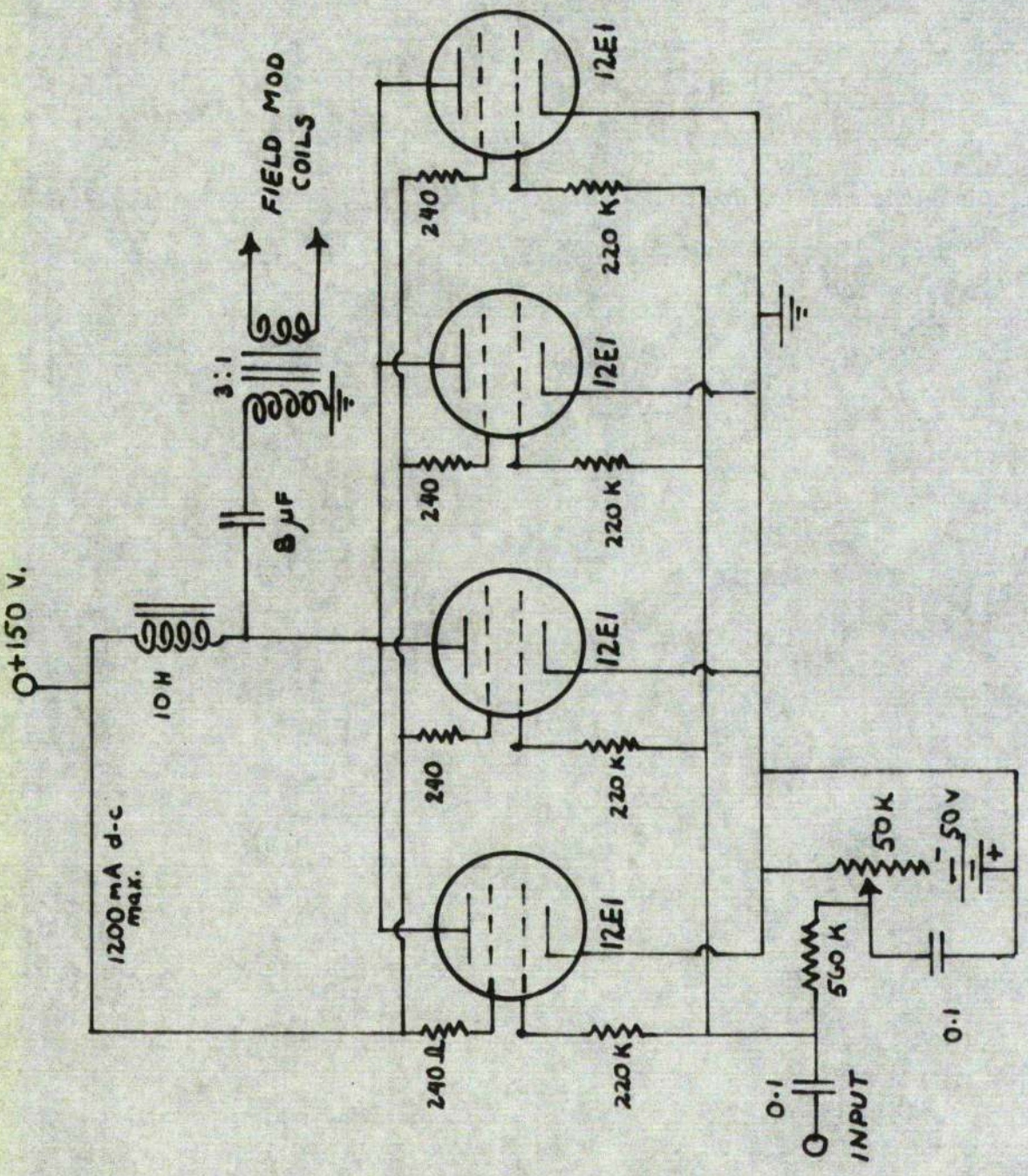

off, was driven by the positive-going sweep voltage from the power-klystron sweep circuit, V4-B. With this system, current sweeps of over 1 amp could be set up in the internal modulating coils.

An additional circuit was designed (V15, V16; V20, V21) for combining inversion and monitor voltage-sweep waveforms. The former waveform could be applied to the grid (E) of V16, while the latter waveform could be applied to the grid (F) of V15. V15 served to amplify the input monitor waveform, while preserving its phase; the resultant waveforms were then added in V16. Diodes V20 and V21, in the grid circuits, served as d-c clamps.

The resultant waveform could be used to drive the power amplifier and modulation coils for inversion and relaxation observations. As it turned out in the thesis investigations however, a field sweep waveform with a low duty cycle was required if the eddy current losses in the TE 102 resonator were to be kept to a minimum. As a consequence, this particular circuit was not applied.

6.5 High-Frequency Alternator

In the initial inversion experiments, high-frequency magnetic field modulation was obtained from a motor-alternator system connected to the external modulation coils, as shown in Figure 19. The motor alternator was a Service Instrument, Type MG-8, with a maximum output of 80 volts at 6.25 amp, 2000 cps.

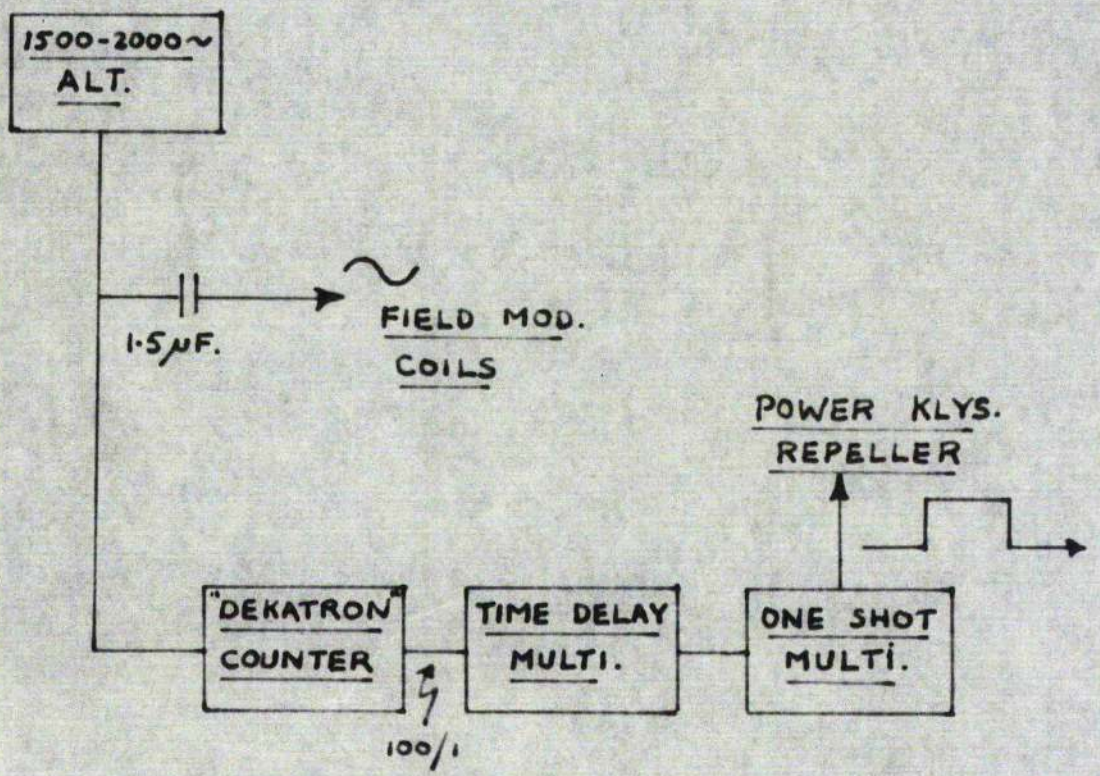

FIGURE 19 ALTERNATOR FIELD SWEEP CIRCUIT

To match the alternator to the modulation coils, a 1.5 μF condenser was connected in series with the latter. In this way a modulation current of 2.5 amp rms was obtained. (Due to coil heating, it was necessary to limit the current to this value.) As will be described in the next chapter, this system was very inefficient and caused the magnet coils to heat considerably. In addition, the eddy current losses in the cryostat were considerable. (A mechanical resonance of the modulation coils in the 1500 - 2000 cps range also caused some discomfort.) This system did, however, provide the necessary information on inversion techniques which led to the final resonant cavity design -- it thus deserves mention.

CHAPTER 7

OPERATION AND RESULTS

Introduction

Transient and steady state spin resonance observations were made on the paramagnetic media described in Chapter 5. The relaxation phenomena could be appraised by both methods of observation as could the inversion criteria. It was possible to observe inversion and amplification with a single MgO crystal at 4.2°K. With an increase in material, spontaneous oscillations were observed at 1.3°K. Irradiated diamond exhibited a shorter spin-lattice relaxation time, and this resonance line could be saturated but not inverted at 1.3°K.

Phosphorous-doped silicon was examined only in passing as detailed resonance and inversion examination had been recently made on such crystals by other workers (Sec. 5.2(c)). Our interest was, however, focussed on the use of a quartz rod light pipe for controlling the spin-lattice relaxation rates in semiconductors.

In addition, the phases in the development of the final system are discussed, and details are given of the operational procedures applicable to each phase.

7.1 Cryostat Performance

In the initial stages, some trouble was experienced in the helium transfer operation as the helium dewar vacuum was

too hard and caused insufficient pre-cooling. With this dewar softened to 5 mm air pressure, the transfer process was quite economical. In an average transfer with a TE 102 resonator, 150 litres (NTP) of helium were expended in level attainment, and an additional 250 litres were expended over the rest of the transfer.

These economical transfers were made with the aid of a CuNi guide tube (length, 15 cm; diameter 1 cm) fitted to the waveguide in the cryostat along the transfer tube axis. The function of the tube (the top of which was 15 cm below the cryostat top plate) was to guide the liquid helium to the bottom of the dewar. Without this device, about 250 additional litres of helium were expended in the transfer process.

The cryostat was carried about 75 feet to the helium liquefier for the transfer operation. After transfer, it was usually necessary to adjust the frame of the liquid air dewar to centre the dewar system between the pole pieces of the magnet. With this system, twenty-four helium temperature experiments were carried out.

The operational time for experiments at 4.2°K (with no eddy current heating) was a maximum of 12 hours. With high frequency heating of the cryostat, the running time at this temperature was a minimum of 3 hours. For experiments below the λ point, the operating period was in the order of 5 hours.

7.2 Spectrometer Sensitivity

To determine the sensitivity of the spectrometer, resonance measurements were carried out on a crystalline sample of the free radical marker DPPH (Diphenylpicrylhydrazyl) which has a line width of 2.7 gauss. The sample, containing about 1.0×10^{18} spins, was mounted in a perspex holder and placed at the point of maximum magnetic field intensity in the resonator. With 50 cps magnetic field modulation, the amplitude of the spin resonance signal was 300 mV at $300^{\circ}K$ when the incident microwave power was 15 μW, as evaluated with the 40 db calibrated attenuator. The noise level was 50 mV peak-to-peak. Detection was by visual display on the Solartron oscilloscope, and in this case the modulation sweep was shifted in phase by 90° (R-C network) and applied to the X-plates for synchronous observation.

For the experiments, it was desirable to ascertain the number of spins that could be detected at helium temperatures with a monitor power of about 15 μW. (In this connection, Feher[26] has shown that spectrometer sensitivity is proportional to the square root of incident power over the range 10^{-1} to 10^{-7} watts.) Thus for this system the sensitivity for DPPH was found to be:

1.65×10^{17} spins at $300^{\circ}K$: 15μW power level ;

which would be

$\sim 1.3 \times 10^{15}$ spins at $4.2^{\circ}K$: 15μW power level

For a paramagnetic sample other than DPPH, therefore, the spectrometer sensitivity would be:

$\sim 4.9 \times 10^{14}$ ΔB spins at 4.2°K ; 15 μW power level

where ΔB is the line width (in gauss) of the specimen under observation, and where it is assumed that: a) the paramagnetic sample is located at the point of maximum field intensity in the resonator, and b) saturation of the sample does not occur at the incident power level employed.

This sensitivity is not high by spectrometer standards, but, as shown by the illustrative examples in Sec. 4.3, it is in the right order for observation with the power levels involved in this investigation.

7.3 Alignment Procedure for Steady-State Resonance Absorption Experiments

For steady-state resonance absorption and saturation measurements, it was usually only necessary to operate with the power klystron and local oscillator klystron in superheterodyne fashion. In some instances, however, the monitor klystron was employed in preference to the power klystron.

For both such requirements, the setting-up procedure would be as follows:

High Power Operation

1) Sweep the power klystron with the saw-tooth voltage sweep; observe by detection on CRO that the cavity dip is in the middle of the klystron mode.

2) Switch on and adjust the LO klystron until beats are observed on the CRO in the above mode.

3) Switch on the IF amplifier and adjust the klystron reflector potentials until the IF response curve is obtained; with the response curve unsaturated, centre the resonant cavity dip.

4) Switch off the power klystron sweep; adjust the reflector voltage of this klystron until the IF second detector meter indicates an output; adjust resonant cavity until this meter shows a dip; connect integrating condenser across the reflector of the power klystron. The system is now set up for spectrometer operation.

Low Power Operation

1) Switch on the monitor klystron repetitive sweep voltage; adjust monitor klystron until the IF response curves are obtained as in steps 2 and 3 above.

2) Switch off monitor klystron sweep; adjust the reflector voltage until IF second detector meter indicates an output; adjust the resonant cavity until this meter indicates a dip; connect 1 μF integrating condenser to the reflector of this klystron. The system is now lined up for low power spectrometer operation.

When primary adjustments were made to the system, prior to each low temperature experiment, it was necessary to consider the 2% shift in the resonant frequency of the cavity which would be experienced when the latter was filled with liquid helium.

7.4 Diamond Specimens -- Steady-State Resonance Phenomena

The diamond specimens were available for investigation some time before the arrival of the MgO crystals, and consequently a number of steady state and transient observations were made to adjudge the maser potentialities of the diamond crystals -- and further, the performance of the equipment. The resonance and saturation characteristics of specimens 29 and 27 were observed and measured at 4.2°K and 1.3°K under steady-state conditions, with 50 cps field modulation and visual (oscilloscope) display. The amplitude of the spin resonance signal obtained with the other specimens was too small to be of value in the investigations. With the specimens concerned, the amplitude of the electron spin resonance signal at resonance was measured on the oscilloscope for each applied level of microwave power. In this way, the absorption at resonance could be plotted as a function of incident power, and thus the saturation factor in Equation 3.15 could be evaluated. Once this was done and T_2 determined from the line width, the spin-lattice relaxation time, T_1, could be evaluated. The usefulness of the specimen as a maser crystal would be determined in part by the result obtained for T_1.

The steady-state measurements could not be made easily and at best, as had been realized, could only lead to approximate results (though certainly within an order of magnitude). To begin with, a series of saturation measurements could not

be taken quickly and as a result considerable trouble was experienced with electrical drifts and with mechanical vibrations. In addition, it was found that the experimental range for observations was limited by saturation effects in the IF amplifier. This saturation could be avoided if the amplifier were operated at reduced gain (Section 6.4(b)). Unfortunately, the valves possessed rather sharp cut-off characteristics and very considerable gain fluctuations were experienced with the biased amplifier, thus making it necessary to operate the system at full gain. Again, the saturation could have been avoided if a variable attenuator had been placed in the crystal detector arm of the microwave circuit. It would have been necessary to use a good, calibrated attenuator in this position, and unfortunately one was not available for this purpose.

Some interesting information on the effects of neutron irradiation was obtained. It was observed that the amplitude of the electron spin resonance signal in Specimen 27 was about one-tenth of that exhibited in Specimen 29 when the two experiments were carried out under the same conditions of temperature, power level and frequency (9.25 kMc/s). From the irradiation specifications in Chapter 5, it would thus appear that colour centre creation in these specimens is directly proportional to neutron dosage.

The saturation characteristics for specimens 27 and 29 at 4.2^{o}K are plotted in Figure 20. From these characteristics

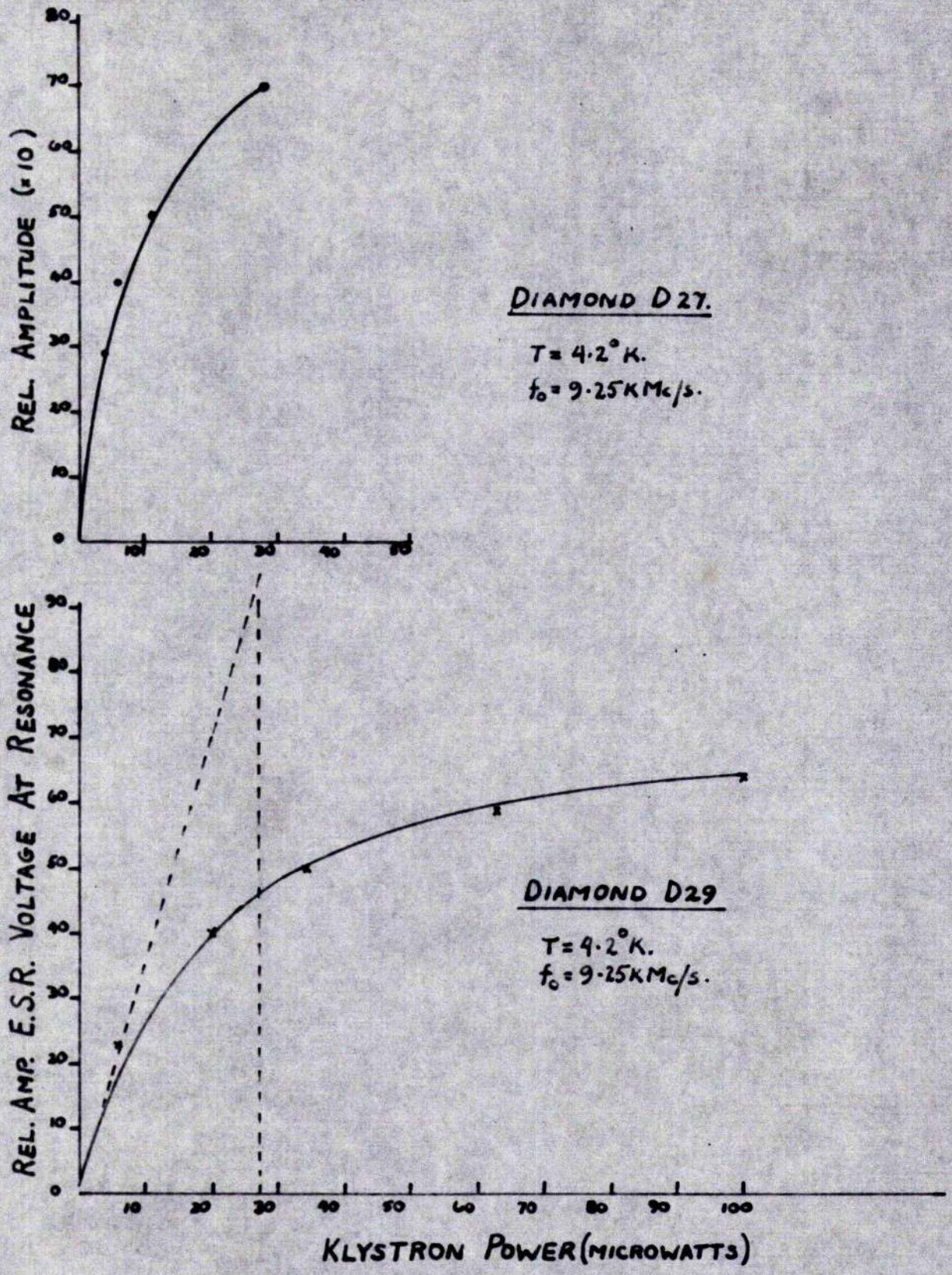

FIGURE 20

SATURATION CHARACTERISTICS FOR IRRADIATED DIAMONDS

the saturation factor of Equation 3.15 can be obtained, and thus T_1, once T_2 and B_1 are known. At resonance, it may be assumed that this saturation factor, $(1 + \gamma^2 B_1^2 T_1 T_2)^{-1}$, will equal $\frac{1}{2}$ when the measured amplitude of the spin resonance signal is one-half of that which would be obtained if the system remained linear. Thus the problem was to evaluate T_2 and B_1 where the amplitude of the microwave magnetic field in the resonant cavity is given by $B = 2B_1 \sin\omega t$.

As shown in Section 3.5, the spin-spin relaxation time, T_2, may be determined from the line width of the electron spin resonance signal. In these experiments, the width of the diamond line was estimated by visual (oscilloscope) comparison with a known marker when 50 cps field modulation was employed. It was desirable to use DPPH as the marker for its line width is known accurately (2.7 gauss); however, since the g-values of diamond ($g = 2.0028$) and DPPH ($g = 2.0036$) are close, the resonance lines of the two specimens might overlap undesirably if both were contained in the resonant cavity. As a result, the diamond spin resonance line was first compared with that of blue plasticene (resonance due to sulphur impurities) which has a g-value of 2.03; and in a second experiment, the blue plasticene line was compared with that of DPPH. From a comparison of the spectra, using 50 cps field modulation, the line width of the plasticene was ~7.5 gauss. This figure is somewhat smaller than the

10 gauss value quoted by Rose-Innes[32]. However, it is possible that the spin-spin interaction varies with different plasticenes.

From the second experiment carried out with diamond and blue plasticene, the line width of specimen 29 was estimated to be ~7.5 gauss. Both experiemtns were conducted at liquid helium temperatures (4.2°K in each case). Then a comparison of the resonance spectra of specimens 27 and 29 indicated that the line widths of the two crystals were of the same order.

These experiments were carried out before the magnet pole pieces were "shimmed", and so some inhomogeneous broadening would be evidenced in the resonance spectra. Thus, a more realistic value for the true line width of the diamond specimens, taking their size into consideration, would be 7 gauss or less at 4.2°K. (The minimum value quoted by Griffiths is 15 gauss at 90°K.)

The resonance spectra for specimen 29 and blue plasticene together are shown in Figure 21. In this figure, the magnetic field is increasing from left to right, and the stronger signal is that of the diamond; 50 cps magnetic field modulation was employed, and the modulating voltage was phase shifted by 90° and synchronously applied to the X-plates of the oscilloscope. It should be mentioned that the spectral lines in this figure have been broadened somewhat by the

FIG. 21 DIAMOND AND BLUE PLASTICENE RESONANCE (4.2°K)

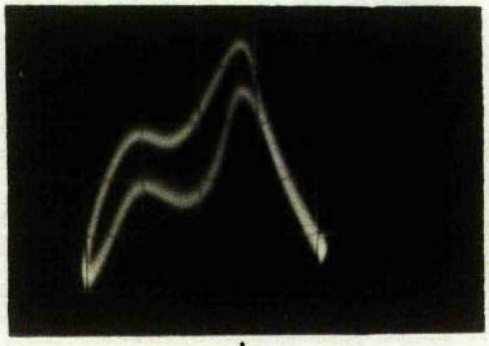

FIG. 22
MgO RELAXATION WITH LOW INVERTING POWER

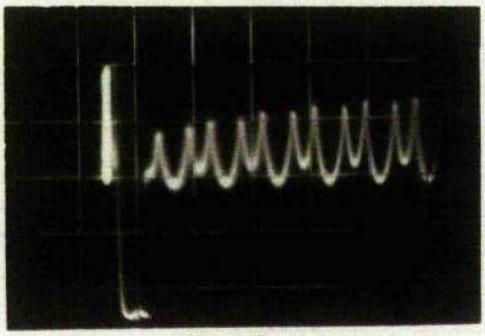

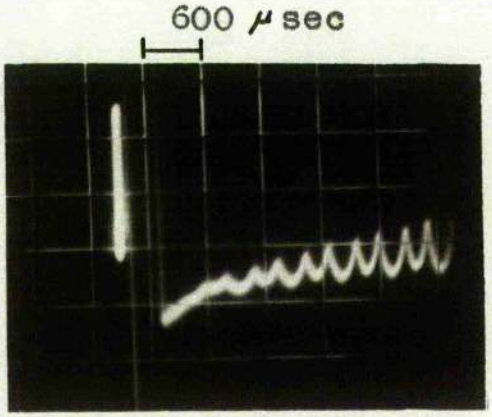

FIG. 23
MgO RELAXATION WITH MED. INVERTING POWER

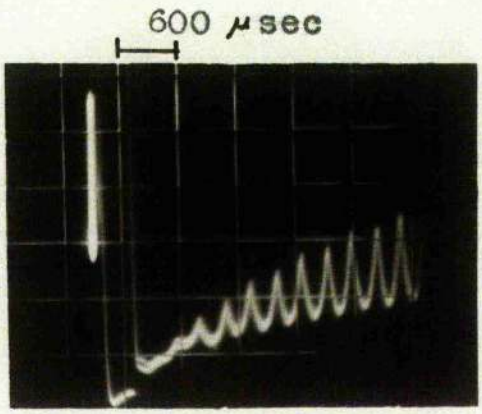

FIG. 24
MgO RELAXATION WITH $\frac{1}{4}$W INVERTING POWER

For Figs. 22, 23, 24, $T = 4.2°K$,

$f_{mod} = 1800$ cps, $N \approx 6 \times 10^{17}$

action of a 0.3 μ F capacitor connected across the IF amplifier output.

Thus T_2 could be determined, but to evaluate T_1 by steady-state methods, it was still necessary to calculate the amplitude $(2B_1)$ of the microwave magnetic field at the specimen. To calculate this field magnitude, it was first necessary to find an expression for the energy stored in the resonant cavity, which in these experiments was the TE 111 cylindrical resonator. This expression, from standard electromagnetic theory[27], is,

$$W = \int^{V_c} \frac{K_o E_m^2 \cdot dV_c}{2} \qquad (7.1)$$

in mks rationalized units, where E_m is the peak amplitude of the electric field in the cavity, and where the integration extends over the volume of the cavity.

For a TE resonator operating far from cut-off, the expression may be rewritten in terms of the amplitude of the microwave magnetic field, namely,

$$W = \int^{V_c} \frac{(2B_m)^2 \cdot dV_c}{2u_o} \qquad (7.2)$$

where $(2B_m)$ is the peak amplitude of the magnetic field over the cavity and $u_o = 4\pi \times 10^{-7}$.

The diamond steady state experiments were carried out with a TE 111 cylindrical resonator, for which Equation 7.2 reduces to a complicated integral of Bessel functions. This equation was not evaluated. Instead, in later calculations, the performance of this resonator was compared with that of the TE 102 resonator. It was observed experimentally that the Q's of the two resonators were alike, as were the cavity volumes. Therefore, to a good approximation in later calculations on the diamond experiments, the energy storage, W, was taken to be that for the TE 102 resonator operating under the same conditions of coupling and frequency. For the TE 102 rectangular resonator, Equation 7.2 becomes a simple volume integral over rectangular co-ordinates, and reduces to,

$$W_{TE\ 102} = \frac{(2B_{1m})^2 \cdot (\text{volume of resonator})}{8u_o} \qquad (7.3)$$

again in rationalized mks units. The stored energy, W, may also be found experimentally from Equation 4.1, since ω, Q_o and P can be measured. If this result is then equated to Equation 7.3, the value for $(2B_{1m})^2$ can be realized. In this experiment, the circuit parameters for a maximum output condition were:

$Q_o \approx 2Q_L = 1.4 \times 10^4$; $f_o = 9.1 \times 10^9$ cps; $P_{KLYS.} = \frac{1}{2}$ w;

$V_c = 10$ cc ; $T = 4.2^oK$

in which it is assumed that the cavity was at, or close to, the matched condition. Thus from Equation 4.1 we have

$$W = 6.15 \times 10^{-8} \text{ joules}$$

and Equation 7.3 gives,

$$W = \frac{(2B_{1m})^2}{1.008} \text{ joules}$$

whence $(2B_{1m})^2 = 6.2 \text{ (gauss)}^2/\tfrac{1}{2}\text{watt microwave power}$

or $(2B_{1m})^2 = 1.34 \times 10^{-5} \text{ (gauss)}^2/ 1\,\mu\text{W microwave power}$ (1:24 ? Surely)

From this expression, therefore, the magnitude of the microwave magnetic field in the cavity could be evaluated at the power level for which the saturation factor was taken to equal $\tfrac{1}{2}$. Thus, at resonance, the saturation term $(\gamma^2 B_1^2 T_1 T_2) = 1$ could be solved for T_1. For diamond specimen 29, it was found (as shown in Fig. 20) that the saturation factor equalled $\tfrac{1}{2}$ when the incident klystron power was 28μW. Further, since $T_2 \approx 1/\pi(\Delta f)$ and $(\Delta f) = 2.8 \times 10^6 (\Delta B) = 19.6 \times 10^6$ cps for a 7 gauss line width; and since $\gamma = 2\pi \times 2.8 \times 10^6$ radians/gauss, the saturation term could be evaluated to give an estimate for T_1, namely,

$$T_1 \approx 1.8 \text{ millisec at } 4.2^\circ\text{K for specimen 29}$$

This value for T_1, derived from steady-state phenomena, is in fair agreement with the value directly measured on the

oscilloscope under transient conditions. With the adiabatic fast-passage frequency sweep method described in Section 7.6, the measured T_1 was $\sim$ 0.5 millisec at 4.2°K. Thus the validity of the above steady-state approximations would appear to be justified. Note that a similar treatment could be applied to the resonance results with specimen 27.

As an additional check on the values obtained for B_1, T_2 and T_1 in the steady-state experiment on specimen 29, these figures were compared with the figures quoted by Bloembergen[34] from experiments on the saturation characteristics of DPPH. In the latter experiments, at the power level corresponding to a saturation factor of $\frac{1}{2}$, the quoted values for $(2B_1)$ and T_1 were 2 gauss and 6.3×10^{-8} sec, respectively. From these values, it can be seen that the products $(B_1^2 T_1)$ for DPPH and specimen 29 are in fact in the same ratio order as the line widths.

The number of spins in diamond 29 was estimated by comparing the amplitude and width of this resonance signal with that of the DPPH sample ($\sim 1.0 \times 10^{18}$ spins) mentioned in Section 7.2. In this way the total number of spins in specimens 29 and 27 were estimated to be

Diamond 29: $N = \sim 2 \times 10^{16}$

Diamond 27: $N = \sim 2 \times 10^{15}$

7.5 MgO Crystals -- Steady State Resonance Phenomena

The resonance spectra of the irradiated MgO crystals were observed under steady state conditions, by the use of the 50 cps magnetic field modulation. The amplitude of the electron spin resonance signal of the Dounreay specimen was compared with that of one of the Harwell specimens. The spectra could be observed at 300°K. It was observed that the amplitudes were of the same order, as were the spectral distributions. Thereafter attention was mainly confined to the Harwell MgO specimens in view of the radioactivity of the Dounreay specimen. As observed, the spin resonance spectrum of an MgO specimen consisted of a main line (at approximately the free electron magnetic field value) and six satellites with a signal amplitude roughly 10% of the main line value. It was observed that the satellite line shapes were asymmetrical about the main line.

The main-line width, when compared with DPPH, seemed to be unusually high -- in the order of 4 gauss. At this time, however, the magnet pole pieces had not been shimmed, and consequently much of the observed distribution was attributed to inhomogeneous broadening over the fairly large MgO sample. Shimming was carried out as previously stated in Section 6.3, and the experiment repeated. It was observed that the line width was reduced to about 1.8 gauss. This observation was made at 300°K to offset possible saturation broadening. Photographs taken for both conditions are reproduced in

Figures 8 and 9. In these photographs, only two of the six satellites can be observed due to the limitation set by the amplitude of the modulating magnetic field. The presentation is with a repetitive sweep on the oscilloscope time base -- hence the double spectrum. In each case, the amplitude of the signal is roughly 5 volts for a temperature of 4.2°K.

In addition to inhomogeneous broadening, some saturation broadening would undoubtedly occur at 4.2°K with the monitor microwave powers employed for observation (6 - 12 μW). To avoid saturation, it would have been necessary to operate with monitor microwave powers of 1 μW or less; system instabilities would have made observations at this power level very inadequate.

The number of spins in each Harwell MgO specimen was estimated to be in the order of 6.7×10^{17} or 1.8×10^{18} per cc. Thus, the spin concentration is in the same order as that employed by Chester in MgO experiments. (Chester quoted a line width of 0.9 gauss for a spin concentration of $\sim 10^{18}$ spins per cc using a 12-in. magnet.)

The spin lattice relaxation time, T_1, was not calculated by steady-state resonance methods, because of the low monitor power difficulties mentioned above. T_1 could, however, be measured directly by transient methods as will be described.

7.6 MgO Crystals -- Transient Resonance Phenomena

The MgO spin-lattice relaxation time could be measured readily by the use of transient-producing techniques. One such technique applied in this investigation was that of the adiabatic rapid-passage, frequency sweep method. The experimental procedure was as follows:

1) With the d-c magnetic field off the resonance value, adjust the resonant cavity coupling (sliding-stub tuner) until the cavity is matched or has a known degree of coupling.
2) Apply a pulse of microwave power ($\frac{1}{4}$ - $\frac{1}{2}$ watt) to the specimen by sweeping the power klystron through the cavity resonance frequency by application of a trapezoidal voltage sweep to the klystron reflector.
3) With the d-c magnetic field at the resonance value, monitor the subsequent transient behaviour of the spin system by sweeping the monitor klystron (5 - 15 μ W) through the cavity resonance frequency in a train of observations -- i.e., by application of a train of saw-tooth voltages to the reflector, as shown in the sequence diagram of Figure 17a.
4) Allow the power klystron frequency to return through the cavity resonance at the end of the monitor period.
5) Repeat this procedure at 12 or 25 cps.

In the timing sequence shown in Fig. 17a, the height of the trapezoidal wave applied to the inverting klystron reflector was 170 volts and the leading edge of the trapezoid was

usually 100 μ sec long, but this was not critical. The amplitude of the monitor pulse train was 90 volts, and the sweep time and sawtooth repitition rate were in the order of 200 μsec and 400 μsec, respectively. The length of the monitor pulse train was equal to one-half of the cycling period mentioned in Section 6.4(d). The resonant cavity employed could be a TE 111 or a TE 102 cavity, as no eddy current losses were incurred in this method.

It should be noted that inversion could not be achieved with this technique. Since the line width of the specimens was larger than the half width of the resonant cavity ($\sim$ 1.5 Mc/s), only a portion of the available spins would be affected by this process. It was possible, however, to effect near-saturation.

An experiment of this type was carried out on the Dounreay MgO specimen at 4.2°K. The result is as shown in Figure 25. In this photograph the sweep is from left to right and compressed so that the successive IF amplifier response curves (with a centrally located resonant cavity "dip") appear as a series of vertical lines. The resonant cavity was adjusted to the matched condition with the d-c magnetic field off the resonance value. In this condition the reflected power would be a minimum, or zero. The applied power klystron pulse produced the initial (large) IF pulse shown in the photograph. Subsequently the spin system would be saturated, and the first monitor-klystron pulse would

FIG. 25
MgO RELAXATION WITH UNDERCOUPLING
(frequency sweep)

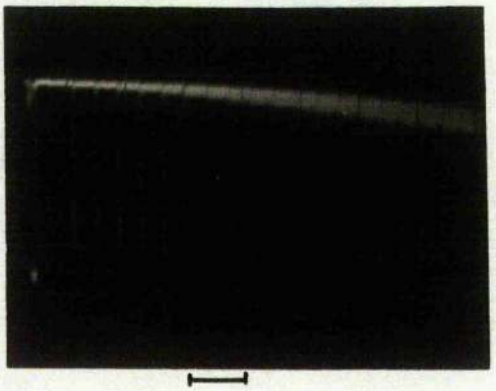

1 msec

FIG. 26
MgO RELAXATION WITH OVERCOUPLING
(frequency sweep)

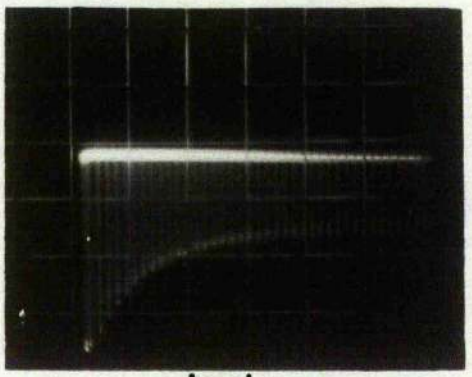

2.5 msec

2 msec

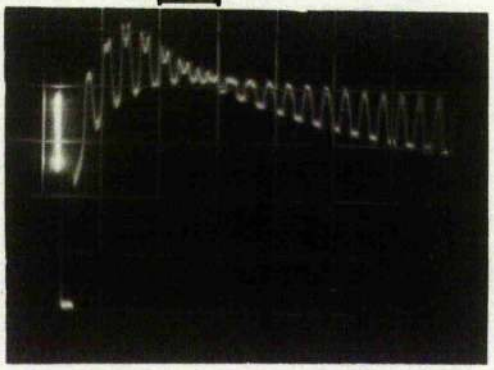

FIG. 27
MgO RELAXATION -- OVER- TO UNDERCOUPLING
(f_{mod} = 1000 cps)

1 msec

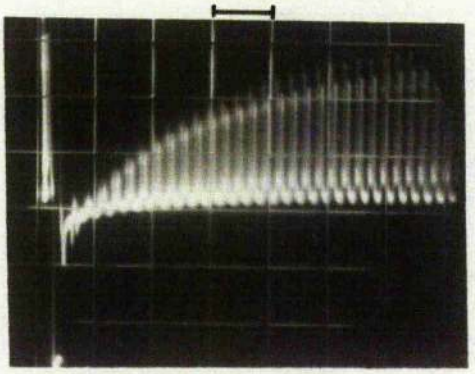

FIG. 28
MgO RELAXATION WITH FIELD SWEEP
(f_{mod} = 5000 cps)

For Figs. 25, 26, 28, $T = 4.2^{\circ}K$; $N \approx 6 \times 10^{17}$
For Fig. 27, $T = 1.3^{\circ}K$; " "

display the matched cavity condition. However, as the spin system returned to equilibrium with the characteristic time constant, T_1, the total Q of the cavity would decrease as the spins absorbed power -- that is the cavity would become more undercoupled, and the reflected power from the cavity would increase, as illustrated. In the figure the sweep rate is 1 millisec/cm, and the time between successive monitor sweeps is 400 μsec. Thus as seen, the spin-lattice relaxation time, T_1 (the time taken for the spin resonance signal to decay to 1/e of its initial value), was about 4 millisec at 4.2°K.

An interesting point is that if the cavity were originally overcoupled with the d-c magnetic field off the resonance value, then in the transient period described above, the total Q would approach that value corresponding to match as the spins absorbed power. Thus, the transient response characteristic would be the inverse of that shown in Figure 25, but the time constant, T_1, would be the same.

One such experiment was carried out on a Harwell MgO specimen at 4.2°K, and the result is shown in Fig.26. In this case the sweep rate is 2.5 millisec/cm, and the spin-lattice relaxation time, T_1, is also about 4 millisec.

Note that the diamond specimen 29, using this frequency sweep method for a transient observation, showed a T_1 measurement of 0.5 millisec at 4.2°K which is a reasonable check on the estimate given in Section 7.4.

7.7 MgO Crystals -- Preliminary Inversion Experiments

As stated, inversion of the MgO line by the frequency-sweep method of adiabatic fast passage was not achieved, as the molecular line width was broader than the width of the resonant cavity response. In consequence, inversion experiments were carried out with the field sweep method of adiabatic fast passage, since in this case all of the available electrons would be acted on by the perturbing radiation field.

Problems were encountered with this method. As the magnet field-modulation coils were mounted as a Helmholtz pair on the magnet pole pieces, transformer action would occur between the main and modulation coils, with the effect prescribed by Lenz' Law. Thus a larger modulating power would be required to sweep the magnetic field at the paramagnetic specimen by the desired amount. In addition, due to the interaction between the main and modulating magnetic fields, much of the circuit path for the modulating field would be through air, and not through the magnet yoke.

In addition to the above coupling drawbacks, at the higher frequencies it was necessary to consider eddy current heating effects on the boiling rate of the liquid helium in the inner dewar. Eddy currents would be set up in the cavity resonator and associated wave guide -- and to a lesser extent in the silvering on the wall of the dewar.

In the original experiments of this investigation, the TE 111 (silver plated) brass resonator was used. With magnetic field modulation applied to this system, it was found that the modulation response at the paramagnetic specimen fell off rapidly for frequencies in excess of 100 cps. This was in agreement with investigations carried out by Hayward[28] on eddy-current effects in cavity resonators. Indeed, to sweep through the MgO main resonance line with the external sweep coils at 2000 cps required a drive of 150 volts rms at 2 amp. In this case the driving source was the high-frequency motor alternator circuit described in Section 6.5. Furthermore, the operating period per experiment at 4.2°K was reduced from about 12 hours to 5 hours as a result of eddy-current heating of the resonator and associated wave guide. (With such a loss rate, therefore, it was impractical to attempt to operate below the λ point.) Despite these drawbacks, however, some initial useful information on inversion and saturation effects was obtained.

Experimentally the method was as follows. The high frequency alternator output was applied to the external sweep coils via a 1.5 μF series capacitor which reduced the circuit impedance. The modulation was simultaneously applied to a Dekatron glow tube scaler and every hundredth pulse was fed from the scaler output to the trigger circuit which initiated the power klystron pulse. The result of

such power pulse application was monitored with the c-w monitor klystron circuit.

In further detail, with reference to Figures 14 and 15, the operation of the pulse circuits is as follows:

1) The scaler output (positive) was amplified and inverted by applying it to Pin 2 of the the triode V1, which was in the "off" position for multivibrator action.
2) The output pulse from V1 triggered the one-shot multivibrator V12, through the trigger diode V17-A.
3) The output of V12 (trailing edge) triggered the one-shot multivibrator V13, through the trigger diode V17-B. This multivibrator applied a 100 volt positive pulse to the cathode-follower clipper circuit V14-A which in turn applied an essentially rectangular 95 volt pulse to the power klystron reflector.

The duration of the power klystron pulse ($\sim$ 500 μ sec) was controlled by the second multivibrator V13, while the time delay of the first multivibrator V12 was adjusted to ensure that the power klystron pulse was applied as the modulated magnetic field swept through the main MgO resonance line.

In these experiments with high frequency sinusoidal magnetic field modulation, it was possible to saturate and partially invert the main resonance line of a Harwell MgO

crystal. Such results are illustrated in Figures 22, 23, and 24. These photographs were taken at an operating frequency of 9.2 kMc/s and temperature of 4.2°K; the field-modulation frequency was ~ 1800 cps. In all three figures, the left-hand pulse is the power klystron pulse, and the sweep rate is ~ 600 μsec/cm. Figure 22 shows the MgO resonance line with the power klystron pulse well attenuated; in this case the resonance line is not saturated. The power klystron pulse was increased to effect saturation of the resonance line as shown in Figure 23; here the transient response of the spin system is displayed. Figure 24 shows, in one sweep, a partial inversion of the resonance line with the application of a power pulse of 250 milliW -- note that the apparent drift of the baseline in this figure was due to the fact that the field modulation was insufficient to sweep completely through the main resonance line.

It was important to know the amount of resonant-cavity coupling in these experiments, if false results were not to be obtained. The amount of coupling could be observed directly by noting whether the spin-resonance signal added to the power reflected from the cavity (undercoupling) or whether it reduced this reflected power (overcoupling) under steady state monitor conditions.

If, under the application of a power klystron pulse, the resonant cavity remained overcoupled for all the possible values of magnetic Q, true inversion would be

displayed on the oscilloscope as an inversion of the spin resonance line. On the other hand, if the cavity were undercoupled for a particular value of magnetic Q_L and passed through the matched condition in a phase of relaxation from a saturated, but not necessarily inverted state, one would observe an apparent inversion of the resonance line. This latter state would be undesirable from the point of view of ambiguity, and this is one reason why an overcoupled cavity was employed in such experiments. Figure 27 shows the effect with a normally undercoupled cavity. In this case, the cavity system is relaxing from an overcoupled to an undercoupled state, following the application of a power klystron pulse, when the power klystron pulse was insufficient for complete inversion. Experimentally, the undercoupled condition was realized with a sliding-stub tuner in the cavity arm of the wave guide circuit. The circuit parameters were $T = 1.3^{\circ}K$; $f_o = 9.2$ kMc/s; $f_{mod} = 1000$ cps; power pulse = 1 millisec duration.

A more complete picture, showing the relaxation phenomena, is given in Figure 28. This observation was made with a Harwell MgO specimen in the TE 102 resonator at $4.2^{\circ}K$ and at an operating frequency of 9.3 kMc/s; $f_{mod} = 5000$ cps; $P_{KLYS} = 200$ milliW. The oscilloscope sweep rate was 1 millisec/cm. The time indicated for T_1 was 4 millisec. This

is in close agreement with the relaxation time measurement made on the same specimen by the frequency sweep method of adiabatic fast passage.

7,8 Inversion Experiments with the TE 102 Resonator

The electromechanical system for field modulation described in Section 7.7 suffered the disadvantage that the modulation frequency of 2000 cps was too low for effective inversion and observation of the MgO resonance line. From observations made on eddy-current effects, however, it was obvious that an increase in the modulation frequency applied to the TE 111 resonator system would shorten the 4.2°K experimental operating time disasterously. Hence, a new field sweep method had to be devised. In this method, a thin wall CuNi TE 102 resonator system was employed, as described in Section 6.2(d).

With the TE 102 resonator, the attenuation of the field sweep at the paramagnetic specimen was lower. The amplitude of an MgO resonance signal, as a measure of the field sweep, decreased only 35% as the (sinusoidal) modulation frequency was increased from 250 cps to 5 kc/s. Even with the TE 102 resonator, however, it was necessary to drive the internal modulation coils with low duty-cycle pulses if eddy-current losses were to be kept to a minimum. For example, with a sinusoidal 12 kc/s field sweep of 5 gauss, an experiment at 4.2°K was shortened from the normal 12 hour period to about 3 hours, as the result of eddy-current heating.

Experimentally, to keep the eddy-current losses to a minimum and to satisfy the inversion criteria, the internal field-modulation coils were driven with a 1.2-amp current trapezoid of duration ~ 400 μsec and repitition rate 12 or 25 cps. In most of the experiments carried out, the leading edge of this trapezoid was 200 μsec long and the trailing edge another 200 μsec.

The d-c magnetic field value was adjusted so that this trapezoidal modulation swept through the spin resonance line twice. (In the case of MgO, this would be the main resonance line.) The two resonance lines were observed with the c-w monitor klystron. The power klystron pulse was then applied while the leading edge of the trapezoid was swept through the spin resonance line, and the result of such power application was observed with the c-w klystron as the trapezoidal sweep returned through the resonance condition. (This method had previously been employed by Chester[8,9], but no circuit details were given.) In these latter experiments, the power klystron pulse was increased to ~ 460 milliwatt with the aid of a sliding-stub tuner placed at the X-13 klystron (Section 6.1(a)). Furthermore, the resonant cavity was left slightly overcoupled.

With reference to Figs. 14, 15, and 18, circuit operation was as follows:

1) The trapezoidal current-sweep output from the power amplifier (Fig.18) was produced by driving this

amplifier (normally biased to cutoff) with the 180 volt trapezoidal positive pulse output from the bootstrap sweep circuit V4. In this case, the driving multivibrator, V1, was in the 12 cps or 25 cps position.

2) As in Section 7.7, the output pulse from V1 triggered the one-shot multivibrator V12 through the trigger diode, V17-A.

3) The output of V12 (trailing edge) triggered the one-shot multivibrator V13 through the trigger diode, V17-B. This multivibrator applied a 100 volt positive pulse to the cathode follower clipper circuit V14-A which in turn applied an essentially flat-topped 95 volt positive pulse to the power klystron reflector.

4) The power klystron quiescent reflector voltage was set to the high frequency edge of the $3\frac{\lambda}{4}$ mode so that the pulse application would bring the klystron frequency to the cavity resonance frequency.

5) The time constant of V12 was adjusted until the power klystron frequency arrived at the resonance value as the field waveform started the first sweep through the resonance line.

6) The time constant of V13 was adjusted until the duration of the power klystron pulse was equal to that time taken by the field sweep circuit to sweep through the resonance line.

7.8 (a) Amplification with MgO at 1.3°K

A field sweep experiment with a Harwell MgO crystal is now described. The experiment was carried out with an over-coupled cavity at 1.3°K and at a frequency f_o = 9.05 kMc/s. The Harwell specimen was cut to size to fit the TE 102 resonator: the weight of a specimen was now 0.72 gms and the

total estimated number of spins $N = 6.7 \times 10^{17}$. The crystal was located along the field sweep axis at the centre of the resonator. Note that the crystal was not cut along any definite crystal axis since it is isotropic in the main resonance line. Nor was it located along any crystal reference axis in the resonator.

Figure 29 shows the sweep voltage applied to the field-sweep power amplifier. As shown, the sweep drive waveform was made slightly asymmetrical in this experiment. The time scale is 100 μsec/cm in this photograph. With this sweep, the two resonance lines displayed by a monitor power of $\sim 1.5 \times 10^{-7}$ watts are as shown in Fig. 31. The apparent difference in line widths is due to the field sweep asymmetry. In Fig. 31, the scales are 200 mV/cm and 100 μsec/cm for Y-modulation and X-modulation, respectively. The result of a 470 milliwatt power pulse application is shown in Fig. 32. In this figure, the large negative pulse is the power klystron pulse which has saturated the IF amplifier, and the following negative-going waveform is the inverted MgO main resonance line. The time and amplitude scales are as in Fig. 31, as is the monitor power. It was estimated that on this amplitude scale a monitor power of 1.5×10^{-7} watts would correspond to $\sim$ 80 mV. Thus the power gain in this case would be $\sim$ 10 db, 100 μsec after inversion. Note that with this specimen it was necessary to use a fairly low monitor power, as it was estimated that the Saturation Factor

FIG. 29
FIELD SWEEP DRIVING VOLTAGE

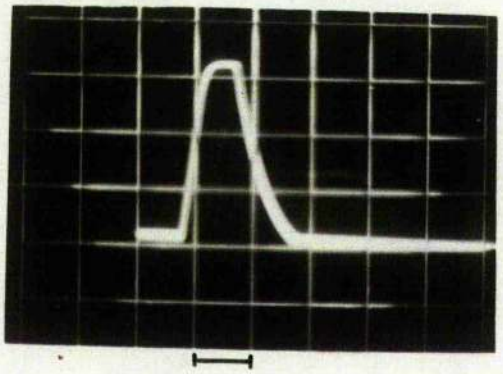

FIG. 30
MgO ABSORPTION AND CAVITY REFLECTION

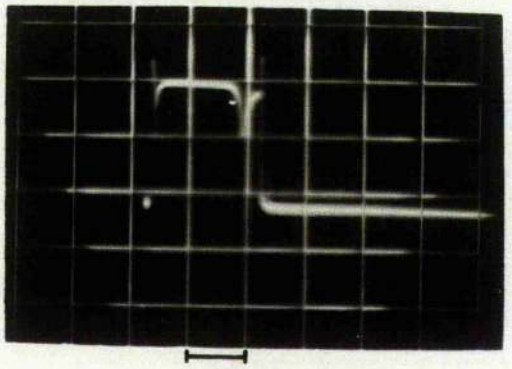

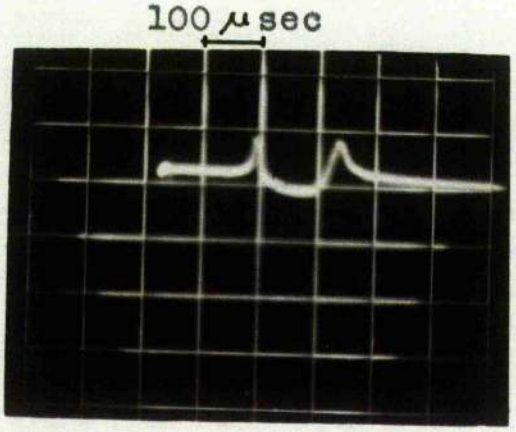

FIG. 31
MgO RESONANCE ABSORPTION
(monitor 1.5×10^{-7}W)

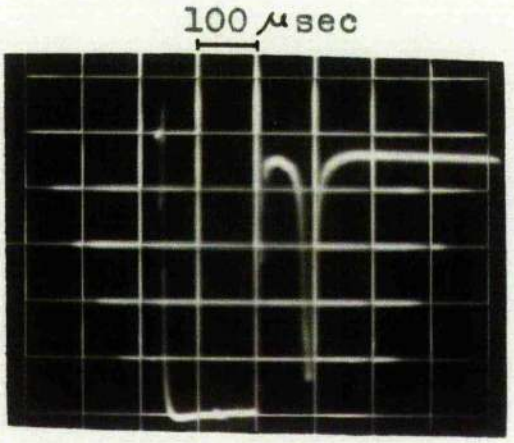

FIG. 32
MgO EMISSION
($\frac{1}{2}$ W inverting power)

For the above figures, $T = 1.3^{\circ}K$;
$N \approx 6 \times 10^{17}$

at resonance $(1 + \gamma^2 B_1^2 T_1 T_2)^{-1}$ would equal $\frac{1}{2}$ for an incident power level of about 3 μ watts.

The power reflected from the cavity during the power pulse application could be observed with straight detection as shown in Fig. 30. The change in power reflected from the cavity occurs as the magnetic field sweeps through the resonance near the end of the pulse. The sweep time is again 100 μ sec/cm.

It was of interest to note that in addition to the main MgO resonance line, it was also possible to invert each of the six satellites. The gain over inversion under such conditions, however, did not appear to exceed unity.

In conclusion it should be stated that the experiment on the main resonance line was also carried out at 4.2°K. At this temperature, however, only a partial inversion of the resonance line could be attained with the technique employed. At this temperature with an MgO specimen containing 10^{17} spins, Chester[8] observed that the inverted state persisted for about 2.5 millisec; in this instance the regenerative gain was 20 db at 125 μsec after inversion and fell to 3 db at 720 μ sec.

7.8 (b) Oscillation with MgO at 1.3°K

In this experiment, which was repeated at f_o = 9.05 kMc/s and T = 1.3°K, the amount of paramagnetic material in the

cavity was doubled. The second Harwell MgO specimen was cut to fit the TE 102 resonator, and was mounted beside the specimen already in the cavity. The total number of spins was then $\sim 1.2 \times 10^{18}$. To ensure rigidity, the two specimens were stuck together with nail varnish before being embedded in the Jabolite that filled the lower half of the cavity. The crystals were inside the area swept by the internal modulation coil. With the sliding-stub tuner, the power klystron was adjusted carefully for maximum output. This adjustment was carried out while pulsing the klystron. From the X-13 klystron operating characteristics, the optimum power at this frequency was estimated to be 470 milliwatts.

Using the technique described in the previous section, a large inverted resonance line was observed with a monitor power of $\sim 1.5 \times 10^{-7}$ watts following the application of the power klystron pulse. This inverted state persisted after the monitor klystron was disconnected from the circuit. Furthermore, this oscillation pulse could be observed with straight detection when the local oscillator klystron was also disconnected.

The oscillation pulse shown in Fig. 33 has the amplitude modulated characteristic observed by investigators[9,29] working with other paramagnetic material. The time scale in this photograph is 70 μ sec/cm. The duration of the pulse was dependent on the field sweep characteristics, and

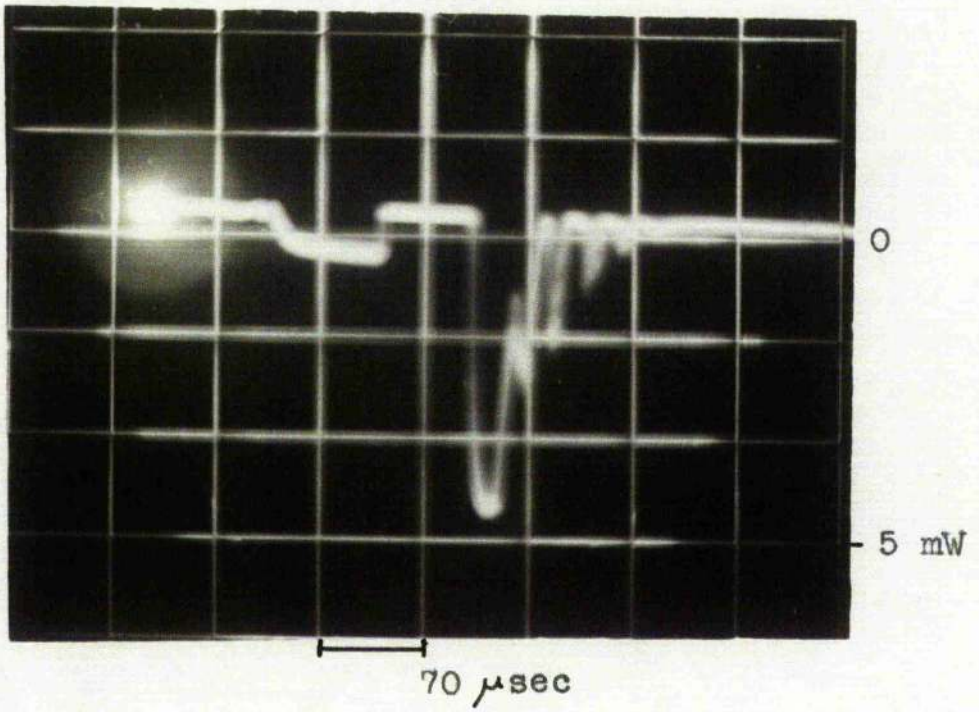

FIGURE 33

MgO OSCILLATION PULSE WITH AMPLITUDE MODULATION

(Field sweep inversion -- ½ watt)

$N \approx 1.3 \times 10^{18}$, $T = 1.3^{\circ}K$, $f_o = 9.05$ kMc/s

thus critically dependent on the quiescent level of the d-c magnetic field. By varying the quiescent field level, the pulse duration could be varied from about 150 μ sec to 50 μ sec -- shorter duration pulses could not be produced. It was noted that the amplitude modulation was most pronounced in the longer pulses. The peak power during a 100 μ sec pulse, such as is shown in Fig. 33, was estimated to be 5 milliwatts. From such an estimate, it was possible to define and evaluate a Conversion Efficiency factor (C.E.) for the system such that

$$C.E = \frac{\text{Peak Oscillatory Power}}{\text{Inverting Klystron Power}} \qquad (7.4)$$

In this case,

$$C.E. = \frac{5 \times 10^{-3}}{470 \times 10^{-3}} = 1.06\%$$

for a conversion at the same frequency.

It is of further interest to define an Emission Efficiency factor (E.E.) for the oscillatory condition, such that

$$E.E. = \frac{\text{Energy Contained in Single Osc. Pulse}}{\text{Spin Energy After Complete Inversion(W)}} \qquad (7.5)$$

In the above, W -- the maximum energy stored in the spin system -- from Equation 3.12, would be

$$W \approx \frac{N(hf)^2}{2kT} \qquad (7.6)$$

where N is the total number of spins. In this experiment, the parameters were: $N = 1.2 \times 10^{18}$ spins; $f = 9.05 \times 10^9$ cps $T = 1.3^\circ K$; ($h = 6.62 \times 10^{-27}$ erg-sec; $k = 1.37 \times 10^{-16}$ erg/degree); so that

$$W \approx 12 \times 10^{-7} \text{ joules}$$

In this experiment, estimated values for the oscillation pulse were $P_{peak} \approx 5$ milliwatts, and pulse duration $\approx$ 100 μsec. Thus, the energy contained in the observed oscillation pulse would be to a first approximation 2.5×10^{-7} joules (neglecting amplitude modulation). Thus the Emission Efficiency would be

$$E.E. = \frac{2.5 \times 10^{-7}}{12 \times 10^{-7}} \approx 20\%$$

As a measure of oscillatory operational efficiency, it is worth while comparing the above results with those calculated from the data given by Chester in oscillation experiments on irradiated quartz. Chester quotes[8], as follows: $N = 10^{18}$ spins; $T = 4.2^\circ K$; $f = 9.0 \times 10^9$ cps; klystron power = 500 milliwatts; peak oscillation power = 12 milliwatts; oscillation pulse duration = 10 μsec. For which case, using the above equations, C.E. = 2.4% and E.E. $\approx$ 20% for irradiated quartz maser.

The conditions for observing an oscillation pulse were quite critical, and several experiments were carried out in which no oscillation pulse was detected. It was found, at this stage, that the Q of the TE 102 resonator had decreased somewhat (due to repeated soldering) and the cavity was, therefore, re-silvered. In the next experiment carried out at 1.3°K, (f_o = 9.0 kMc/s, $Q_L \approx$ 7000), an oscillation pulse of about 5 milliwatt was observed as shown in Figs. 34, 35 and 36. In each of these figures, the sweep time is 200 μsec/cm.

In Fig. 34, the gain of the IF amplifier has been reduced so that the oscillation pulse does not saturate the amplifier. It can be noted that this 100μ sec oscillation pulse does <u>not</u> have the amplitude-modulated characteristic observed with the previous experiment.

In Fig. 35, the gain of the IF amplifier has been increased to the maximum, and the amplifier is saturated by both the inverting and oscillation pulse. It was found, that if the local oscillator reflector voltage was shifted slightly, the amplifier output would have the form shown in Fig. 36. In this figure, the IF amplifier is unsaturated for part of the inverting period when the magnetic field sweeps through the molecular resonance. It is not exactly understood why the inverting pulse and oscillation pulse

FIGURE 34
MgO OSCILLATION PULSE
WITHOUT AMPLITUDE MODULATION

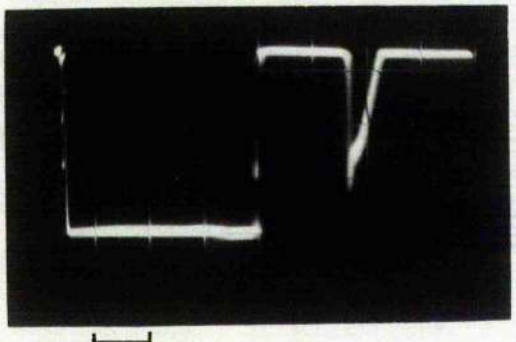

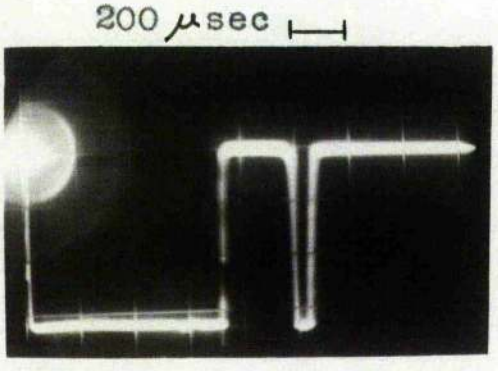

FIGURE 35
MgO OSCILLATION PULSE --
INTERMEDIATE FREQUENCY
AMPLIFIER SATURATED

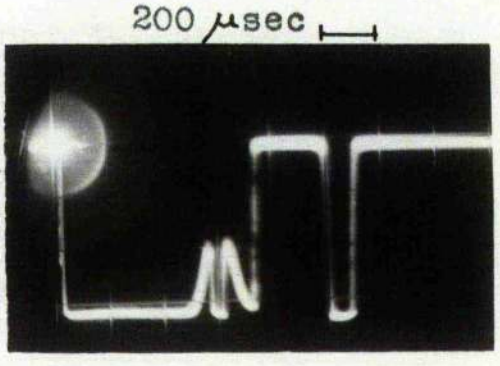

FIGURE 36
MgO OSCILLATION PULSE --
AMPLIFIER UNSATURATED
DURING INVERSION

In all figs., $T = 1.3^{\circ}K$, $f_o = 9.0$ kMc/s, $N \approx 1.3 \times 10^{18}$

displays decreased at different rates as the local oscillator frequency was taken off the superheterodyne value. It is possible that the local oscillator is "pulled" slightly by the power klystron during the inverting pulse, in which case the inverting and oscillation pulse displays would differ slightly with the local oscillator frequency variation. This could be checked by increasing the isolation factor in the local oscillator circuit.

The difference in the shape of the oscillation pulses in Figures 33 and 34 was even more puzzling. The theories formulated[33,35,36] to explain the nature of an oscillation pulse seemed to be somewhat inadequate and it was felt that the oscillatory behaviour should be further examined. Following a suggestion made by Prof. Stevens[37] an attempt was made to monitor the behaviour of the longitudinal component of magnetization during the oscillation pulse. We postulated that if the energy in the cavity was oscillating between the spin system and microwave field at say 50 kc/s (as might be inferred from Fig. 33), it should cause a measurable voltage to be induced in a coil wound around the MgO crystals in the cavity. It was estimated that a peak voltage of $\sim \frac{1}{2}$ millivolt might be picked up with a 50 turn coil at the 50 kc/s frequency. When a coil was wound around the specimens (with the coil axis along the main field axis) it was found that the Q of the cavity was seriously affected, despite the fact that the coil was located along the plane of the microwave

magnetic field. The Q was affected seriously when more than two turns of 42 gauge copper wire were wound around the crystals. Thus, the experiment had to be abandoned. A possible alternative method is, however, given in Chapter 8.

7.8 (c) Saturation with Diamond at 1.3°K

Following the successful oscillatory experiments with the irradiated MgO specimens, a similar experiment was carried out on an irradiated diamond specimen to see if inversion could be attained. Using the method described in Section 7.8, a pulse of klystron power (470 milliwatt) was applied to specimen 29 and the result of such application was monitored 100 μsec later with the c-w klystron ($\sim 1\mu W$). Saturation of the diamond resonance line was observed with this pulse power at $f_o = 9.2$ kMc/s and T = 1.3°K. Inversion, however, was not attained. This result might be anticipated from paragraph 2a of Section 5.1 covering the adiabatic fast passage conditions, since in this case the relaxation time, T_1 ($\sim$ 0.5 millisec) is not long compared with the field sweep time.

As a means of studying the degree of saturation of the system as a function of "inverting" power, the amplitude of the resonance absorption characteristic was monitored as a function of pulse power 100 μsec after the pulse application, and the results are plotted in semi-logarithmic

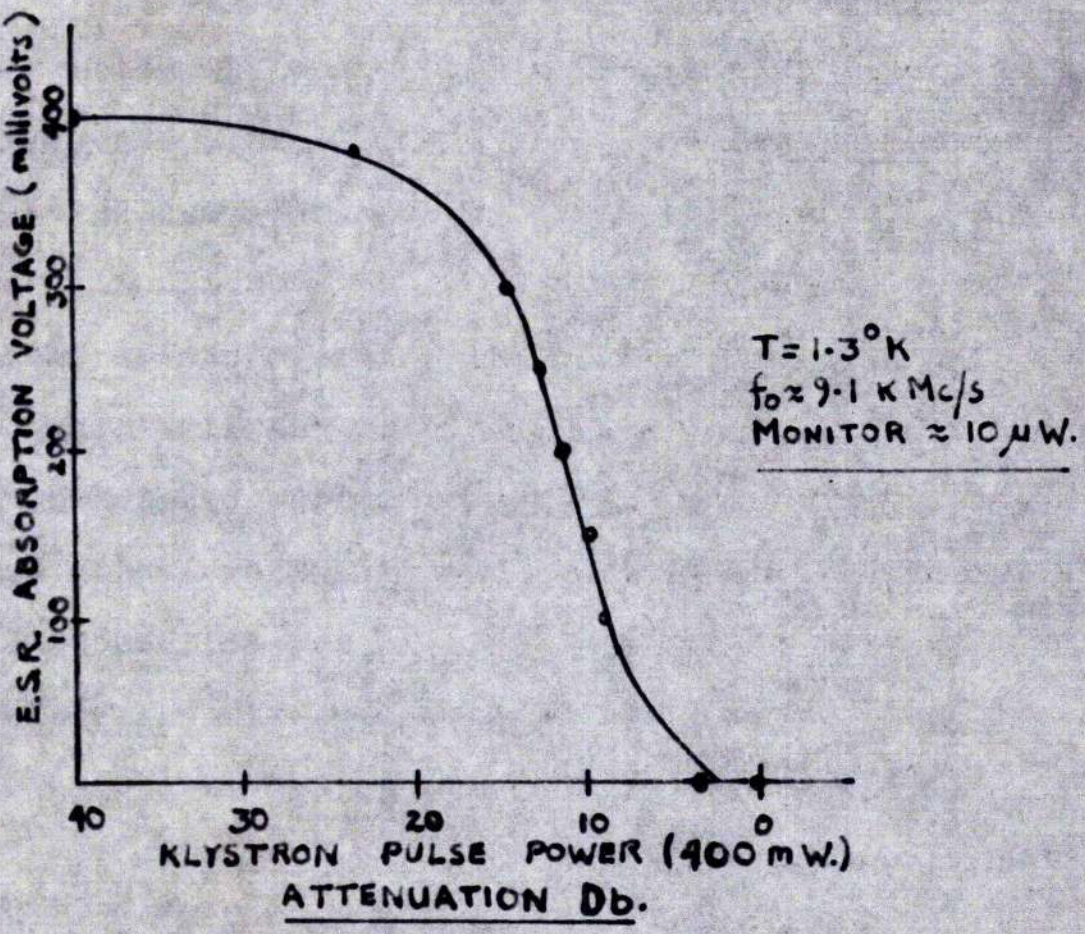

FIGURE 37

DIAMOND 29 SATURATION CHARACTERISTIC

100 μsec AFTER POWER PULSE

(Field sweep method)

fashion in Fig. 37. It can be seen that the relationship between degree of saturation and "inverting"power is non-linear.

7.8 (d) Resonance Experiment with Phosphorous-Doped Silicon

A spin resonance experiment was carried out on one of the phosphorous-doped silicon crystals. This experiment was incidental as this type of crystal had been extensively studied in a two-level maser by Waters at S.R.D.E., Christchurch. The specimen (weight $\approx$ 1.4 gm; thickness 3mm; $N = 1 - 3 \times 10^{16}$ spins) was mounted on Jabolite along the TE 102 resonator field-sweep axis with its broad face normal to the incident power vector. The resonator length was shortened to counteract the effect of the silicon ($K = 11.83$) on the resonant frequency. With this specimen, the length of the TE 102 resonator was reduced to 35 mm for operation at 9.05 KMc/s and $1.3^{o}K$.

With a c-w klystron power of 10 μW (which was well into saturation under steady-state conditions), a resonance spectra was observed which consisted of two equal and narrow absorption lines. The amplitude of the resonance lines was less than 10 millivolts on the oscilloscope and as this level was smaller than that for the Harwell MgO crystal by a factor of 500, it was thus at the threshold of the spectrometer.

The amplitude of the resonance signal could, however, be increased to 10 millivolts -- with the same incident power

level -- by shining "white" light down the quartz tuning rod. In this case the light source was a 6.3 volt, a-c, 0.15 amp bulb mounted on a frame about the quartz tuning rod as shown in Figures 4 and 5.

Since relaxation times in the order of minutes had been observed by Waters with similar crystals, the inversion technique of this investigation could not be suitably applied. An inversion of the resonance lines was attempted by a) mechanically sweeping the magnetic field through the resonance condition with the power klystron fully "on"; b) attenuating this klystron fully (70 db); c) returning the d-c magnetic field to the resonance condition; and d) monitoring the resonance signal with this low klystron power. Some degree of saturation and relaxation was observed with this rather crude method. The signal was, however, so close to the spectrometer threshold that no qualitative measurments could be made other than an approximation of T_1, which was judged to be of the order of many seconds.

CHAPTER 8

CONCLUSIONS AND RECOMMENDATIONS

With this maser design it has been possible to produce oscillation pulses at the inversion frequency. Thus, the thesis aim has been achieved, and in this respect the following conclusions and recommendations may be made.

With the MgO crystals investigated, the available klystron power (~ 460 milliwatt) was just sufficient to effect oscillation at the lowest working temperature of 1.3°K. The generation of oscillations would therefore be much more certain if the inverting klystron power and sample size (or concentration) could be increased.

If the paramagnetic sample were made to fill the cavity completely, the system could be much more easily tuned. In this case, the operating frequency at liquid helium temperatures would be essentially the same as at room temperatures. To reduce the eddy-current losses incurred with the field sweep method, the cavity could be made from a section of MgO (or other crystal) covered with a thin deposit of silver. While the silver deposit would be effective in containing the microwave fields within the cavity, it would permit the application of a sweep field to the specimen. Furthermore, a pick-up coil could be wound around the outside of the cavity to detect low-frequency changes in the longitudinal

component of magnetization. The pick-up circuit would have to be designed so that it would not respond to the swept field. If this effect proved troublesome, the adiabatic frequency sweep method of inversion could be re-investigated.

With this system it should be possible to produce oscillation pulses at a frequency higher than the "inverting" frequency. Using a pulsed magnetic field for this purpose, care would have to be taken to ensure that the oscillatory energy were emitted only in the desired mode. From the investigations in this thesis it would appear that oscillation in an undesirable mode would not occur if the rate of field sweep were sufficiently high.

APPENDIX A

PRINCIPAL MICROWAVE COMPONENTS

Component	Type
Medium power klystron	Varian X-13
Low power klystron	English Electric K311
Sliding-stub tuners	Microwave Instruments Ltd. 32/1400
30 db variable attenuators	M.I.L. 32/670
40 db calibrated attenuator	M.I.L. 32/635
10 db directional coupler	M.I.L. 32/1700
Flexible Wave guide	Sanders FG-16-6PC
Wave guide flanges:	
choke	American type UG40 A/U
plain	" " UG39 /U

REFERENCES

1) A.S. McWhorter, J.W.Meyer and Strum, 1957, "Noise Figure of a Solid State Maser", Phys. Rev. 108, 1642.

2) A.Einstein, 1917, "Zur Quantentheorie der Strahlung", Phy. Zeit 18, 121.

3) J.Weber, June 1953, "The Possibility of Amplification of Microwaves by Systems not in Equilibrium", I.R.E. Transactions on Electron Devices.

4) J.P.Gordon, H.Z.Zeiger and C.H.Townes, 1954, "The Maser - A New Type of Microwave Amplifier, Frequency Standard and Spectrometer", Phys. Rev. 95, 282.

5) J.Combrisson, A.Honig and C.H.Townes, 1956, "Utilisation de la resonance de spins electronique pour realiser un oscillateur ou un amplificateur en hyperfrequences", Comptes Rendus Academie francaise, 242, 2451.

6) N.Bloembergen, 1956, "Proposal for a New Type Solid State Maser", Phys. Rev. 104, 324.

7) H.Scovil, G.Feher and H.Seidel, 1957, "Operation of a Solid State Maser", Phys. Rev. 105, 762.

8) P.F.Chester, P.E.Wagner and J.G.Castle, 1958, "Two Level Solid State Maser",Phys. Rev. 110, 281.

9) P.F.Chester, P.E.Wagner, J.G.Castle, 1958, "Quarterly Progress Report No. 6 - Maser Studies", Research Report AF33(616)5258-R6, Westinghouse Research Labs, Pittsburgh.

10) Burkhardt et al, 1958, "Theory of Two-Level Masers" Final Report, Contract Nonr 2254(00), Hycon Eastern Inc, Cambridge, Massachusetts.

11) See for example, P.A.M.Dirac, 1958, "Principles of Quantum Mechanics", Cambridge University Press.

12) See for example, L.Schiff, 1955, "Quantum Mechanics", McGraw Hill.

13) F.Bloch, 1946, "Nuclear Induction", Phys. Rev. 70, 460.

14) J.P.Wittke, 1957, "Molecular Amplification and Generation of Microwaves", Proc.I.R.E. 45, 291.

15) E.R.Andrew, 1955, "Nuclear Magnetic Resonance", Cambridge University Press.

16) D.J.E.Ingram, 1958, "Free Radicals as Studied by Electron Spin Resonance", Butterworths Scientific Publications.

17) E.G.Cullwick, 1948, "Fundamentals of Electromagnetism", Cambridge University Press.

18) D.I.Bolef and P.F.Chester, 1958, "Some Techniques of Microwave Amplification and Generation using Electron Spin States in Solids", I.R.E. Transactions on Microwave Theory and Techniques, MTT6, 47.

19) D.I.Bolef and P.F.Chester, 1957, "Superregenerative Masers", Proc. I.R.E. 45, 1287.

20) D.M.Bagguley and J.Owen, 1957, "Microwave Properties of Solids", Reports on Progress in Physics, 20, 304.

21) R.A.Weeks, R.H.Silsbee, J.E.Wertz and P.Auzins, 1957, "Electron Spin Resonance of F Centers in Magnesium Oxide - Confirmation of the Spin of Magnesium-25", Phys.Rev.107, 1535.

22) R.A.Weeks, 1958, Private communication.

23) J.H.Griffiths, J.Owen and J.M.Ward, 1954, "Magnetic Resonance in Irradiated Diamond and Quartz", Physical Society, Defects in Crystalline Solids - Report of 1954 Bristol Conference, 81.

24) "Radar Systems and Components", 1949, Staff of Bell Telephone Co.

25) M.E.Rose, 1938, "Magnetic Field Corrections in the Cyclotron", Phys. Rev. 53, 715.

26) G.Feher, 1957, "Sensitivity in Microwave Paramagnetic Resonance Absorption Techniques", Monograph 2782, Bell Telephone System Technical Publications.

27) "Principles of Radar", 1952, M.I.T. Staff, Technology Press.

28) R.D.Hayward, 1959, "Eddy Current Effects in Microwave Cavity Resonators", Ministry of Supply, S.R.D.E. Technical Memorandum No. RES 230.

29) G.Feher, J.Gordon, E.Buehler, E.Gere and C.Thurmond, 1958, "Spontaneous Emission of Radiation from an Electron Spin System", Phys. Rev. 109, 221(L).

30) G.Feher and R.C.Fletcher, 1956, Bull. Amer. Phys. Soc. 1 Ser. 2, 125. Also see ref. 20.

31) H.Torrey, 1949, "Transient Nutations in Nuclear Magnetic Resonance", Phys. Rev. 76, 1059.

32) C.Rose-Innes, 1954, "Interaction of Microwaves and Matter at Low Temperatures", Ph.D. Thesis, Clarendon Lab., Oxford.

33) K.W.Stevens and B.Josephson, 1959, "The Coupling of a Spin System to a Cavity Mode", Proc. Phys. Soc. 74, 561.

34) N.Bloembergen and Wang, 1954, "Relaxation Effects in Para and Ferromagnetic Resonance", Phys. Rev. 93, 72.

35) J.C.Kemp, 1959, "Theory of Maser Oscillations", J. App. Phys. 30, 1451(L).

36) K.W.Stevens, 1958, "The Wave Mechanical Damped Harmonic Oscillator", Proc. Phys. Soc. 72, 1027.

37) K.W.Stevens, 1960, Private Communication.